Optical Investigations of Biological Samples in Far Infrared

Von der Fakultät Mathematik und Physik der Universität Stuttgart
zur Erlangung der Würde eines Doktors der Naturwissenschaften
(Dr. rer. nat.) genehmigte Abhandlung

Vorgelegt von
Adriana Matei
aus Bukarest

Hauptberichter: Prof. Dr. M. Dressel
Mitberichter: Prof. Dr. J. Wrachtrup
Tag der mündlichen Prüfung: 23.05.2005

1. Physikalisches Institut Universität Stuttgart
Universität Stuttgart
2005

TABLE OF CONTENTS

SUMMARY

Terahertz radiation that spans the frequency range between microwave and infrared, which is ~0.3 - 20 THz, was for long time inaccessible for study. Because of this, the frequency region was referred as the "THz-gap".
The present work was performed in the frame of the EU project "Terahertz radiation in Biological Research, Investigations on Diagnostics and study of potential Genotoxic Effects". The main purposes of this project were:

(1) To bridge the existing gap of knowledge regarding the effects of Terahertz (~0.3 THz to 20 THz) radiation on biological systems;
(2) To make a first research step of European, dimension before implementing THz technology in biological and biomedical diagnostics.

This thesis contributes to the database of the far infrared spectral properties of biomolecules. The samples investigated here are: standard amino acids, polyglycine, proteins (lipase, acylase and beta-lactamase), and human blood serum.

The first chapter is bringing the motivation of the present study.
This thesis tries to answer several questions arising in the context of imaging:
(1) How can an unknown substance be identified by means of THz imaging?
(2) Can one identify the presence of a specific amino acid in a protein by means of infrared spectroscopy?
(3) Is it possible to identify an unknown substance when one knows the absorption pattern of its basic components?

In the Chapter 2 "Sample presentation", details are given about the four categories of samples that were investigated. Amino acids are classified

according with their side chain. A few details are given about the physiological point of view. Peptides are shortly reviewed, starting from the condensation reaction. Proteins are discussed in terms of secondary structure (α-helix and β-sheet), structure characteristics in far infrared and glassy behaviour at low frequencies. Here is given a review of Boson peak occurrence in spectra of different proteins. Water is the main absorbing material in far infrared in the liquid samples investigated, and makes one of the subjects of the Chapter 2. The absorption coefficient of water is presented as a function of frequency. In addition, the main vibration modes that appear in infrared are shown. A very short description of blood and plasma (which makes approximately 55% of the blood volume) composition is closing the chapter.

Chapter 3 introduces elements of theory of the radiation interaction with matter and details about the measurement technique. Starting from the simple model of diatomic molecule as harmonic damped oscillator, the real and imaginary parts of the complex dielectric function[1] are derived. This optical characteristic is used for fitting the spectra and for calculating the absorption properties of the samples. For fitting a spectrum, this is approximated with a sum of lorentzians, in order to find the resonant frequencies for the molecular vibrations. To each absorption band is associated an oscillator. Oscillators are defined by three parameters: its strength, its damping constant, and its frequency.

Spectra between 10 and 650 cm^{-1} were recorded with the instrument Bruker IFS 113v using a mercury lamp and two helium cooled bolometers.

For liquid samples, a cuvette with silicon windows was constructed together with a support for it that enables one to perform consecutive measurements in reproducible experimental conditions.

[1] Complex dielectric function = relative permittivity $\varepsilon = \varepsilon' + i\varepsilon''$.

The polycrystalline solid samples were mixed with polyethylene (PET) and pressed as pellets. The ratio sample/PET matrix was 1:10 for the frequency range 50 – 650 cm^{-1}, and 1:4 or 1:1 for the range 10 – 50 cm^{-1}. Transmitance spectra are fitted using the program WinASF, developed in the 1st Physics Institute. The fitting helps to determine the vibrational modes. Sample absorbance is calculated from the transmitance of the pellet sample/PET when the contribution from PET was removed.

The results of the investigations are described and commented in the Chapters 4 – 7.

Chapter 4 is dedicated to amino acids measurements. 18 amino acids have been investigated by means of far infrared transmission spectroscopy. The absorbance (A) has been calculated for each of them as A = log (1/T), where T is the transmitance.

Spectra of different amino acids resemble each other, what is expected considering the similarities of their chemical structure: they all have NH_3^+ and COO^- as end groups, and a CCN "backbone". However, this resemblance is limited to a few general features. The individual features are sufficiently different to be used in identifying the compounds.

The results are presented starting with glycine (Gly) and following the evolution of the spectra complexity, as the molecule is getting bigger and more complex. Glycine is the smallest amino acid that has also the simplest spectrum. The strongest absorption peaks that are observed are situated at 135 cm^{-1} (CC torsion), 200 cm^{-1} (H bonds), 357 cm^{-1} (CCN bending), 526 cm^{-1} (NH_3^+ torsion) and 502 and 607 cm^{-1} (COO^- modes). The torsion mode seen at 548 cm^{-1} appears as a shoulder of low intensity. Its presence is often subject for controversies in literature. Here is with no doubt present, especially at low temperature (10K) where it becomes extremely intense. In the other amino acids, starting with alanine, this NH_3^+ mode is visible as an individual absorption peak. Measurements with isotope replacement performed for glycine support the peak assignment.

The side chain is influencing strongly the shape of the spectrum. The changes are analysed for a few couples of amino acids, like: glycine and alanine, alanine and phenylalanine (Phe), tyrosine (Tyr) and phenylalanine, isoleucine and leucine, valine and isoleucine, glutamic acid and aspartic acid, glutamine and asparagine. A few of them are summarized here.

Starting already with alanine, the vibrational spectra of amino acids become more structured compared with glycine. In the alanine absorption spectrum, the COO^- modes are shifted to higher frequencies. For alanine, the NH_3^+ torsion peak is very distinct compared with glycine, and is located at 486 cm^{-1}. Four peaks of medium to strong intensity are found in alanine between 278 cm^{-1} and 409 cm^{-1} and all of them have their origin in the $CC^{\alpha}N$ deformation and CH_3 torsion. In the glycine spectrum the equivalent to those modes is the peak at 357 cm^{-1}. The shoulder present in glycine at 233 cm^{-1} is not visible in the spectrum of alanine; instead of it, there is a maximum developing at 216 cm^{-1}, described as COO^- torsion. Another peak in alanine at 258 cm^{-1} is described also as COO^- torsion.

Starting from the established assignment of the bands for glycine and alanine, we can now assign some bands in the spectra of the other amino acids, even without normal mode calculations.

Phenylalanine is alanine that has a phenyl group replacing a hydrogen atom. This substitution is determining big changes in the shape of the spectrum. Although phenylalanine is a heavier molecule, with a phenol ring, alanine shows more spectral features. Phenylalanine has only four peaks above 200 cm^{-1}, and they are distributed along on the frequency axis in a way that reminds of glycine spectrum. The CCN mode around 350 cm^{-1} is visible for both Phe and Gly, both samples have a strong peak at ~200 cm^{-1}.

Tyrosine is phenylalanine plus an OH group attached to its phenol group. The difference between the two is small, but not the same can be said about the difference in the vibrational spectra. Looking at the differences between the Phe and Tyr spectra, the first to be noticed is at 248 cm^{-1}. Tyr has here a very strong peak in absorption, while Phe has a minimum.

According to the literature, the benzene ring should be prevalent in the spectra, and the ring substitute could be treated as point masses. The reality looks different. There is no evidence that most of the lines are due to the benzene ring. There is a prominent peak in Phe, at ~365 cm^{-1}, that has as correspondent in Tyr three peaks of lower intensity, at 310, 335, and 377 cm^{-1}. Phenylalanine and tyrosine have a common peak, a benzene mode, situated around 525 cm^{-1}: in Phe at 525 cm^{-1} and in Tyr at 529 cm^{-1}. The peak might show also the influence of COO^- modes, like bending, rocking, and wagging, modes which appear in many amino acids, starting with Ala.

Leucine and isoleucine have four methyl groups in their side chain and are isomers of each other. Their spectra are alike, but not as much as the spectra of isoleucine and valine are. Valine is isoleucine less a CH_3 group. The CH_3 group behaves as a heavier atom, leaving the valine spectrum almost unchanged. Absorption maxima at lower frequencies (<100 cm^{-1}) appear in valine and isoleucine at about the same positions. The same is true for the peaks between 100 and 500 cm^{-1}. Isoleucine has the bands slightly displaced to higher frequency, compared with leucine; the shift is bigger below 300 cm^{-1}. The NH_3^+ torsion mode is not visible in leucine, while it appears very clear in isoleucine at 490 cm^{-1}.

After looking at all the spectra, one can conclude upon the absorption bands that these amino acids have in common. There are four categories of vibrational modes that are present in all amino acids: the H bond, CCN, NH_3^+, and COO^- modes. The region below 200 cm^{-1} belongs mainly to the H bond modes. Other vibrations appear here as well: the lattice vibrations, the backbone deformations, and the vibrations of the ending groups NH_3^+ and COO^-. Around 270 – 380 cm^{-1} the most visible vibrations are the CCN deformations. The NH_3^+ modes appear around 380-480 cm^{-1}, and the COO^- modes – at frequencies above 480 cm^{-1}, as well as between 220 and 300 cm^{-1}.

Amino acids share common features, enough to make them a "class of molecules", where each of the members is still and individual. The individuality is given by the position of absorption maxima - each amino acid

has a distinct absorption pattern - and by their intensity. As is shown further, this absorption pattern is smeared out in oligomers and proteins.

In Chapter 5 are showed the far infrared spectra of glycine oligomers, up to hexamer, of polyglycine, and those of alanyl-glycine and glycyl-leucine.
Investigation of the glycine followed the evolution of the spectra from monomer up to hexamer and to polypeptide. In the progression toward longer Gly oligomers, the crystal structure becomes less precisely defined because of the difficulty of forming crystals, and the absorption lines broaden and shift to lower frequencies. This is exemplified by the spectrum of polyglycine: there are only three spectral features in the frequency region 0 – 400 cm^{-1}. For a peptide, the spectrum becomes broad in the same manner the water spectrum does. Single amino acids cannot be identified in the spectrum of a peptide. For alanyl-glycine and glycyl-leucine, the spectra are still made up of four regions, like it was discussed in the previous chapter, in case of amino acids. However, the features are not a sum of those from the individual amino acids, but they indicate a new sample.
In the frequency range 0 - 650 cm^{-1}, oligomers and peptides spectra show the intramolecular and intermolecular modes. These modes are: torsions about the skeletal bonds, skeletal bending, end group vibrations, and intermolecular bonds involving the hydrogen bond and the side-groups interactions. The lattice modes are visible below 200 cm^{-1}.
A skeletal torsional mode frequency depends on conformation, and so comes that the spectra can be used as indicators for conformation of the chain. Like in the case of alanine, glycine oligomers, starting with Gly_3 take the β-form. This conclusion is determined by the presence of four different bands that were previously presented and appear in our studies too. These are: 466, 572, 606, 648 cm^{-1} for Gly_3; 468, 578, 605, 639 cm^{-1} for Gly_4; 467, 580, 602, 610, 536 cm^{-1} for Gly_5; and 467, 583, 606, 634 cm^{-1} for Gly_6. Simultaneously, the α-helix characteristic band at 365 cm^{-1} is absent. The polyglycine spectrum became very noisy in the experimental conditions that were ideal for the

oligomers. In consequence, the highest frequency value that is displayed in the spectrum is at 400 cm^{-1}, too low to observe the expected feature at 410 cm^{-1}, characteristic for β-form.

The results of protein studies are described in Chapter 6. Three different proteins, acylase, lipase and beta lactamase, have been investigated in the frequency range 0 – 350 cm^{-1}.

For each of them, the peptide chain is arranged in a α-helix structure: for beta lactamase 80 % of the total length is twisted in helical form, for lipase and acylase only 50 %. The other 50 % of the lipase and acylase chain is arranged in β-sheet structure.

The absorption pattern that is characteristic for amino acids, is smeared out in proteins: the absorption spectra of the three proteins show only a few broad features. Acylase and lipase are characterized by a large absorption band at ~200 cm^{-1}, beta lactamase by a broad peak, at 148 cm^{-1}.

This shift in frequency indicates the presence of different secondary structures: whereas for beta lactamase the maximum at 148 cm^{-1} shows the vibrations of the hydrogen bonds responsible for the stability of the helix, in acylase and lipase, the absorption maximum indicates the presence of more than one secondary structure.

Considering former assignments, the modes of acylase at 143 and 222 cm^{-1}, and those of lipase at 135 and 264 cm^{-1}, can be taken as indicators for the presence of α-helix structure. Beta lactamase has absorption maxima, at 148, 229, and 306 cm^{-1}. The first two are indicating the presence of α-helix.

At low frequencies, below 50 cm^{-1}, proteins exhibit an absorption feature that is temperature independent. In glasses, a similar feature, of unknown origin, is called boson peak. Proteins that display such a peak are considered to have a "glassy behaviour".

Two of the protein samples show a low-lying feature that could be associated with the boson peak: acylase at 25 cm^{-1} and lipase at 22 cm^{-1}. These peaks

have low intensity, and they can be distingushed only by fitting the spectra with a sum of lorentzians.
The origin of this low frequency behaviour can be tentatively explained in two ways. On one hand, it can be the boson peak, on the other hand, the feature could be connected with the secondary structure of the proteins. As lipase and acylase have 50% of their chain length in β-form, and they are the samples to disyplay such a peak, maybe there is a straightforward connection between the two facts; the peak could be either related to the hydrogen bonds the β-sheet forms, or with a specific amino acid, or with the hydration level of the proteins. However, these ideas are not supported yet by further measurements, but would make sense to follow them.

Investigations on human blood serum are presented in Chapter 7. The optical properties of human blood serum have been measured in reflection in the frequency range 50 – 650 cm^{-1}. A cuvette with silicon windows was used in this purpose. The data analysis was done using a home-made fitting software package.
Due to its high water content (> 90%), the infrared properties of blood serum do not exhibit either sharp features or strong deviations compared to water. Water has an overwhelming absorption compared with other seum components. Any effect that the far infrared radiation can have on the blood is felt by the water.

In Chapter 8 are presented the conclusions of the studies.

In Annex are gathered results from previous studies that help to complete the picture about amino acids and amino acid chains properties in far infrared.

ZUSAMMENFASSUNG

Terahertz-Strahlung, welche sich über die Frequenzspanne zwischen Mikrowellen und Infrarot erstreckt – also von ca. 0.3 – 20 THz, ist lange Zeit experimentellen Studien unzugänglich gewesen. Deshalb ist in diesem Zusammenhang auch immer noch der Begriff „THz-Lücke" geläufig.

Die vorliegende Arbeit wurde im Rahmen eines Projektes der Europäischen Gemeinschaft mit dem Titel „**T**era**h**ert**z** radiation in **B**iological **R**esearch, **I**nvestigations on **D**iagnostics and study of potential **G**enotoxic **E**ffects" (THz-Bridge) angefertigt. Dieses Projekt hatte folgende wesentlichen Zielsetzungen:

- Schließen der bestehenden Wissenslücke bezüglich des Einflusses von Terahertz-Strahlung (0.3 – 20 THz / 10 – 600 cm^{-1}) auf biologische Systeme.
- Durchführung erster Erforschungen auf europäischer Ebene, bevor Terahertz-Technologien in der biologischen und biomedizinischen Diagnostik Einzug erhalten.

Diese Doktorarbeit stellt einen Beitrag dar, in welchem die ferninfraroten spektralen Eigenschaften von Biomolekülen in einer Datenbank zusammengefasst werden. Folgende Proben wurden dabei untersucht: Aminosäuren, homopolymeres Polyglyzin, Proteine (Lipase, Acylase, beta-Lactamase) sowie menschliches Blutserum.

Das erste Kapitel umreißt die Motivation der vorliegenden Studien und steckt einen größeren Rahmen ab.

Die Doktorarbeit versucht, mehrere Fragen zu beantworten, die sich im Kontext bildgebender Verfahren basierend auf Terahertzspektroskopie-Techniken stellen:

- Wie kann eine unbekannte Substanz mittels THz-Bildgebung identifiziert werden?
- Kann das Vorhandensein einer spezifischen Aminosäure in einem Protein detektiert werden?
- Ist es möglich, eine unbekannte Substanz komplexer Struktur zu erkennen, falls die Absorptionsmuster deren einzelner Bestandteile bekannt ist?

Im Kapitel 2 „Probenpräparation" werden die vier verschiedenen Probentypen, die untersucht worden sind, detailliert beschrieben. Die Aminosäuren werden gemäß ihrer Seitenkette klassifiziert. Ebenso werden einige physiologische Aspekte der untersuchten Proben geklärt. Ein kurzer Überblick über die Polymere, d.h. Ketten von Aminosäuren, wird gegeben ausgehend von der Kondensationsreaktion. Die Eigenschaften der Proteine werden anhand ihrer sekundären Struktur (α-Helix und β-Faltblatt), der Strukturcharakteristik im Ferninfraroten und des Glasverhaltens bei niedrigen Frequenzen behandelt. Des weiteren wird das Vorkommen des sog. „Boson-Peaks" in den Spektren verschiedener Proteine besprochen. In den untersuchten flüssigen Proben absorbiert im ferninfraroten Frequenzbereich hauptsächlich der Wasseranteil, und daher wird der Einfluss von Wasser in der Transmissionsspektroskopie in Kapitel 2 näher untersucht. Der Absorptionskoeffizient von Wasser wird als Funktion der Frequenz dargestellt. Zusätzlich werden zum besseren Verständnis die dominanten Vibrationsmoden im Infrarotbereich herangezogen. Mit einer kurzen Beschreibung über die Zusammensetzung des menschlichen Bluts und Blutplasmas, welche zusammen ungefähr 55% des gesamten Blutvolumens ausmachen, endet dieses Kapitel.

Kapitel 3 gibt einerseits eine Einführung in die Theorie der Wechselwirkung zwischen Strahlung und Materie sowie andererseits eine detaillierte Beschreibung der verwendeten Messtechnik. Ausgehend vom einfachen Modell eines zweiatomigen Moleküls als gedämpfter harmonischer Oszillator

wird der Real- und Imaginärteil der komplexen dielektrischen Permittivität abgeleitet. Diese optischen Charakteristika werden benutzt, um die Spektren anzupassen und um die Absorptionseigenschaften der Proben zu berechnen. Das Anpassen eines Spektrums geschieht näherungsweise durch die Superposition mehrerer Lorentzfunktionen. Dieses Vorgehen erlaubt, die Resonanzfrequenzen der molekularen Vibrationsmoden aufzufinden. Jedem Absorptionsband wird ein Oszillator zugeordnet.

Mit dem Fouriertransformationspektrometer „Bruker IFS 113v" wurden Spektren von 10 bis 650 cm^{-1} aufgenommen. Als Strahlungsquelle diente eine Quecksilberlampe, und zwei heliumgekühlte Bolometer sind im Einsatz gewesen.

Um aufeinanderfolgende Messungen der flüssigen Proben unter reproduzierbaren experimentellen Bedingungen zu gewährleisten, wurde eine Küvette mit Siliziumfenstern und einer speziellen Befestigungsvorrichtung entworfen.

Die festen polykristallinen Proben wurden als Pulver mit Polyethylen (PET) vermischt und zu kleinen, flachen Tabletten gepresst. Das Massenverhältnis von Probe zu PET-Matrix betrug 1 zu 10 im Frequenzbereich von 50 bis 650 cm^{-1} bzw. 1 zu 4 oder 1 zu 1 in der Region von 10 bis 50 cm^{-1}. Die Transmissionsspektren wurden angepasst unter Verwendung der Software WinASF, einer Entwicklung des 1. Physikalischen Instituts der Universität Stuttgart. Die derart angepassten Spektren dienen der Bestimmung der Vibrationsmoden.

Das Absorptionsvermögen der ursprünglich zu untersuchenden Substanzen wird errechnet, indem der Beitrag der PET-Matrix vom Transmissionsverhalten der Tablette abgezogen wird.

Die Ergebnisse der Untersuchungen werden in den Kapiteln 4 bis 7 beschrieben und interpretiert.

Kapitel 4 widmet sich den Messungen der Aminosäuren. 18 verschiedene Aminosäuren wurden mittels Transmissionsspektroskopie im ferninfraroten Frequenzbereich untersucht.

Das Absorptionsvermögen (A) wurde gemäß der Beziehung A=log(1/T) bestimmt, wobei (T) für das Transmissionsvermögen steht.

Erwartungsgemäß ähneln sich die Spektren verschiedener Aminosäuren, da deren chemische Struktur viele Gemeinsamkeiten untereinander aufweist: Sie alle besitzen NH_3^+ und COO^- Endgruppen genauso wie ein CNN-„Rückgrat". Nichtsdestotrotz beschränken sich diese Gemeinsamkeiten auf einige allgemeine Merkmale. Die individuellen Eigenschaften der Aminosäuren sind jedoch hinreichend unterschiedlich, sodass deren „Signatur" eindeutig identifiziert werden kann.

Die Ergebnisse werden beginnend mit Glycin (Gly) (Fig. Z1) vorgestellt und nach steigender Komplexität, die hier mit zunehmender Molekülgröße einhergeht, geordnet.

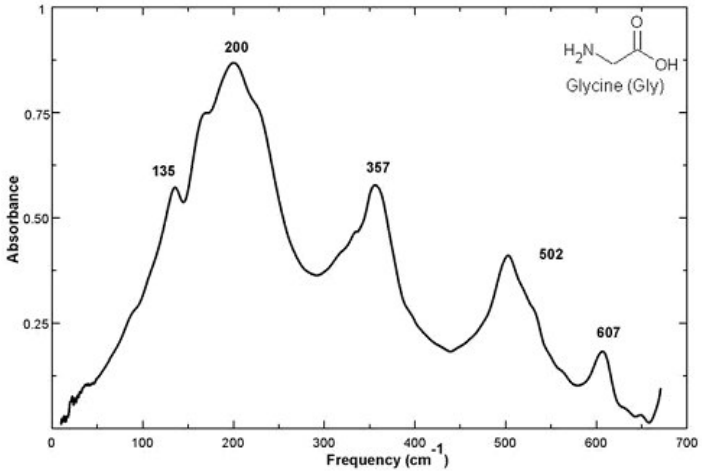

Fig. Z1. Absorptionsspektrum von Glycin.

Bei Glycin handelt es sich um die „kleinste" Aminosäure, welche auch das einfachste Spektrum aufweist. Die ausgeprägtesten Absorptionsmaxima bei Raumtemperatur, die beobachtet wurden, liegen bei 135 cm^{-1} (CC-Torsion), 200 cm^{-1} (H-Brücken Moden), 357 cm^{-1} (CCN Verbiegungen), 526 cm^{-1} (NH_3^+-Torsion) sowie 502 und 607 cm^{-1} (COO^- Moden). Die in der Literatur kontrovers diskutierte Torsionsmode bei 548 cm^{-1} konnten wir als Schulter

zweifelsfrei beobachten. Mit Abkühlung auf T=10 K tritt sie äußerst intensiv zu Tage. Von Alanin an erscheint diese NH_3^+-Mode als eigenständiges Absorptionsmaximum.. Messungen von Glycin mit verschiedenen Isotopen untermauern die Eindeutigkeit, mit der diese Absorptionsschulter der zuvor genannten NH_3^+-Mode zugeordnet werden kann.

Die Seitenkette beeinflusst maßgeblich die Gestalt des Spektrums. In diesem Kontext werden die Unterschiede für verschiedene Paare von Aminosäuren herausgearbeitet. Folgende Paare werden betrachtet: Glycin und Alanin, Alanin und Phenylalanin (Phe), Tyrosin (Tyr) und Phenylalanin, Isoleucin und Leucin, Valin und Isoleucin, Glutaminsäure und Asparaginsäure, Glutamin und Asparagin. Bereits das Vibrationsspektrum für Alanin besitzt im Vergleich zu Glycin mehr Strukturen. Ebenso erkennt man, dass im Absorptionsspektrum von Alanin die COO^- Moden zu höheren Frequenzen hin verschoben sind. Des weiteren liegt bei Alanin das Maximum der NH_3^+-Torsionsmode bei 486 cm^{-1} und ist im Gegensatz zu Glycin sehr ausgeprägt. Vier Absorptionsmaxima mittlerer bis starker Intensität werden im Alaninspektrum zwischen 278 cm^{-1} und 409 cm^{-1} vorgefunden. Diese sind alle auf die $CC^{\alpha}N$-Verformung und CH_3-Torsion zurückzuführen. Im Glycinspektrum findet man nur ein einziges entsprechendes Absorptionsmaximum bei 357 cm^{-1}. Die Schulter, die im Falle von Glycin bei 233 cm^{-1} zu erkennen ist, ist im Alaninspektrum nicht auflösbar. Stattdessen erscheint ein Maximum bei 216 cm^{-1}, welches als Torsions-Mode der COO^- Gruppe verstanden werden kann. Ein weiteres Maximum im Alaninspektrum bei 258 cm^{-1} wird gleichermaßen durch eine Verwindungsmode der COO^- Gruppe verursacht.

Ausgehend von den bekannten Zuordnungen der Bänder für Glycin und Alanin kann man nun diese Bänder in den Spektren anderer Aminosäuren identifizieren, ohne auf Berechnungen der Normalmoden angewiesen zu sein.

Phenylalanin geht aus Alanin hervor, indem ein Wasserstoffatom durch eine Phenylgruppe ersetzt wird. Diese Ersetzung führt zu Veränderungen in der

Gestalt des Spektrums. Obwohl das Phenylalanin-Molekül mit seinem Phenol-Ring schwerer ist, zeigt Alanin das reichhaltigere Spektrum. Phenylalanin besitzt nur vier Maxima jenseits von 200 cm^{-1}, welche in einer Art und Weise über den Frequenzraum verteilt sind, die an das Spektrum von Glycin erinnert. Die CCN Mode in der Nähe von 350 cm^{-1} ist sowohl für Phe als auch für Gly vorhanden. Beide Proben zeigen darüber hinaus ein starkes Absorptionsmaximum in der Region um 200 cm^{-1}.

Hängt man an den Phenolring von Phenylalanin eine OH-Gruppe an, so erhält man Tyrosin. Der strukturelle Unterschied zwischen diesen beiden Aminosäuren fällt also klein aus, ganz im Gegensatz zu den Differenzen im Vibrationsspektrum. Augenfällig weicht das Phe-Spektrum von demjenigen von Tyr bei 248 cm^{-1} ab: Tyr besitzt hier ein starkes Absorptionsmaximum, während das Phe-Spektrum ein Minimum durchläuft.

Entsprechend der Literatur sollte der Benzolring im Spektrum prävalent sein. Die Experimente können dies jedoch nicht bestätigen. Es gibt keine plausible Erklärung, warum die meisten Linien auf den Benzolring zurückzuführen sein sollten. Phe zeigt ein markantes Absorptionsmaximum bei ungefähr 365 cm^{-1}, welches in Tyr dreifach für 310, 335 und 377 cm^{-1} vorhanden ist. Phenylalanin und Tyrosin haben einen gemeinsamen Absorptionsscheitelpunkt – eine Benzol-Mode - in der Nähe von 525 cm^{-1}: für Phe bei 525 cm^{-1} und für Tyr leicht verschoben bei 529 cm^{-1}. Dieser Scheitelpunkt ist möglicherweise auch durch COO^- Moden beeinflusst, darunter Biegungs-, Kipp- sowie Wagging-Mode, welche in vielen Aminosäuren wie z.B. Alanin vorkommen.

Leucin und Isoleucin besitzen vier Methylgruppen in ihrer Seitenkette und sind isometrisch zueinander. Ihre Spektren gleichen sich, jedoch nicht in dem Maße, in welchem sich die Spektren von Isoleucin und Valin einander ähneln. Valin entspricht Isoleucin, besitzt aber einer CH_3-Gruppe weniger. Die CH_3-Gruppe verhält sich wie ein schweres Atom, welches das Valinspektrum kaum beeinflusst. Die Positionen der Absorptionsmaxima bei tieferen Frequenzen (<100 cm^{-1}) für Valin und Isoleucin sind nahezu identisch. Gleiches gilt auch für die Positionen der Scheitelwerte der beiden Spektren

zwischen 100 und 500 cm^{-1}. Die Absorptionsbänder Isoleucins sind im Vergleich zu Leucin geringfügig zu höheren Frequenzen hin verschoben; unterhalb von 300 cm^{-1} ist diese Versetzung ausgeprägter. Die NH_3^+ Torsionsmode ist im Spektrum von Leucin nicht auszumachen, hingegen erscheint sie sehr deutlich im Spektrum von Isoleucin bei 490 cm^{-1}.

Zwischen 270 und 380 cm^{-1} sind die meisten sichtbaren Vibrationen auf CCN Deformationen zurückzuführen. Die NH_3^+-Moden erscheinen im Intervall von 380 bis 480 cm^{-1} und die COO^--Moden für Frequenzen sowohl oberhalb von 480 cm^{-1} als auch von 220 bis 300 cm^{-1}.

Nach Betrachtung aller aufgenommenen Spektren sind nachstehende Folgerungen bezüglich der den Aminosäuren gemeinsamen Absorptionsbänder möglich (Fig. Z2). Die Vibrationsmoden können in vier Kategorien eingeteilt werden, die in allen Aminosäuren vorkommen: die Wasserstoffbindungs-, die CCN-, die NH_3^+- und die COO^- Moden. Die Region unterhalb 200 cm^{-1} ist im wesentlichen von den Wasserstoffbindungsmoden dominiert.

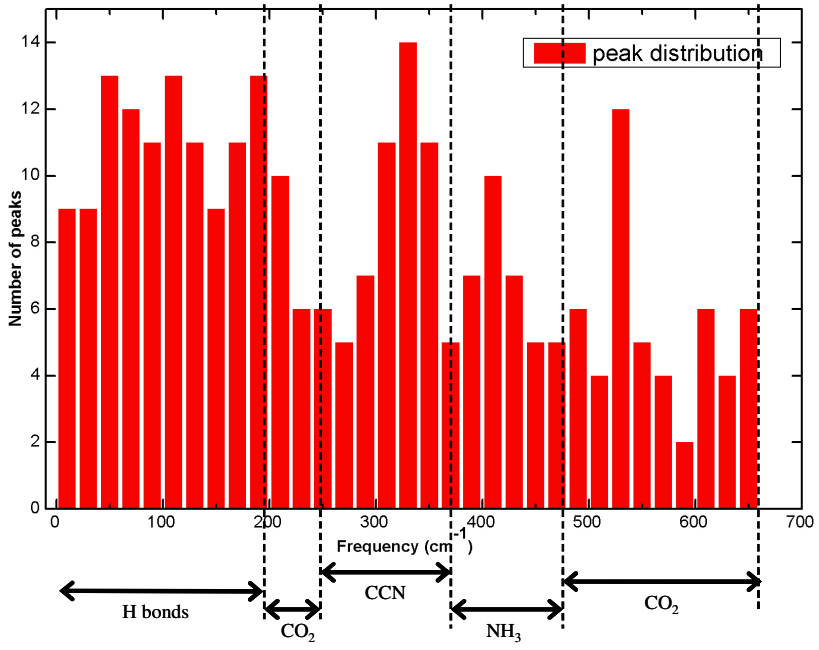

Fig. Z2. Verteilung der Absorptionsmaxima von Aminosäuren.

Andere Vibrationen kommen hier allerdings auch vor: Gitterschwingungen, Rückgratverformungen und Vibrationen der Endgruppen NH_3 und COO^-. Aminosäuren besitzen im Ferninfraroten so viele Gemeinsamkeiten, dass man sie als eigene Molekülklasse auffassen kann, in welcher dennoch jedes Mitglied individuelle Merkmale besitzt. Die Individualität liegt in der Position der Absorptionsmaxima - jede Aminosäure besitzt ihr charakteristisches Absorptionsmuster – und in deren Intensität. Wie später gezeigt wird, verschmiert dieses Absorptionsmuster bei Oligomeren und Proteinen.

In Kapitel 5 werden die ferninfraroten Spektren der Oligomere des Glycins (bis zu hexameren Molekülketten), dasjenige von Polyglycin selbst und in gleicher Weise diejenigen von Alanylglycin und von Glycylleucin präsentiert.

Die Untersuchungen an Glycin folgen der Evolution der Spektren von der monomeren über die hexamere Anordnung bis hin zum Polypeptid. Mit dem Fortschreiten zu längeren Gly Oligomeren geht gleichzeitig auch der zunehmende Verlust kristalliner Strukturen einher, ein Verbreitern der Absorptionslinien und eine Verschiebung der Absorptionsmaxima zu tieferen Frequenzen hin. Dies wird anhand des Spektrums von Polyglycin beispielhaft erläutert: Im Frequenzintervall von 10 bis 400 cm^{-1} gibt es einzig drei spektrale Merkmale. Das Spektrum eines Peptids verbreitert sich in gleicher Weise wie das Spektrum von Wasser. Einzelne Aminosäuren können im Spektrum eines Peptids nicht erkannt werden. Im Fall von Alanylglycin und Glycylleucin kann das Spektrum weiterhin in vier Regionen eingeteilt werden, wie es im vorangehenden Kapitel für Aminosäuren diskutiert worden ist. Dennoch können deren Merkmale (die von Alanylglycin und Glycylleucin) nicht als Summe der Eigenschaften der einzelnen, sie aufbauenden Aminosäuren verstanden werden. Vielmehr sind sie als eigenständige Proben aufzufassen.

Zwischen 10 und 650 cm^{-1} zeigen die Spektren von Oligomeren und Peptiden intra- und intermolekulare Moden. Unter diesen Moden befinden sich Torsionen um die Bindungen zwischen den Kettengliedern, Verbiegungen der Kette, Vibrationen der Endgruppen und Verformungen der

zwischenmolekularen Bindungen (Wasserstoffbrückenbindungen und Bindungen basierend auf Wechselwirkungen zwischen den Seitengruppen). Die Gitterschwingungen werden unterhalb von 200 cm^{-1} sichtbar.

Da die Frequenz der Verwindungsmoden von der Konformation der Molekülkette abhängt, kann man das Spektrum als Indikator diesbezüglich verwenden. So erkennt man zum Beispiel, dass das Glycinoligomer Gly_3 die β-Form einnimmt. Diese Feststellung basiert auf dem Vorkommen von vier verschiedenen Bändern, die aus der Literatur bekannt sind und durch die vorliegenden Studien bestätigt werden. Diese Absorptionsbänder befinden sich für Gly3 bei 466, 572, 606 und 648 cm^{-1}, für Gly4 bei 468, 578, 605 und 639 cm^{-1}, für Gly5 bei 467, 580, 602, 610 und 636 cm^{-1} sowie für Gly6 bei 467, 583, 606 und 634 cm^{-1}. Gleichzeitig kann das für die α-Helix charakteristische Absorptionsband um 365 cm^{-1} nicht aufgefunden werden. Das Polyglycinspektrum war unter den experimentellen Rahmenbedingungen, die sich als ideal für die Oligomere erwiesen hatten, sehr verrauscht. Deshalb wird das Spektrum nur bis zu einer Maximalfrequenz von 400 cm^{-1} abgebildet und ist somit ungeeignet, das für die β-Form charakteristische Absorptionsband bei 410 cm^{-1} aufzuzeigen.

Die Ergebnisse der untersuchten Proteine werden in Kapitel 6 beschrieben. Acylase, Lipase und beta-Lactamase sind für Frequenzen zwischen 10 und 350 cm^{-1} beobachtet worden.

In allen drei Fällen liegt die Peptidkette in der α-Helix Struktur vor: 80 % der Gesamtlänge von beta-Lactamase ist spiralförmig verdreht. Bei Lipase und Acylase sind es nur 50 %, und die restlichen 50 % der Kette besitzen die β-Faltblattstruktur.

Das Absorptionsmuster der Proteine "zerfließt" im Vergleich zu dem der Aminosäuren, und deren zugrundeliegenden Konturen sind nur noch schwer zu erkennen: Die Absorptionsspektren der drei untersuchten Proteine zeigen nur einige großstrukturierte Merkmale. Die Spektren von Acylase und Lipase zeichnen sich durch ein breites Absorptionsband aus, welches um den Wert

von 200 cm^{-1} zentriert liegt, das Absorptionsband von beta-Lactamase besitzt sein Zentrum bei 148 cm^{-1}.

Diese Frequenzverschiebung deutet auf unterschiedliche sekundäre Strukturen hin: Während das Absorptionsmaximum von beta-Lactamase bei 148 cm^{-1} ein Indiz für die Vibrationen der Wasserstoffbrückenbindungen ist, die für die Stabilität der α-Helix verantwortlich sind, weist das Absorptionsmaximum von Acylase und Lipase darauf hin, dass mehr als nur eine einzige sekundäre Struktur vorhanden ist. Unter Berücksichtigung der Ergebnisse früherer Arbeiten können die Moden von Acylase bei 143 und 222 cm^{-1} und diejenigen für Lipase bei 135 und 264 cm^{-1} als Indikatoren für das Vorhandensein der α-Helix-Struktur angesehen werden. Die Absorptionsmaxima von beta-Lactamase liegen bei 148, 229 und 306 cm^{-1}, wobei die ersten beiden für die α-Helix-Struktur sprechen.

Für tiefe Frequenzen unterhalb von 50 cm^{-1} zeigen Proteine ein Absorptionsmerkmal, welches temperaturunabhängig ist. Gläser zeigen ein ähnliches Merkmal unbekannten Ursprungs, welches „Boson-peak" genannt wird. Ähnliche Eigenschaften werden auch in Polymeren beobachtet. Proteinen, deren Spektren ein solches Absorptionsmerkmal aufweisen, wird in diesem Zusammenhang ein glasartiges Verhalten zugesprochen.

Zwei der Proteinproben zeigen ein tieffrequentes Merkmal, welches mit dem „Boson-Peak" assoziiert werden könnte: Acylase bei 25 cm^{-1} und Lipase bei 22 cm^{-1}. Diese Maxima sind schwach ausgeprägt und können nur durch Anpassung der Spektren mit mehreren überlagerten Lorentzkurven aufgefunden werden.

Der Ursprung dieses niederfrequenten Verhaltens kann in zweierlei Weise verstanden werden. Auf der einen Seite könnte es sich tatsächlich um den „Boson-Peak" handeln; auf der anderen Seite könnte dieses Merkmal auch mit der sekundären Struktur des Proteins zusammenhängen. Da Lipase und Acylase die Proteine sind, die zu 50 % β-gefaltet sind und bei denen dieses tieffrequente Absorptionsmaximum auftritt, liegt es nahe zu vermuten, dass eine direkte kausale Verknüpfung zwischen diesen beiden Tatsachen existiert;

die Absorptionslinie könnte entweder auf die Wasserstoffbrückenbindungen, die die β-Faltblattform bilden, oder auf eine spezifische Aminosäure oder auf den Hydratationsgrad der Proteine zurückzuführen sein. Zum jetzigen Zeitpunkt gibt es jedoch keine weiterführenden Messungen, die eine dieser Ideen bevorzugen würde. Es wäre jedoch allemal lohnenswert, hier die Forschungen fortzusetzen.

Die Untersuchungen an menschlichem Blutserum werden in Kapitel 7 vorgestellt. Die optischen Eigenschaften menschlichen Blutserums wurden reflektionsspektroskopisch für Frequenzen zwischen 50 und 650 cm^{-1} gemessen. Für diese Belange wurde eine Küvette mit Siliziumfenster benutzt. Die Datenanalyse wurde unter Verwendung der am Institut entwickelten Software WinASF vorgenommen.

Aufgrund des hohen Wasseranteils der Proben (> 90 %) sind die Infraroteigenschaften des Blutserums nur schwer von denen reinen Wassers zu unterscheiden. Wasser besitzt ein Absorptionsverhalten, welches das der Bestandteile des Serums weit übersteigt. Jeglicher Effekt, welcher die ferninfrarote Strahlung auf das Blut hat, wird durch den Wasseranteil vermittelt.

Kapitel 8 liefert die Schlussfolgerungen der Untersuchungen.

Im Anhang werden die Ergebnisse vorangegangener Studien zusammengefasst und hinzugezogen, um das Bild der Aminosäuren und der Aminosäurenketten im Ferninfraroten zu vervollständigen.

Chapter 1

INTRODUCTION

Terahertz radiation (1 THz = 10^{12} Hz) that spans the frequency range between microwave and infrared, from ~0.3 THz to 20 THz was for long time inaccessible for study. The reason is that it lies beyond the normal range of electronic and optical measurement techniques that are used in microwave or in infrared regions. Due to the facts, the frequency region was referred as the "THz-gap" (Fig. 1).

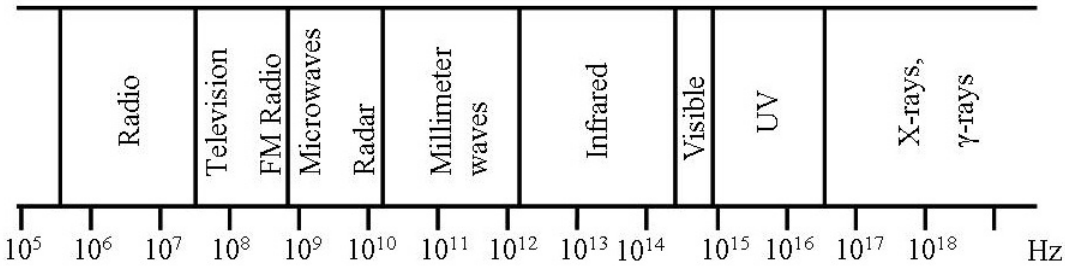

Fig. 1. Electromagnetic spectrum.
The terahertz gap lies between ~300 GHz (0.3 THz) and 20 THz.

Only recently, it has become scientifically available, with the development of broadband sources of moderate intensity. Nowadays, wave-guides for terahertz rays are still improved **[Wan2004]**.

In the last years, terahertz radiation started to be considered attractive for different applications. One of the most important applications for terahertz radiation is imaging, which evolved as a possible non-invasive investigation method for medicine **[Hu1995]**, as well as for security **[Zon2003]**. Terahertz rays are able to peer through clothing and reveal concealed weapons and explosives. Imaging with THz could be useful in detecting structural defects

in materials as well as skin cancer **[Woo2003]**. Also wireless telecommunication systems, which presently extend in frequency up to 30 GHz, are gradually approaching the THz region from the low-frequency side, with an increasing demand of high frequency domains.

However, for these applications there are no check studies that investigate the negative effects THz region could induce in living matter. The region 6 – 120 THz is dominated by the normal vibrational modes of small molecules. Lattice modes and acoustic modes extend the low frequency end of the range down to ~0.3 THz **[Bow1989]**.

Different projects tried to assess the damaging potential of the THz radiation for the living tissues. The present work was performed in the frame of the EU project "Terahertz radiation in Biological Research, Investigations on Diagnostics and study of potential Genotoxic Effects". The main purpose of this project was to bridge the existing gap of knowledge regarding the effects of Terahertz radiation on biological systems. The work was meant as the first research step of European dimension before implementing THz technology in biological and biomedical diagnostics.

This thesis tries to answer several questions arising in the context of imaging:

(1) How can an unknown substance be identified by means of THz imaging?

(2) Can one identify the presence of a specific amino acid in a protein by means of infrared spectroscopy?

(3) Is it possible to identify an unknown substance when one knows the absorption pattern of its basic components?

The present study provides the far infrared absorption spectra of samples of relevant biological importance. These are presented in the order of increasing complexity: the standard amino acids, oligopeptides, amino acid chains, proteins (beta-lactamase, acylase, and lipase), and human blood serum. Samples were presented in crystalline state (amino acids, peptides, proteins) and liquid state (water, human blood serum). Spectra were recorded in transmission (amino acids, oligopeptides, amino acid chains, proteins) or in reflection (human blood serum).

Chapter 2

SAMPLES

2.1 Amino Acids - Molecular Crystals

Crystalline solids are classified as ionic, covalent, metallic, and molecular crystals. Amino acids are an example of molecular crystals.

They represent a class of molecules of crucial importance for life processes. Stand-alone amino acids are not typical for living bodies. More often, they are found in proteins. If an organism is irradiated by infrared light, it is highly probable that some of its proteins will feel the effect. In order to decide which this effect is, we considered investigating firstly the amino acids behaviour in far infrared. The next step is to observe the proteins under the same conditions.

Infrared spectroscopy of molecular crystals reveals absorption bands in the low frequency region that are due to the vibrations of the lattice and to intramolecular vibrations. These vibrations are small translational and rotational motions of the molecules about their equilibrium positions; they are called external modes, in contrast to the internal modes, which are intramolecular vibrations. Usually the internal and external vibrations are decoupled of each other and separated in frequency. Combinations of internal and lattice modes can appear as multiphonon bands. Multiphonon absorption occurs when two or more phonons interact and produce an electric moment to which the incident radiation may couple. In Figure. 2.1 are presented the typical group frequencies that are visible in infrared. The figure will be later completed with the results of our experiments.

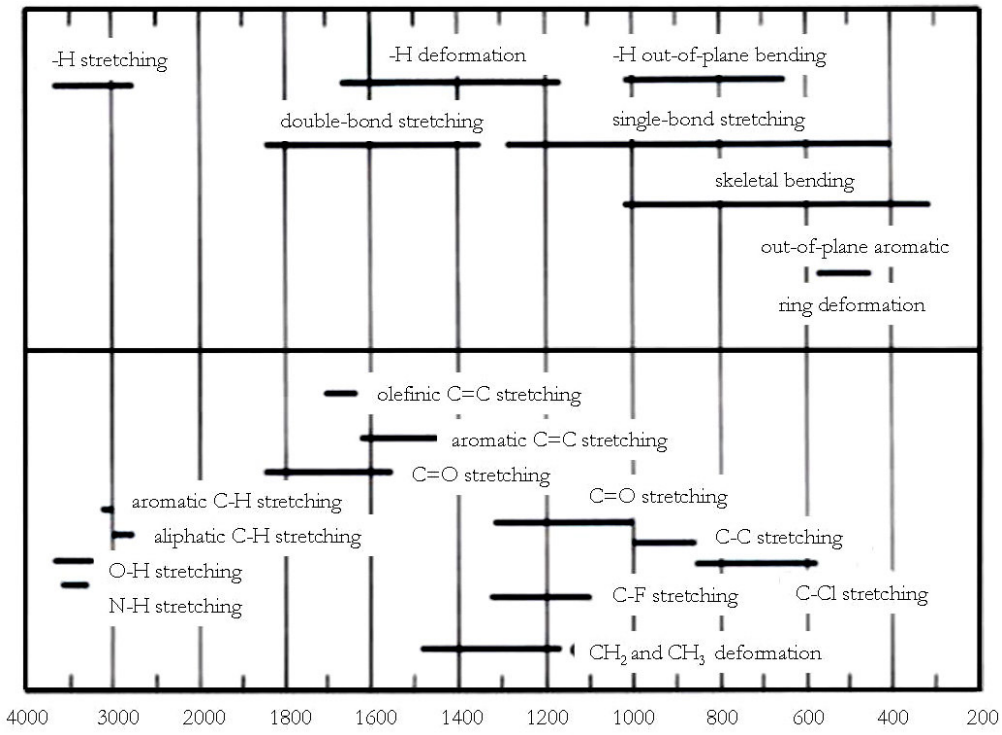

Fig. 2.1 Group frequencies **[Bow1989]**. The upper part of the diagram shows the frequency region where some general categories of vibration may be observed. The lower part indicates more specific examples of these general types.

In amino acids, multiphonon absorptions can be observed below 200 cm^{-1}. As it is reported in **[Sus1983]**, at low frequency the internal modes couple with intermolecular vibrations, in particular for serine where the vibrations of the OH•••O hydrogen bonds occur in the same frequency region as low frequency intermolecular modes.

All proteins are polymers of the 20 standard amino acids. Naturally occurring proteins contain only L-amino acids (Fig. 2.1) that rotate the plane of plane-polarized light counterclockwise.

Except of proline, amino acids have a primary amino group ($-NH_2$) and a carboxilic acid group (-COOH) substitutent on the same carbon atom (C^{α}). The third substitution on the α-carbon is an atom of hydrogen. Proline has a secondary amino group (-NH).

What makes the amino acids distinct from each other is the radical group attached to the same α-carbon.

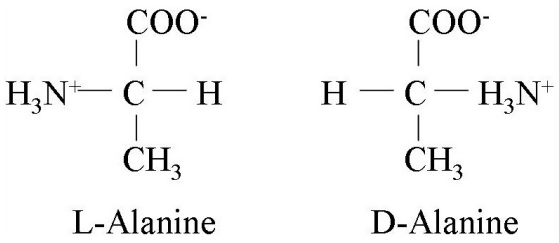

Fig. 2.1 The two enantiomers of alanine. They are mirror image of each other.

The radical group (the side chain of an amino acid) is responsible for the biochemical properties of the protein. The side chain can be:

- Nonpolar (hydrophobic): Gly, Ala, Phe, Pro, Trp, Val, Leu, Ile, Met (Fig. 2.2);
- Polar (hydrophilic): Ser, Cys, Thr, Tyr, Gln, Asn (Fig. 2.4);
- Negatively charged: Asp, Glu (Fig. 2.3);
- Positively charged: Arg, His, Lys (Fig. 2.5).

These side chains stick out from the backbone of the molecule, and help determine the properties of the proteins that they form. In the crystal, the amino acid molecules is zwitterionic and the nytrogen atom participates in intermolecular hydrogen bonds of different strength **[Sim1966]**, **[Des1988]**, **[Leh1972]**.

Polar side chains tend to be present on the surface of a protein where they can interact with the aqueous environment from the cells. The nonpolar amino acids reside mainly within the centre of the protein where they can interact with similar nonpolar neighbours. This can be the case of enzymes, where a hydrophobic region is created within the molecule, and chemical reactions undergo in a nonpolar medium. Amino acids have different physiological functions.

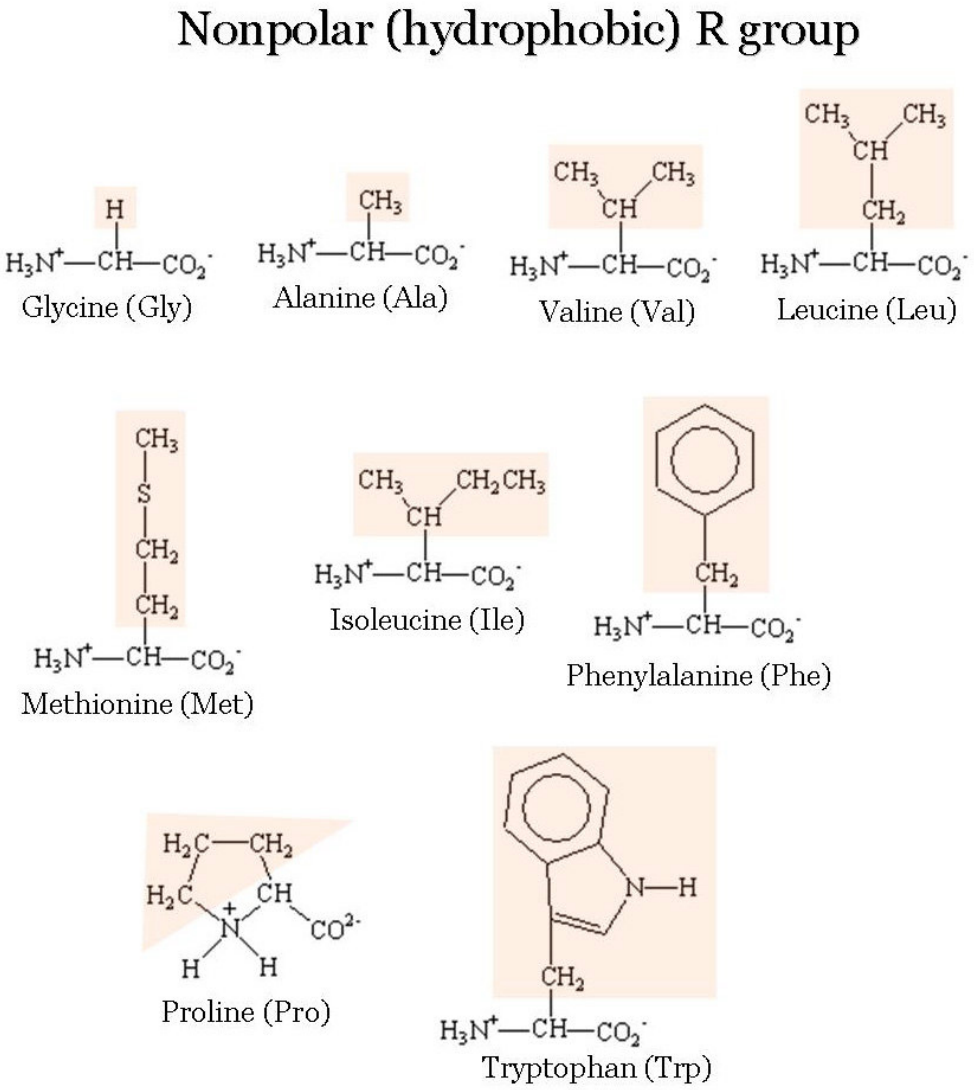

Fig. 2.2 Amino acids with nonpolar R group.

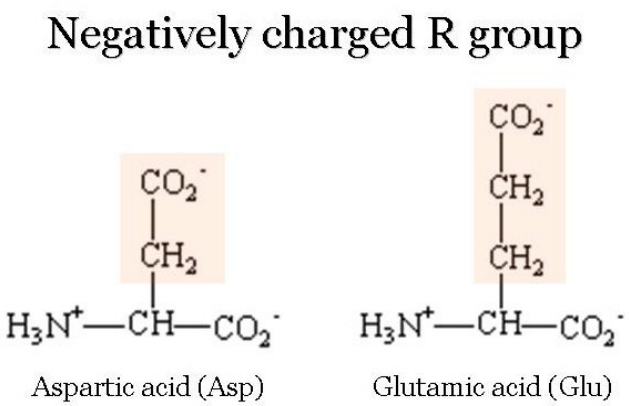

Fig. 2.3 Amino acids with negatively charged R group.

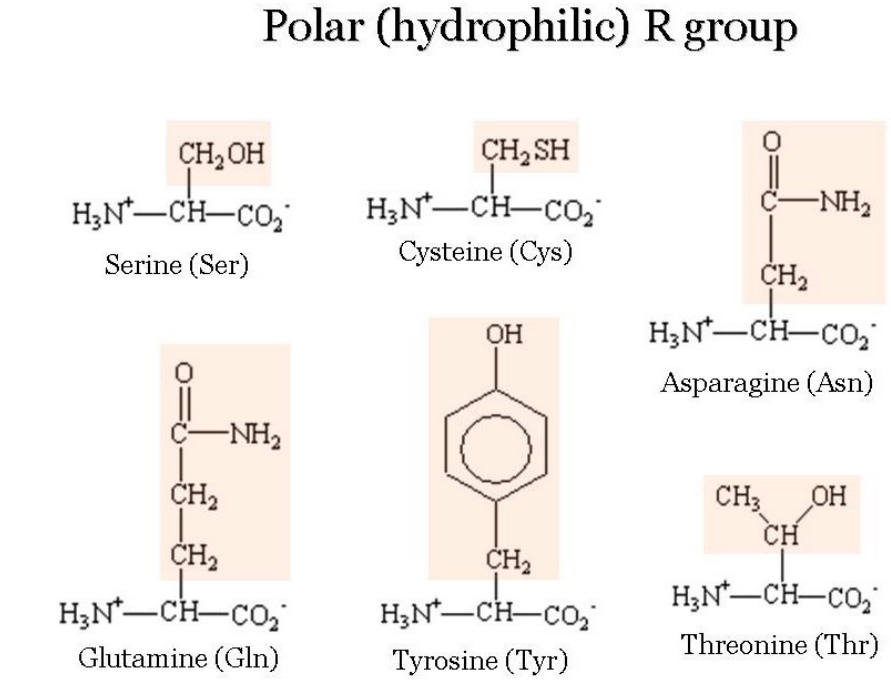

Fig. 2.4 Amino acids with polar R group.

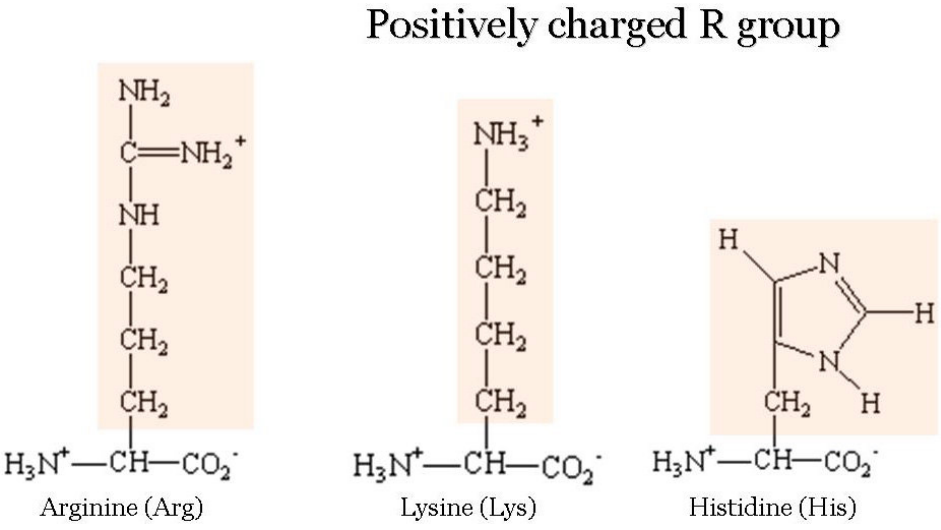

Fig. 2.5 Amino acids with positively charged R group.

Glycine (Gly - G) (Fig. 2.6) is the simplest amino acid and the only one that has no stereoisomer. It is important for the biosynthesis of nucleic acids, ATP, proteins, peptides, purines, haemoglobin, glucose, glycogen, and for other amino acids. Except collagen, which is about one-third glycine, most proteins contain only small quantities of glycine. Glycine is also a neurotransmitter in the central nervous system

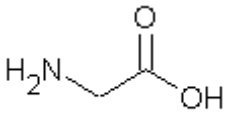

Glycine (Gly)
Fig. 2.6

Alanine (Ala – A) (Fig. 2.7), the most used amino acid in proteins, is an important source of energy for brain and central nervous system as well as for muscle tissue.

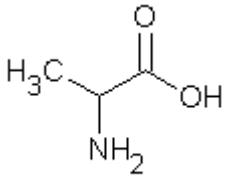

Alanine (Ala)
Fig. 2.7

L-valine (Val – V) (Fig. 2.8) is a branched-chain essential amino acid with stimulant activity: It promotes muscle growth and tissue repair. The lack of L-valine may influence the growth of body, and cause anemia.

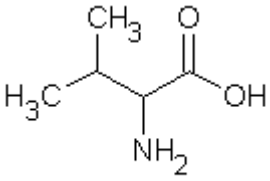

Valine (Val)
Fig. 2.8

L-leucine (Leu – L) (Fig. 2.9) is a branched-chain amino acid important for hemoglobin formation.

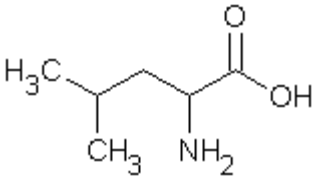

Leucine (Leu)
Fig. 2.9

L-isoleucine (Ile – I) (Fig. 2.10), an isomer of leucine, is a branched-chain aliphatic amino acid found in many proteins. It is important in haemoglobin synthesis.

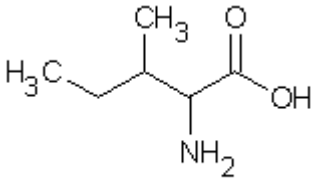

Isoleucine (Ile)
Fig. 2.10

The three branched-chain amino acids

valine, leucine, and isoleucine enhance energy, increase endurance, and aid in muscle tissue recovery and repair. This group can also lower elevated blood sugar levels and increase growth hormone production.

L-serine (Ser – S) (Fig. 2.11) is a constituent of brain proteins. It is also important in metabolism of purines and pyrimidines. In skin creams serine is used as natural moisturizer.

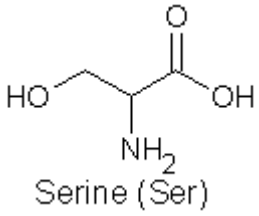

Serine (Ser)
Fig. 2.11

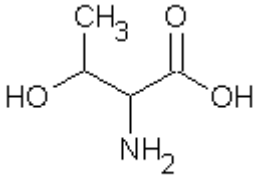

Threonine (Thr)
Fig. 2.12

L-threonine (Thr – T) (Fig. 2.12) has a function in the formation of collagen, elastin, and tooth enamel.

L-cysteine (Cys – C) (Fig. 2.13) is a sulphur-containing non-essential amino acid that aids the collagen production.

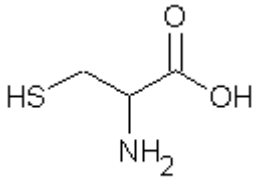

Cysteine (Cys)
Fig. 2.13

L-methionine (Met – M) (Fig. 2.14) is one of the sulphur-containing protein amino acid. It is important for many bodily functions: it helps prevent problems of the skin and nails, it acts as a lipotropic agent to prevent excess fat build-up in the liver and the body, and may be useful in some cases of allergy because it reduces histamine release.

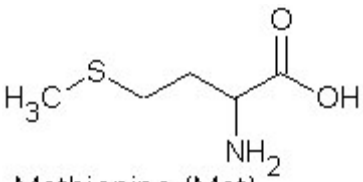

Methionine (Met)
Fig. 2.14

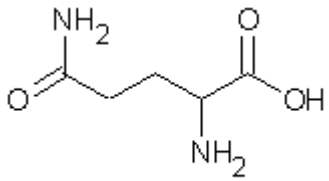

Glutamine (Gln)
Fig. 2.15

L-glutamine (Gln – Q) (Fig. 2.15) is classified as non-essential amino acid but it becomes essential in conditions of stress,

when the body cannot produce it anymore. It can be found in all types of proteins.

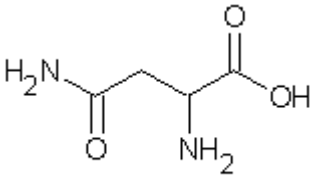

Fig. 2.16

L-asparagine (Asn – N) (Fig. 2.16) is involved in the metabolic control of cell functions in nerve and brain tissue.

L-aspartic acid (Asp – D) (Fig. 2.17) is alanine with one of the β hydrogen atoms replaced by a carboxylic acid group. It is found in animals and plants (especially in sugar cane and sugar beets). Together with **L-glutamic acid (Glu – E)** (Fig. 2.18) play important roles in enzyme active centres and in maintaining the solubility and ionic character of proteins.

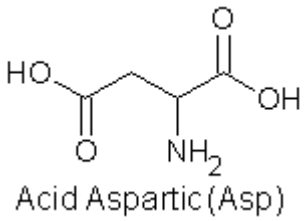

Fig. 2.17

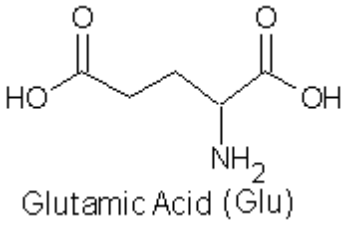

Fig. 2.18

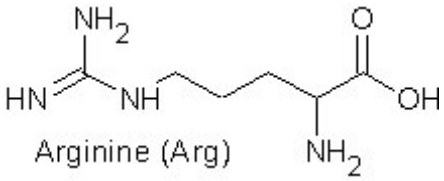

Fig. 2.19

L-arginine (Arg – R) (Fig. 2.19) acts as a growth hormone stimulant.

L-lysine (Lys – K) (Fig. 2.20) helps in calcium absorption in bones.

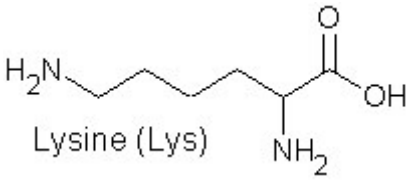

Fig. 2.20

L-histidine (His – H) (Fig. 2.21) is involved in metabolic processes involving blood cell production (it is present in haemoglobin), in the production of histamine, which is involved in

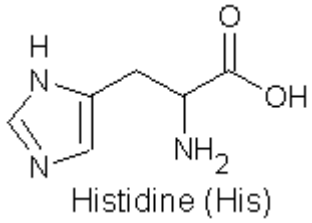

Fig. 2.21

many allergic and inflammatory reactions, and in tissue formation or repair.

L-phenylalanine (Phe – F) (Fig. 2.22) is a protein amino acid, which is also used by the body to build neurotransmitters norepinephrine, epinephrine, dopamine, and tyramine.

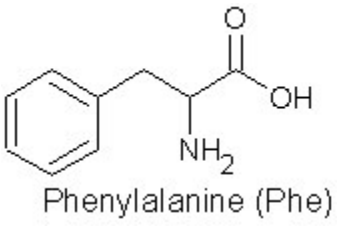

Phenylalanine (Phe)
Fig. 2.22

L-tryptophan (Trp - W) (Fig. 2.23) is essential to the human body for the production of neurotransmitter serotonin.

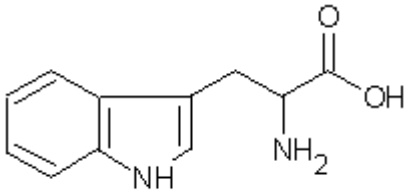

Tryptophan (Trp)
Fig. 2.23

L-tyrosine (Tyr – Y) (Fig. 2.24) combines with iodine within the thyroid gland to form the thyroid hormone thyroxin. Thyroxin has many important functions in the body: controls the metabolic rate, promotes growth, and is involved in carbohydrate and fat metabolism.

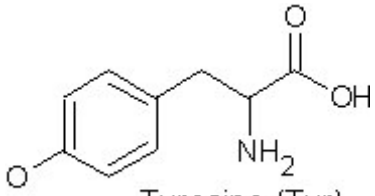

Tyrosine (Tyr)
Fig. 2.24

L-proline (Pro – P) (Fig. 2.25) is one of the main amino acids found in collagen.

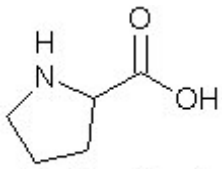

Proline (Pro)
Fig. 2.25

Some of the above presented amino acids can not be synthesized in the body. They are known as essential amino acids and they have to be supplied as part of the diet. These are: tryptophan, lysine, methionine, phenylalanine, threonine, valine, leucine and, isoleucine.

The vibrational properties of amino acids have been studied for a long time. In 1935, Heintz performed the first representative investigation of the far-

infrared absorption of some[2] amino acids **[Hei1935]**. As soon as it was noticed the potential of the infrared spectroscopy in studies of molecular structure, new reports followed: in 1939 N. Wright published "The infrared absorption spectra of amino acids" **[Wri1939]** where is presented, among other samples, the glycine spectrum in the range 400-3000 cm^{-1} [(3)].

Since that time much attention was devoted to the FIR spectra of smallest of the amino acids, glycine **[Tsu1958]**, **[Suz1963]**, **[Mac1977]**, **[Has1983]**, **[Gen1983]**, **[Wri1939]**, **[Dov1998]**, and alanine **[Gen1983]**, **[Wri1939]**,

Amino acid	Chemical formula	Number of vibrations (3N-6)	Space group/ Reference
α-Glycine	$C_2H_5NO_2$	24	$P2_1/n$ **[Alb1939]**
L-Alanine	$C_3H_7NO_2$	33	$P2_12_12_1$ **[Sim1966]**
L-Leucine	$C_6H_{13}NO_2$	60	$P2_1$ **[Kha1970]**
L-Isoleucine	$C_6H_{13}NO_2$	60	$P2_1$ **[Tor1971]**
L-Asparagine	$C_4H_8N_2O_3$	48	$P2_12_12_1$ **[Ver1972]**
L-Glutamine	$C_5H_{10}N_2O_3$	54	$P2_12_12_1$ **[Coc1952]**
L-Aspartic acid	$C_4H_7NO_4$	42	$P2_1$ **[Der1968]**
L-Glutamic acid	$C_5H_9NO_4$	51	$P2_12_12_1$ **[Hir1955]**
L-Tyrosine	$C_9H_{11}NO_3$	66	$P2_12_12_1$ **[Bog1971]**
L-Tryptophan	$C_{11}H_{12}N_2O_2$	75	Pmmm **[Kha1969]**
L-Histidine	$C_6H_9N_3O_2$	54	$P2_1$ **[Mad1972]**
L-Phenylalanine	$C_9H_{11}NO_2$	63	$P222_1$ **[Kha1985]**
L-Methionine	$C_5H_{11}NO_2S$	54	$P2_1$ **[Kha1970]**
L-Threonine	$C_4H_9NO_3$	45	$P2_12_12_1$ **[Sil1998]**
L-Serine	$C_3H_7NO_3$	36	$P2_12_12_1$ **[Kis1974]**
L-Proline	$C_5H_9NO_2$	45	$P2_12_12_1$ **[Wri1949]**
L-Lysine	$C_6H_{14}N_2O_2$	66	unknown
L-Valine	$C_5H_{11}NO_2$	51	$P2_1$ **[Tor1971II]**
L-Arginine	$C_6H_{14}N_4O_2$	72	unknown
L-Cysteine	$C_3H_7NO_2S$	36	$P2_1$ **[Har1968]**

Table 2.1. List of amino acids with their chemical formulas and the number of molecular vibrations according to 3N-6. In the last column the space group symmetries of the amino acids crystals are listed according to the literature.

[2] D-L-alanine, L-cystine, L-leucine, L-glutamic acid, D-arginine (carbonate), D-L-proline, phenylalanine, tyrosine, L-histidine (monochlorhydrate)

[3] [Wri1939] in Annex amino acids, tables 1&2, page 1

[Fuk1959], **[Suz1959]**, **[Ban1983]**, **[Mac1978]**, while for other amino acids measurements of low-frequency vibrations have been reported only sporadically **[Dov1998]**.

Nevertheless, the information about them remains incomplete: unlike mid-infrared studies (see for instance **[Bar2000]**), there are still gaps in the far-infrared (FIR) characterization of amino acids.

In this thesis is presenting the absorbance spectra of 18 amino acids[4] (Table 2.1) in the frequency range between 10 and 650 cm^{-1} and is discussing the features they have in common.

2.2. Polymers

Two or more amino acids can link together through a condensation reaction forming a peptide (Fig. 2.26). Peptides consist of only a few amino acids. Some antibiotics, hormones, neurotransmitters, and antitumor agents are peptides.

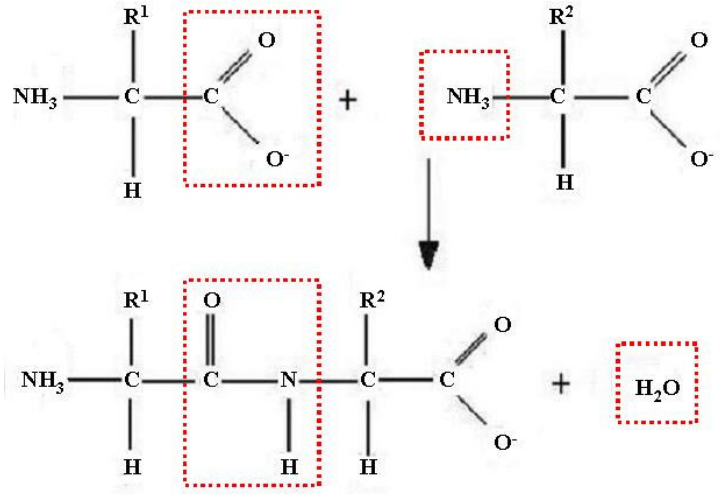

Fig. 2.26 Condensation of glycine to glycyl-glycine.

[4] without arginine and cysteine

Polymers are a class of macromolecules, which consist, approximately, of a set of regularly repeated identical chemical units. As a polymer molecule may contain thousands of atoms that involve 3N-6 normal modes of vibration, its infrared spectrum is expected to be very complicated.

Surprisingly, for most polymers the absorption spectrum looks rather simple. The complexity of the spectrum is reduced not only by the selection rules. The basic reason is that for a homopolymer the molecule consists of chemically identical units, each of them having tens of atoms or even less. In this way, many normal vibrations have almost the same frequency. Each repeating unit has a different local environment, which implies a broadening of the absorption coming from group vibrations. This is particularly true for the vibrations that involve the side-group atoms.

For an irregular polymer chain, all normal modes are potentially infrared active because of the lack of molecular symmetry.

For a polymer chain in a crystalline region of the polymer only a fraction of the vibrational modes are visible in infrared. There are many repeat units within one wavelength[5], which makes the interaction between polymer and radiation to depend on the sum of the interactions between the repeat units and radiation. If the polymer chain possess a high symmetry only a small fraction of the normal modes are visible in infrared spectrum. The other modes are mainly standing wave modes in which the vibrations of the chain units are similar but not in phase. In these modes the interaction cancels out over the length of the chain **[Bow1989]**.

The frequencies of the normal vibrational modes of small molecules lie in the region 200-4000 cm^{-1}. Very low frequency torsional vibrations of small molecules or polymers, and crystal lattice modes extend the low frequency end to ~10 cm^{-1}.

[5] The typical size for a repeat unit is 1nm, while the infraed radiation absorbed by the molecule is greater than 1 mm (10 cm^{-1}).

2.3. Proteins

A protein is a polypeptide chain made up of amino acid residues linked together in a definite sequence **[Ric1981]**. A peptide chain is assuming a secondary structure as the length of the chain is growing. Studies have indicated that a secondary structure can be detected already when the chain consists of only three molecules: in **[Sho1974]** it was shown that the oligomers of alanine (n = 3-6) assume β-form. Some proteins contain only one polypeptide chain while others, such as haemoglobin, contain several polypeptide chains all twisted together. The three dimensional shape of the protein is called native conformation. Under certain conditions, the protein can change its conformation and loose its activity. One talks in this case about denaturation.

In the next section, we will discuss the protein structure, the structure characteristics in IR, and the glassy behaviour of proteins at low frequencies.

2.3.1 Protein Structure

The sequence of the amino acids in a protein determines its primary structure. The sequence of amino acids in each polypeptide or protein is unique for every protein. The change of a single amino acid in the sequence can potentially change the protein's ability to function. For instance, sickle cell anaemia appears because of the change of one amino acid in one of the haemoglobin polypeptides. The result is that the red blood cells are deformed and unable to carry oxygen properly.

The secondary structure of the proteins is determined by the three dimensional organization of the polymeric chain. The most important secondary structures are α-helix, β sheets, turns, and random coil.

The hydration level conditions the existence of one type or another of secondary structure in a polymer. As X-ray studies of poly-L-arginine have

shown **[Suw1972]**, the polymeric chain assumes α-helical structure for a hydration of five molecules of water per arginine residue and β structure for the case 5-20 water molecules per residue. Dehydration of the chain (<5 water molecules per residue) had as result a very diffused α pattern.

The α-helix (Fig 2.27) is *the* classic element of protein structure and the dominant helical conformation found in globular proteins **[Ric1981]**. One helix can influence the stability of a protein more than any other individual structure element. A single α-helix can have as many as 35 residues, while the longest β strand has maximum 15. It was Pauling in 1951 **[Pau1951]** that first described the α-helix as a stable and favourable structure for the X-ray diffraction pattern of peptides; this structure has 3.6 residues per turn and a hydrogen bond between the CO of residue *n* and the NH of residue *n+4*.

Single stranded intramolecular hydrogen-bonded helices are designated by the symbol n_m **[Bra1950]**, where *n* represents the number of residues per turn (negative for a left-handed helix) and *m* the number of atoms contained in the "ring" joined by the hydrogen bond. The standard α helix is a 3.6_{13} helix. The α helix has 5→1 hydrogen bonds, meaning that the NH group on residue 5 along the chain bonds to the CO group back on residue 1. The 3_{10} helix is similar to the α helix, except that it has a 4→1 hydrogen-bonding pattern.

2.3.2. Secondary Structure Characteristics in FIR

Conformational changes in the secondary structure can be observed in IR. Native sperm-whale myoglobin **[Chi1973]**, protein for which 77% of the amino acids residues are included in helical segments, shows two absorption maxima between 30 and 280 cm^{-1} (at 140 and 226 cm^{-1}), and four explicit peaks in the region 280 – 500 cm^{-1} (at 324, 376, 420, and 470 cm^{-1}). After denaturation, the last three bands disappear and two wide bands appear at 128 and 160 cm^{-1}. The disappearance of the three peaks is an indication that they are characteristic for the helical structure. One might interpret the myoglobin spectrum in the FIR region by correlating it with spectra of helical

polypeptides. Poly-L-norvaline, poly-L-norleucine, and poly-L-leucine possess a α-helical structure that shows characteristic strong bands at about 100, 150 and 380 cm^{-1}.

It appears obvious that these polypeptides and myoglobin share the band at 380 cm^{-1}. However, one must be careful in assigning peaks or bands to the α-helical structure: in myoglobin, the changes in the bands near 324, 420, and 476 cm^{-1} are related not only to deformations of the polypeptide chain, but they reflect also changes in the conformational state of the side groups.

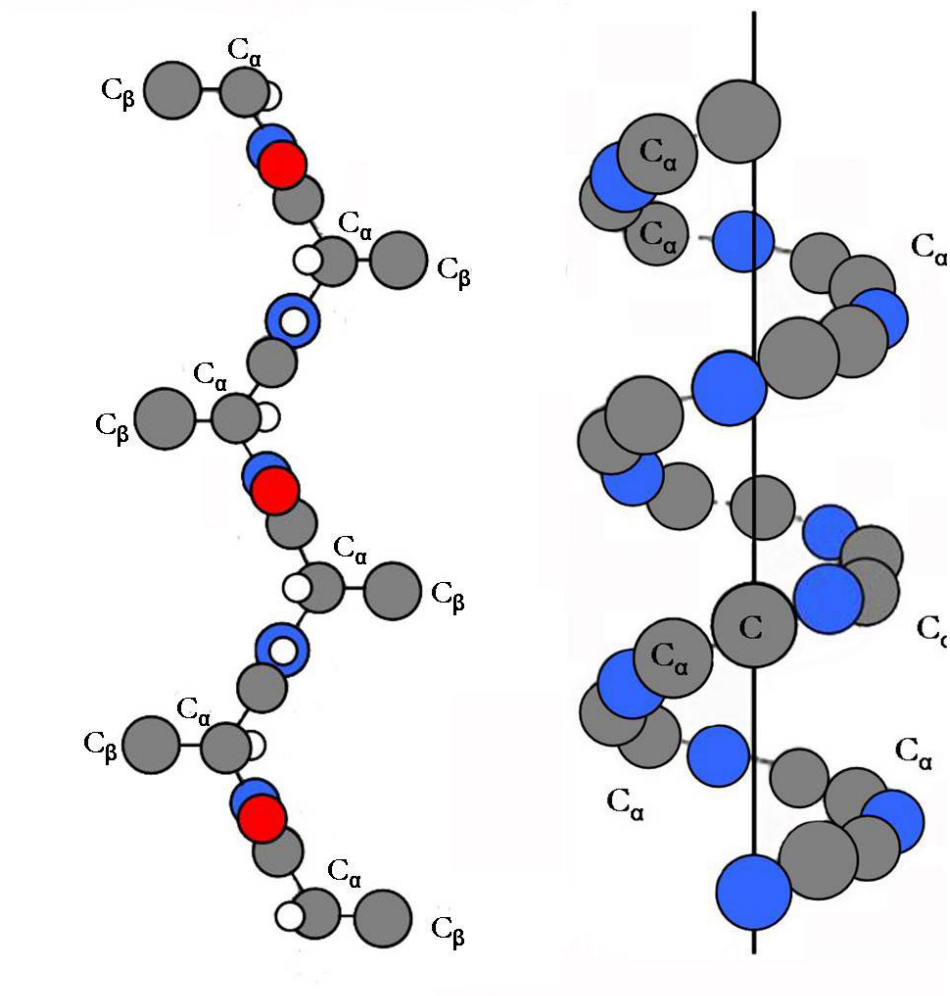

Fig. 2.27 The most important elements of protein secondary structure are the β-sheet (left image) and the α-helix (right image).

An extended polypeptide chain with a sheet-like arrangement stabilized by lateral hydrogen bonds forms a β-structure (Fig. 2.27 left). The β-sheet is for some proteins the main secondary structure component (concanavalin A); in others it appears in conjunction with α-helical segments. Often it is present as a mixed sheet of parallel and antiparallel strands. The characteristic IR frequencies of the polyglycine with β-sheet have been found at 140, 217, 285, 321, 589, 614, and 628 cm^{-1} **[Moo1976I]**. Poly-L-alanine with parallel β-sheet structure shows vibration frequencies at: 122, 240, 326, 432, 448, 615, and 629 cm^{-1} **[Ito1972]**.

However, the changes in the secondary structure cannot be always observed in FIR absorption spectra. The spectra of cytochrome c in native and denatured state presented in **[Yam2002]** indicated almost identical absorption for the two samples in the frequency range below 150 cm^{-1}. There was no doubt that the conformation has been changed, the MIR have proven it.

Proteins are different from homopolymers: not only that they contain different amino acids, but also the portions with a definite secondary structure are shorter. Because of these features, it is expected to see a broadening in the FIR peaks of the proteins compared with homopolymers. A further broadening is determined by the tertiary structure of proteins. Nonperiodic intramolecular interactions through hydrogen bonds, electrostatic effects, van der Waals forces, hydrophobic groups, tightly bound water lead to a broadening of the FIR absorption spectrum. Haemoglobin absorption spectrum for instance shows a broad structure with a peak at ~130 cm^{-1}, similar with other proteins **[Gen1983I]**. The peak was assigned to the stretching modes of the backbone peptide hydrogen bonds NH•••OC that stabilize the secondary structure of proteins.

These assumptions have been proved also in **[Buo1971]** and **[Yam2002]**. In **[Buo1971]** it has been shown that seven different globular proteins have a rather featureless absorption in FIR, in spite of the large differences in the structure. Globular proteins like myoglobin (~70% helix), ribonuclease (<15% helix), lysozyme, haemoglobin, serum albumin, ribonuclease,

chymotripsin, and subtilisin have quite similar spectra. For lysozyme, the FIR spectrum is not affected by the treatment with solvents, which induce conformational changes, or by the treatment with trypsin, that produces partial digestion.

2.3.3 Glassy Behaviour of Proteins

For terms as "amorphous" and "glassy," it is difficult to elaborate universally accepted definitions. Glass is a solid material, usually transparent or translucent, hard, brittle, made by cooling molten ingredients fast enough so that no crystals form. Glasses form through a process of "glass transition". This is a phenomenon in which a solid amorphous phase exhibits change in derivative thermodynamic properties (as heat capacity or thermal expansivity) from solid-like to liquid-like values with change of temperature. The thermodynamic parameters change less abruptly than in the case of melting.

While melting is a transition which occurs in crystalline polymers, the glass transition happens to amorphous polymers.

A liquid that is cooled can follow one of the two possible scenarios: crystallization, at the melting point $T_{m,}$ or supercooling to temperatures under T_m, becoming more viscous with decreasing temperature and turn into a glass. Glass formation is a matter of bypassing crystallization.

As experimental studies proved, the hydrated protein is a glass. Hydrated lysozyme powders show a dielectric relaxation, which is typical of the glassy behaviour of ferroelectric spin glasses, magnetic glasses and relaxors **[Car1999]**, **[Lev1999]**, **[Pey2001]**.

Protein folding is believed to be a phase transition similar to a spin glass[6] transition **[Bry1987]**. The transition between denatured and native protein can be interpreted as a loss of some liquid degrees of freedom, which defines

[6] A spin glass is a disordered material that exhibits high magnetic frustration. Atomic spins in a frustrated magnet cannot simultaneously minimize the energies of their local interactions. Instead, they fluctuate continuously, even at low temperatures **[Mir2002]**.

the formation of a glass **[Ang1995]**. The relaxation process that governs the large-scale motions in proteins is nonexponential in time. Its temperature dependence does not follow an Arrhenius law, analogous to glass-forming liquids **[Piz2001]**.

The role played by hydration water in determining the glassy character of a protein is not definitively clarified. Moreover, the relation between the liquid and the glass phases of water are still under active debate. One of the subjects of the debate is the identification of the glass transition temperature T_g[7] for bulk water.

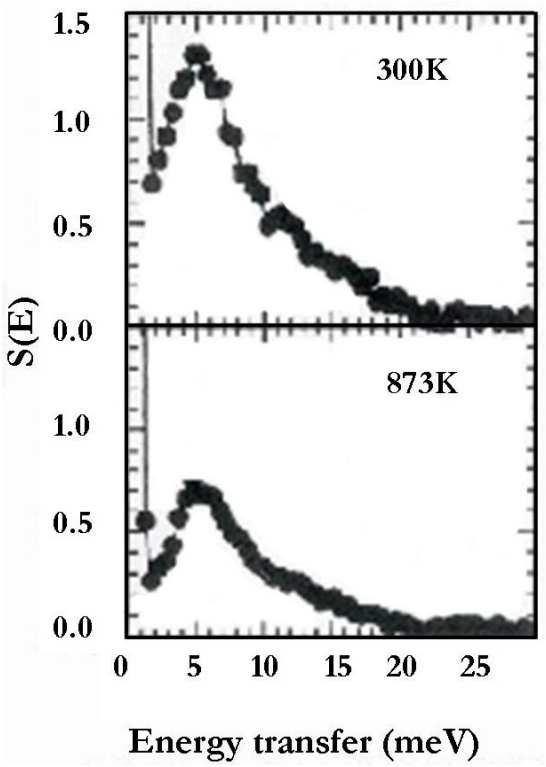

Fig. 2.28 The inelastic neutron scattering function, S(E), for vitreous silica measured at temperatures of 300 and 873 K indicate an absorption maximum at ~5 meV. This is reffered as boson peak. **[Har2000]**

[7] The glass transition temperature T_g is defined as the temperature of onset of the C_p jump during heating.

Two different temperatures were considered in literature as the point of glass transition: 136 K **[Hal1989]**, **[Ito1999]**, **[Mis1998]** and 165 K **[Vel2001]**, **[Gio2004]**. The latest studies agreed upon the second one as being correct.
This vibration anomaly, where the number of vibrational modes exceeds the one estimated by the Debye level, is called boson peak (Fig. 2.28).

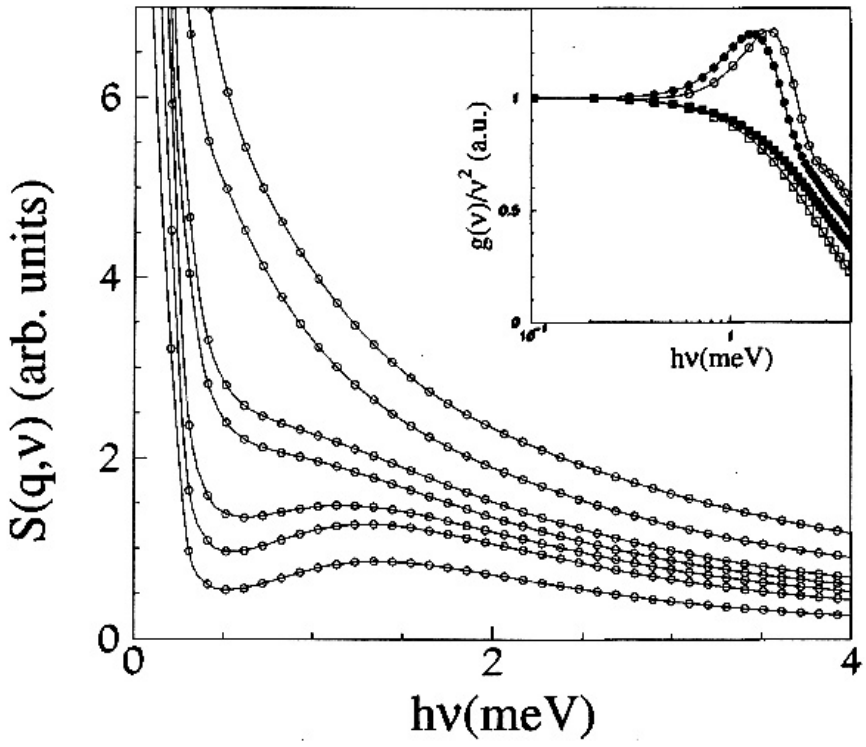

Fig. 2.29 Molecular dynamics simulations show the existence of an excess of low frequency vibrational modes in the density of states of hydration water around plastocyanin (PC) **[Biz2000]**.
Incoherent dynamical structure factor S(q, ν) is represented as a function of energy at a fixed q value (q = 2 $Å^{-1}$) of the water oxygen atoms around PC for different temperatures: 100, 150, 180, 200, 220, 260, and 300 K from bottom to top. Inset: Density of states divided by $ν^2$ as a function of energy at 100K (white circles), 180 K (black circles), 200K (black squares), and 220 K (white squares). Solid lines are a guide to eye. Incoherent dynamic structure factor is the Fourier transform of the Intermediate scattering function. (1meV = 8 cm^{-1})

Bounded water behaves different from bulk water. Neutron scattering experiments **[Set1996]** evidenced the anomalous diffusion of hydration water near the protein surface.

Molecular dynamics simulations **[Pac1998]**, **[Biz2000]** (Fig. 2.29) and neutron scattering experiments **[Pac1999]** showed the existence of an excess of low frequency vibration modes in the density of states of hydration water around plastocyanin.

In Debye approximation[8], the density of states g(ν) at low frequency is proportional to ν^2. The reality is different for proteins, as it can be seen in the inset in the Fig. 2.29. The presence of a boson peak is essential to the approach to glasses. The term refers to the fact that the temperature dependence of its intensity is scaling a Bose-Einstein distribution.

The origin of the boson peak is not completely understood; it is believed that it appears from a flattening of the dispersion of the transverse acoustic modes **[Lea1969]**, **[Ell1996]**, **[Tar1997I]**, **[Tar1997II]**, **[Dov2000]**, **and [Har2000]**.

Indications about a low-frequency band in proteins came also from Raman spectroscopy of α-chymotripsin (29 cm^{-1}) and pepsin (32 cm^{-1}) at room temperature **[Bro1972]**.

These peaks were vanishing upon denaturation, showing that they are dependent on the conformation (secondary structure or tertiary structure) of the protein molecule. Raman spectroscopy of several globular proteins **[Pai1982]** revealed an absorption peak at 25 cm^{-1}, for lyophilized chymotripsin a broad absorption maximum at ~30 cm^{-1}.

Raman spectroscopy of several globular proteins **[Pai1982]** revealed an absorption peak at 25 cm^{-1}, for lyophilized chymotripsin a broad absorption maximum at 30 cm^{-1}. Neutron scattering experiments on polycrystalline lysozyme **[Gen1976]** confirmed the existence of a peak at 25 cm^{-1} previously seen in Raman measurements. Low temperature inelastic neutron scattering of trypsin inhibitor, myoglobin, haemoglobin, lysozyme, and red blood cells

[8] A common approximation for the density of states in a crystal: $\rho_D(E) = \begin{cases} 9N\frac{E^2}{E_D^3}, (0<E<_D) \\ 0 otherwise \end{cases}$

[Cus1989], **[Cus1990]**, **and [Dos1989]** confirmed the results and showed a broad maximum in the incoherent dynamic structure factor at around 24 cm^{-1}. Synchrotron-FIR transmission of dry lysozyme showed a minimum at 24 cm^{-1} **[Moe1992]**. Normal mode analysis of bovine pancreatic trypsin inhibitor **[Bro1983]** proved the existence of a peak in the density of states near 50 cm^{-1}. The protein low frequency spectrum was interpreted in different ways. On one hand, it was suggested that the low-frequency modes could be related to accordion like modes of α-helical secondary structure of the proteins, and were calculated in the range 19-30 cm^{-1} **[Cho1985]**. On the other hand it was recognized the contribution of the hydrogen atoms from the side chains of the protein inner region to the existence of the band at 24 cm^{-1} in myoglobin **[Mel1999]**.

In conclusion, the presence of a boson peak in a sample indicates a glassy behaviour. Proteins exhibit such a low-frequency vibrational mode, which legitimate their comparison with glasses. The origin of this mode in proteins is not clarified yet.

2.4. Water properties in far infrared

Water is omnipresent in the samples and is the main absorbing material in far infrared for the samples here investigated. It is very difficult to obtain a sample that is completely lyophilised. Due to its importance, this subchapter is dedicated to the water molecule, revealing its properties, as they are known by now. Water molecule belongs to the symmetry group $\mathbf{C_{2v}}$, and has a

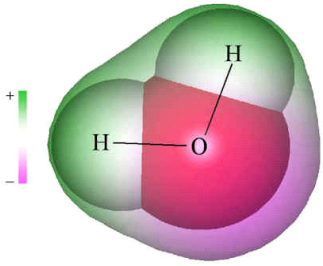

Fig. 2.30 The water molecule

permanent dipole moment of 2.95 ± 0.2 D (liquid, 27°C) **[Gub2002]**. The charge distribution in a water molecule is presented in Fig. 2.30: the oxygen is the negative pole and the hydrogen atoms represent the positive pole.

The dipole moment of the molecule varies during the normal mode motion, which makes the water molecule infrared active.

The water molecule may vibrate in a number of ways. In the gas state, the vibrations involve combinations of symmetric stretch (ν_1 = 3657 cm^{-1}), asymmetric stretch (ν_3 = 3756 cm^{-1}) and bending (ν_2 = 1595 cm^{-1}) of the covalent bonds **[Ber2002]**. In liquid water, the infrared and Raman spectra become more complex (Fig. 2.31 & 2.32) due to:

(1) Vibrational overtones and combinations with librations[9];

(2) The hydrogen bonds (a minor libration band L_1 appears at 395.5 cm^{-1}; a major libration band L_2 appears at 686.3 cm^{-1}, both at 0°C; the absorbance of L_1 increases with temperature whereas the absorbance of L_2 decreases **[Zel1995]**);

(3) Intramolecular stretching (184 cm^{-1}) and bending (40 - 60 cm^{-1}) of the hydrogen bonds **[Cha]**;

(4) Cluster vibrations, such as translational vibrations involving combinations of stretching and bending at around 200 cm^{-1} **[Gai2001]**.

On raising the temperature or pressure, the molecular stretch vibrations in liquid water shift to higher frequency. The reason is that the hydrogen bond weakens, while the covalent O-H bonds strengthen, causing the first to vibrate at higher frequencies.

In the same conditions, the intramolecular and molecular bend vibrations shift to lower frequencies. The stretching bands are loosing from intensity when the temperature is increased.

Due to this divergent behavior of bending and stretching vibrations, it is possible to distinguish between their contributions to combination bands.

[9] Librations are restricted rotations; *i.e.* rocking motions

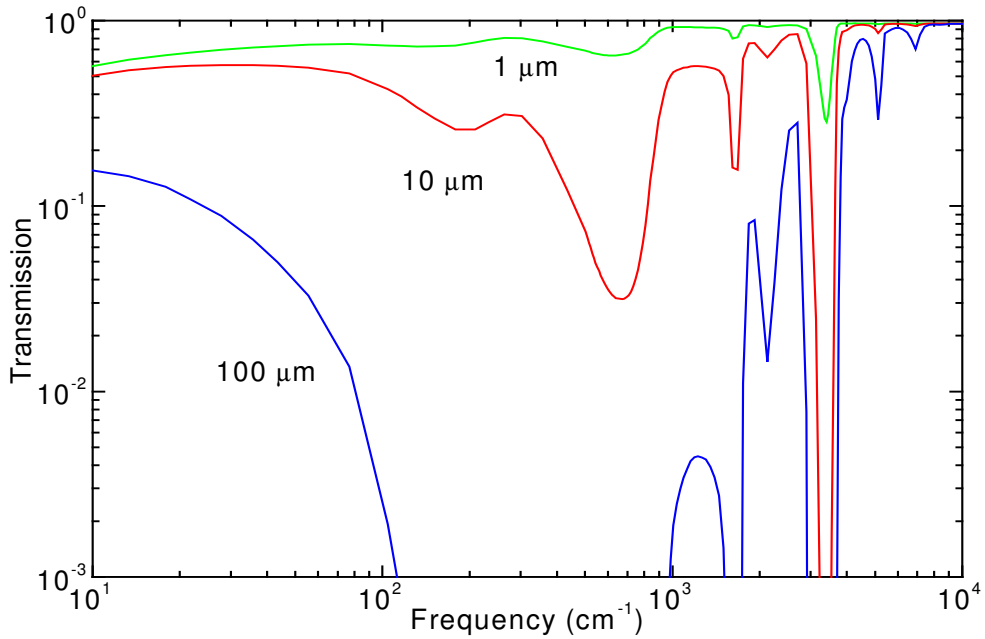

Fig. 2.31 Transmission of water in layers of different thickness.

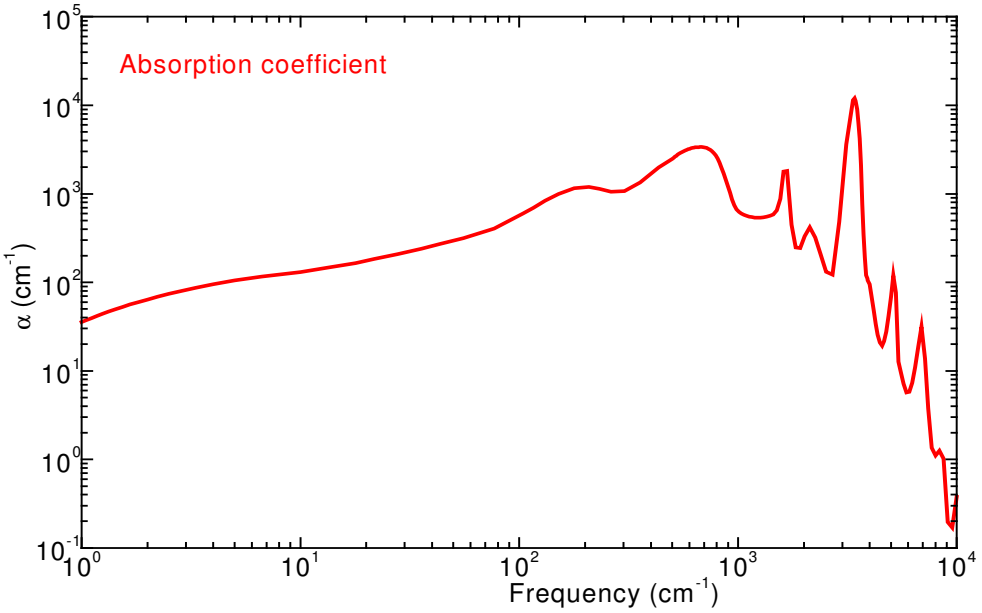

Fig. 2.32 Absorption coefficient of water. **[Pal1991]**

Thus, combinations of stretching vibrations shift to higher frequency with temperature with this trend reduced when bending vibrations are also combined. It was found from early experiments that in the low-frequency range, liquid water shows two broad bands: one is situated around 60 cm^{-1}, and the other one at 170 cm^{-1} (Table 2.2, Fig. 2.33).

Although the first measurements of this kind were made more that 70 years ago (**[Seg1931]**, **[Bol1932]**), there is no general agreement yet concerning the interpretation of these features. These two studies were concerned with Raman spectroscopy measurements. The same bands were identified later by absorption spectroscopy in far infrared (**[Dow1975]** detected the high frequency band, and **[Has1985]** found the low frequency band).

It was observed for both bands that they weaken when the temperature is increased. This leads to the assumption that the bands are due to the breakdown of the intermolecular structure.

Table 2.2. Assignment of the vibrational absorption spectrum of liquid water **[Cha]**.

Wavelength (cm^{-1})	Assignment
60	Cage effect
183.4	Intramolecular stretch
395.5	L_1, librations
686.3	L_2, librations
1645	v_2, bend
2150	$v_2 + L_2$
3277	v_3, asymmetric stretch
3490	v_1, symmetric stretch

Normal mode calculations showed that the low-frequency bands are hindered translational vibrations. The band at 60 cm^{-1} is attributed to the frustrated translations due to the local structure around a given atom (molecule) that

produces the cage effect **[Pad2003]**, **[Pad2004]**. The existence of this band should not be associated with the existence of hydrogen bonding. Low-frequency features, centered on 60 cm^{-1}, are observed not only in water, but also in the spectra of dense non-associated liquids, such as the noble gasses; it might be an indication that the low-frequency features of proteins are not related with hydrogen bonds.

The frequency band around 170 cm^{-1} is attributed to the stretching of hydrogen-bonded molecules.

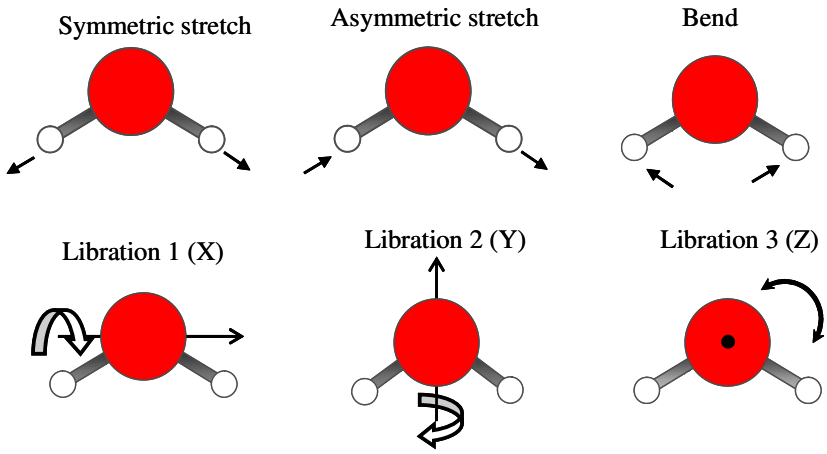

Fig. 2.33. The main vibrations ocurring in water. The dipole moments change in the direction of the movement of the oxygen atoms as shown by the arrows.

2.5. Blood

Blood is one of the body fluids that flow close to the body surface. When the body is irradiated, blood is one of the exposed tissues. This is why we decided to use blood in order to observe how it absorbs in far infrared. The average adult has about five litres of blood inside of their body, flowing through the vessels, delivering essential elements, and removing harmful wastes. Blood transports:

- Oxygen from the lungs to body tissue,

- Carbon dioxide from body tissue to the lungs,
- Nourishing products from digestion (glucose, lipids, amino acids),
- Hormones from glands throughout the body,
- Antibodies to the tissue and waste to the kidneys.

Approximately 55% of blood is plasma, a straw-coloured clear liquid. The liquid plasma carries the solid cells and the platelets, which help the blood to clot. Its composition is seen in Table 2.3.

Component	**Percentage**
Water	~ 92
Proteins	6-8
Salts	0.8
Lipids	0.6
Glucose	0.1

Table 2.3. Plasma composition.

We use in our measurements liquid plasma because of its preponderance in blood.

By now, there are no far infrared studies of blood plasma. Other blood constituents, like hemoglobin, have been often investigated in this frequency range. Absorption spectrum of hemoglobin **[Gen1983I]** shows a broad structure with a peak at ~130 cm^{-1}, assigned to the stretching modes of the hydrogen bonds N-H•••OC that stabilize the secondary structure of proteins. This behavior is typical for proteins. For blood plasma is expected a behavior comparable with water, rather than with that of proteins.

C h a p t e r 3

THE TECHNIQUE

3.1 The interaction of radiation with matter

Molecules consist of atoms bound together by chemical bonds. Atoms behave like a set of coupled harmonic oscillators (Fig.3.1). This means that under the influence of a perturbation the atoms vibrate in such a way that the motion can be considered a superposition of simple harmonic vibrations. *Normal modes* are oscillations in which all atoms vibrate with the same frequency and phase. In a normal mode each atom passes simultaneously through its equilibrium position.

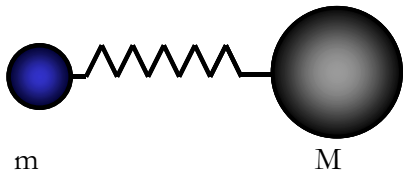

Fig. 3.1 A simple model for the vibration of a diatomic molecule.
The oscillator is called harmonic if it obeys the Hooke`s law:
Restoring force = f = -kx, k is the elastic constant of the spring.

There are three principle methods used for the study of molecular vibrations **[Bow1989]**: infrared spectroscopy, Raman spectroscopy and inelastic neutron scattering.

Infrared spectroscopy was used here for investigations. In this chapter are presented the theoretical and experimental details of this method.

The different parts of the electromagnetic spectrum have very different effects upon interaction with matter. Each region of the electromagnetic

spectrum can induce certain types of physical processes in matter. The energy levels for physical processes at the atomic and molecular levels are quantized. If the energy of the radiation matches the difference between two atomic or molecular energy levels, than the radiation will be absorbed in the material. If there are no available quantized energy levels with spacing, which match the quantum energy of the incident radiation, then the material will be transparent to that radiation.

Following the interaction with the electromagnetic radiation, a vibrating molecule may: (1) absorb radiation, when the latter has the same frequency as one of the normal modes of vibration, (2) scatter, or (3) transmit the radiation. The frequency of the incident radiation can change after interaction (Raman scattering), or can stay the same (Rayleigh scattering). An infrared spectrum indicates what fraction of the incoming radiation is absorbed at each value from the frequency range.

Using selection rules, one can predict whether a molecular vibration is infrared active or not. During the interaction between the photon and the molecule the total angular momentum in the electronic ground state has to be conserved, and this involves that only specific transitions are possible. Molecular vibrations symmetric with respect to the center of symmetry of the molecule are forbidden in the infrared spectrum, while molecular vibrations, which are antisymmetric to the center of symmetry, are forbidden in the Raman spectrum. Infrared absorption is detected if the dipole momentum μ in a molecule changes during the normal vibration. Because of these selection rules, IR spectroscopy gives detailed information about functional groups.

A molecule with N atoms has 3N-6 normal vibrations that appear in infrared spectra. In the gaseous state, the molecules are free and their spectrum shows mainly rotation-vibration features. Liquids, due to the irregular intermolecular interactions, show hardly any rotational fine structure in their spectra. In the crystalline state, the interactions are the same for each molecule and the spectral features are sharper than in liquids.

Electromagnetic radiation that propagates through a medium is modified by the interaction with the medium. Radiation can be scattered, transmitted, or absorbed by the medium. When the frequency of the incoming radiation is resonant with the transition frequencies of the electrons, atoms, or molecules, the radiation is absorbed. Infrared radiation frequency corresponds to vibrational transitions in molecules. Following the interaction, the intensity of the radiation is attenuated in the material according with the Lambert-Beer´s law:

$$I(r) = I_0 \exp(-\alpha r) \tag{3.1.1}$$

where $I(r)$ is intensity at the point defined by r, I_0 is the intensity at the incidence, α is the absorption coefficient[10].

A further decrease in the intensity is due to the scattering of the radiation **[Fox2001]**:

$$I(r) = I_0 \exp(-N\sigma_s r) \tag{3.1.2}$$

where N is the number of scattering centers per unit volume and σ_s is the scattering cross section. In standard transmission experiments, like ours, the scattering cannot be identified, and it sums up to the absorption. As the scattering is proportional with the scattering cross section, one way to limit the scattering effects is to prepare samples with very fine granulation.

3.2 The Lorentz oscillator model

The atom-field interactions can be described using the Lorentz oscillator model. This represents the classical model of a damped harmonic oscillator. Lorentz considered an atom as a mass (the nucleus) connected by a spring (of elastic constant k) to another smaller mass (the electron). The spring is set into motion by an oscillatory electric field of an electromagnetic wave electric field that is interacting with the negative charge of the electron. The spring is

[10] α is defined as the fraction of absorbed power per unit length.

compressed when the field is repelling the electron, and stretched when the field is attracting the electron. An oscillator of mass m[11] and charge e is acted upon by: a linear restoring force $K\vec{r}$, where K is the spring constant (stiffness) and $\vec{r}$ is the displacement from equilibrium; a damping force $b\frac{d\vec{r}}{dt}$, where b is the damping constant; and a driving force produced by the electric field $\vec{E}(t)$. The equation of motion for such an oscillator is written as:

$$\frac{d^2\vec{r}}{dt^2} + b\frac{d\vec{r}}{dt} + K\vec{r} = e\vec{E}(t) \qquad (3.2.1)$$

This is the simplest picture of atom-field interaction.

The model can be extended to the case of molecules (Fig. 3.1) where the spring is considered to connect different atoms in the same molecule. In this case, the oscillatory electric field is the driving force for the molecular dipoles, and the mass from (3.2.1) is the reduced mass of the dipole.

When the electric field has an exponentially dependence on time $\vec{E} \sim \vec{E}_0 \exp(-i\omega t)$, the solution of (3.2.1) is **[Fox2001]**:

$$\vec{r}(\omega) = \frac{e\vec{E}/m}{(\omega_0^2 - \omega^2) - i\omega\gamma} \qquad (3.2.2)$$

where $\omega_0^2 = K/m$ and $\gamma = b/m$. For $\gamma \neq 0$, the proportionality factor between $\vec{r}$ and $\vec{E}$ is complex, which means that the displacement and field are not, in general, in phase.

The optical properties of the material can be determined considering a system of such damped harmonic oscillators. There are two sets of quantities used for description of optical properties: the real and imaginary parts of the complex refractive index $N = n + ik$, and the real and imaginary parts of the complex dielectric function (relative permittivity) $\varepsilon = \varepsilon' + i\varepsilon''$. The relations between the two are[12]:

---

[11] m is the reduced mass of the system nucleus-electron

[12] we assume a nonmagnetic material $\mu=\mu_0$

$$\varepsilon' = n^2 - k^2, \tag{3.2.3}$$

$$\varepsilon'' = 2nk \tag{3.2.4}$$

$$n = \sqrt{\frac{\sqrt{\varepsilon'^2 + \varepsilon''^2} + \varepsilon'}{2}} \tag{3.2.5}$$

$$k = \sqrt{\frac{\sqrt{\varepsilon'^2 + \varepsilon''^2} - \varepsilon'}{2}} \tag{3.2.6}$$

In the next it will be shown how to obtain the complex dielectric function for an oscillator and for a set of oscillators.

The induced dipole moment of an oscillator is:

$$\hat{\vec{p}} = -e\hat{\vec{r}}(\omega). \tag{3.2.7}$$

For *N* oscillators per unit volume, the polarization $\vec{P}$ [13] is

$$N\vec{p} = Ne\vec{r} \tag{3.2.8}$$

or

$$\vec{P} = \frac{\omega_p^2}{\omega_0^2 - \omega^2 - i\gamma\omega}\varepsilon_0\vec{E} \tag{3.2.9}$$

where ω_p is the plasma frequency defined as $\omega_p^2 = Ne^2 / m\varepsilon_0$ (3.2.10). The complex dielectric constant for a simple harmonic oscillator is:

$$\hat{\varepsilon}(\omega) = 1 + \frac{\omega_p^2}{(\omega_0^2 - \omega^2) - i\gamma\omega} \tag{3.2.11}$$

with real and imaginary parts:

$$\varepsilon' = 1 + \frac{\omega_p^2\left(\omega_0^2 - \omega^2\right)}{\left(\omega_0^2 - \omega^2\right)^0 + \gamma^2\omega^2}, \tag{3.2.12}$$

[13] the polarization is defined as dipole moment per unit volume.

$$\varepsilon'' = \frac{\omega_p^2 \gamma \omega}{\left(\omega_0^2 - \omega^2\right)^0 + \gamma^2 \omega^2} \qquad (3.2.13)$$

In the Lorentz model with several oscillators, the complex dielectric function is given by:

$$\hat{\varepsilon}(\omega) = 1 + \sum_{j=1}^{k} \frac{f_f \omega_p^2}{\left(\omega_0^2 - \omega_j^2\right) - i\omega\gamma_j} = \varepsilon_1 + i\varepsilon_2, \qquad (3.2.14)$$

where ω_p is the plasma frequency; N is the number of oscillators with frequency ω_j, oscillator strength f_j, and damping constant γ; ε_1 and ε_2 are the real and imaginary parts of the complex dielectric function, respectively.
In our fitting program, the spectra are approximated with a sum of lorentzians, in order to find the resonant frequencies for the molecular vibrations: for every absorption band is associated an oscillator. Each oscillator is defined by three parameters: its strength, its damping constant, and its frequency.

3.3 Spectrometer Bruker IFS113v

Our measurements in far infrared were performed with a modified rapid-scan Fourier transform spectrometer Bruker IFS 113v (Fig. 3.2). In the Fourier transform spectrometer, radiation of all wavelengths passes through the sample to the detector simultaneously. The detector measures the total transmitted intensity as a function of the displacement of one of the mirrors in the interferometer. A computer does the separation of the different wavelengths.
The spectrometer Bruker IFS 113v is appropriate for measurements between 10 and 10000 cm^{-1}. The machine is equipped according to a Genzel arrangement of the Michelson interferometer. It is supplied with three light sources (mercury, tungsten, and Glowbar lamp) and up to six different

detectors. For far infrared, one can use as source the mercury lamp and two He bolometers (4.2 and 1.2 K) as detectors. The first detector covers the frequency range 50 – 650 cm^{-1}, the second bolometer 10-50 cm^{-1}. There is one more detector for far infrared: the DTGS detector. This has the advantage of working at room temperature and does not necesitate long time for preparing an experiment. Compared with bolometers, it has some drawbacks: slow response time and low signal-to-noise ratio.

Fig. 3.2 Bruker IFS 113v spectrometer has four different chambers:
I - for sources, II – interferometer chamber, III – sample chamber, IV – detectors.
a – sources; b – aperture for adjusting the beam waist, c – beamsplitter;
d – semitransparent mirror, e – mirror; f – moving mirror; h & i – sample positions; k – detectors.

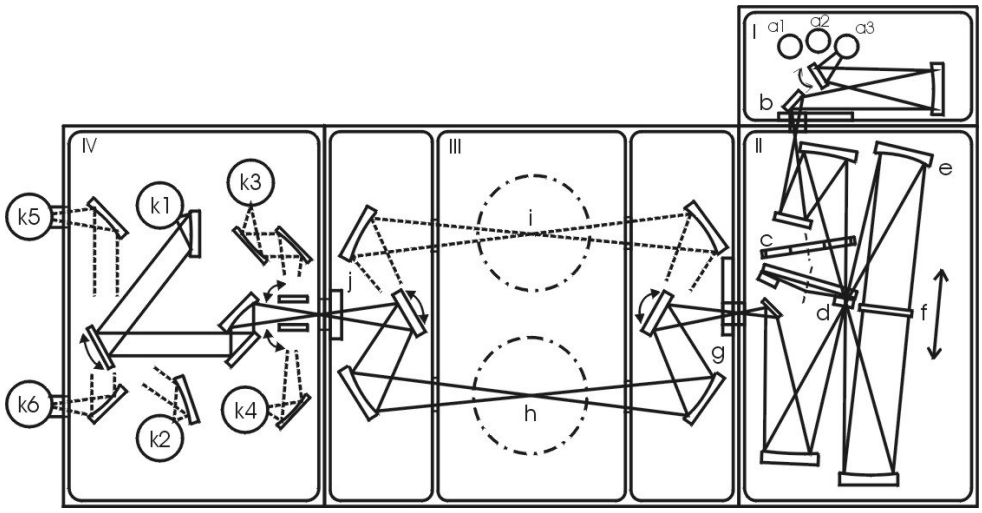

The resolution of a measurement can go up to 0.03 cm^{-1}, but is typically of 1 cm^{-1}. The signal-to-noise ratio is limited only by the stability of the machine[14]. One can obtain an optimum signal-to-noise ratio by averaging over many measurements (up to 500 scans).

[14] i. e. the stability of the source and the properties of the detector

The fast Fourier transformation of the signal is produced by a computer and further analysed. As the spectrometer gives only the absolute value of the transmission and reflection, the refraction index and the absorption coefficient are determined by Kramers-Kronig analysis of the data. This is done by data extrapolations to low and high frequencies, which might influence the result. All the experiments were performed at room temperature. In Annex D is presented the way a spectrum is produced using a Fourier transform spectrometer.

3.4 Liquid measurements in far infrared - silicon as window

For the liquid samples, we designed a cuvette (Fig. 3.3) that can be used under vacuum. The thickness of the liquid chamber can be adjusted by using different Mylar spacers.

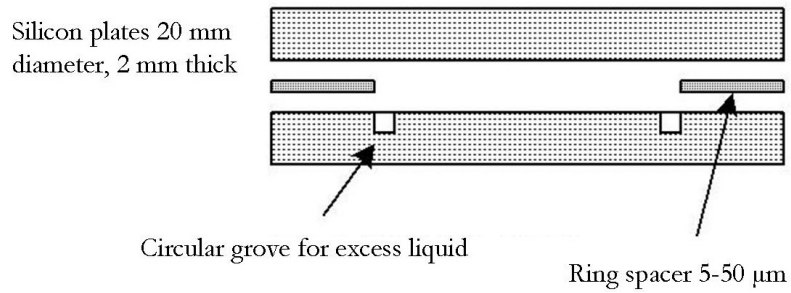

Fig. 3.3 The cuvette for liquid samples: two silicon plates separated by a ring that defines the thickness of the sample layer. A few μl of sample are pipetted on the plate, inside the ring. One of the plates has a circular grove for extra liquid to flow. The plates are enclosed in a metal support (Fig. 3.4).

Polyethylene is transparent in far infrared, which makes it suitable for use as windows. It has one disadvantage: it is too soft to be used for cuvette windows in vacuum, where the distance between the two faces should be fixed during the measurement.

Fig. 3.4 The transmission cell. The two silicon plates (the dark discs in the image) are mounted inside the metal support, which closes with three screws. The cell is placed in front of the beam.

Silicon with low doping concentration seems to be the best choice, because of its optical and mechanical properties: it is transparent in far infrared and has a hardness of 6.5 on Moh`s scale. Being so hard, it can be transformed in windows of very well defined thickness (error of 1 μm).

The material has also disadvantages: (1) it is opaque in the visible range, so that a visual investigation of the inside of the cuvette is excluded, and (2) has a high refractive index (~3.4). Figure 3.5 shows the transmission spectrum of a silicon plate of 2 mm thickness. Once in vacuum, the windows will tend to bend, increasing the space between them. As this space is filled with liquid, the optical path will increase. From calculations of material resistance, we agreed that windows of 2 mm thickness after bending would modify the pathway in the error limit. When water is present in samples, identifying features from the recorded spectra turns out to be a very difficult task. Because of the high absorption in far infrared, it is preferable to use dry samples. The problem of low transmission due to the presence of water can

be overcome by recording spectra in reflection. In this case, the optical arrangement will look like in Fig. 3.6.

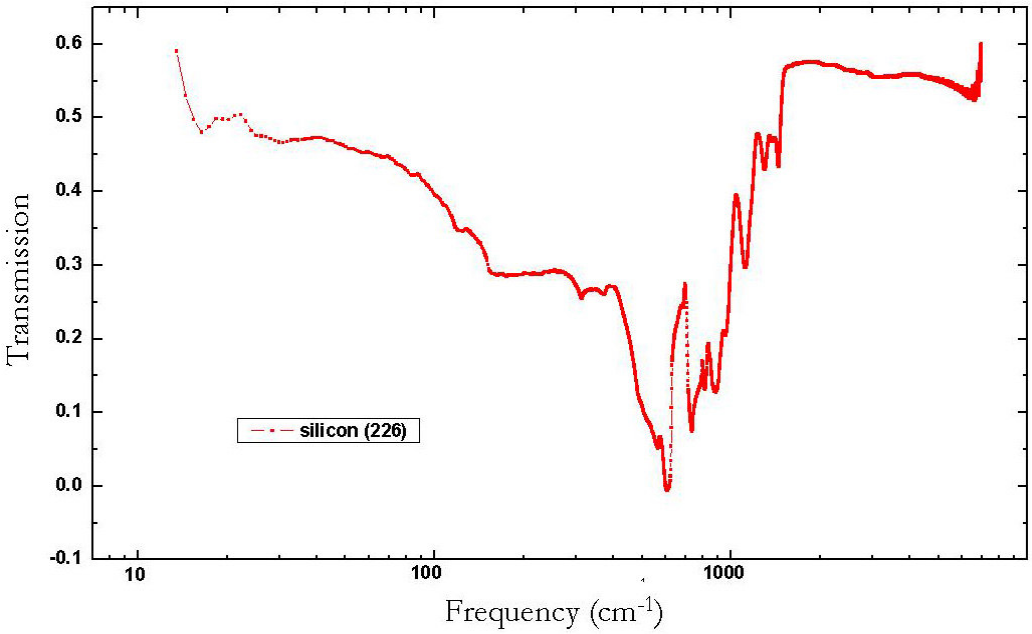

Fig. 3.5 Transmission of silicon.

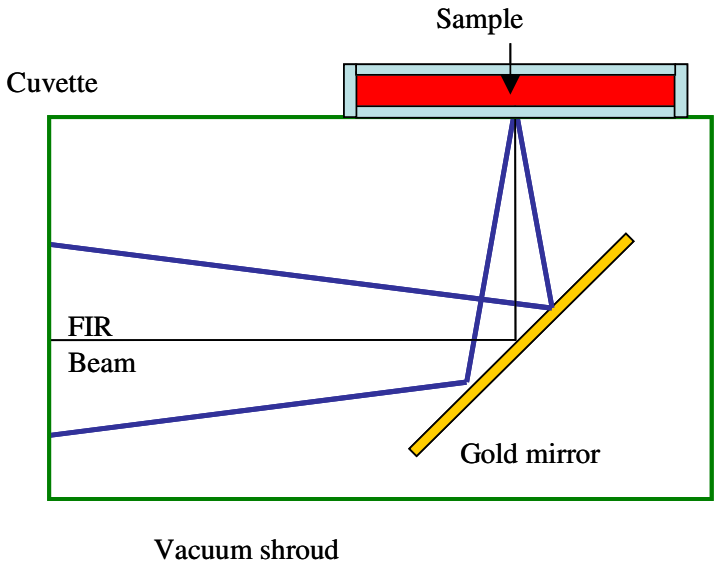

Fig. 3.6 Arrangement for reflection measurement.

The cuvette with silicon windows can be used for transmission and reflection measurements. In the case of reflection, the sample can be prepared as layer of a few millimetres thickness (or even more). Figure 3.6 shows the arrangement for reflection measurements: the cuvette is lying flat on the spectrometer, the beam is directed by means of a golden mirror to the lower silicon window, is passing through the window, and is reflected back to the golden mirror, before reaching the detector.

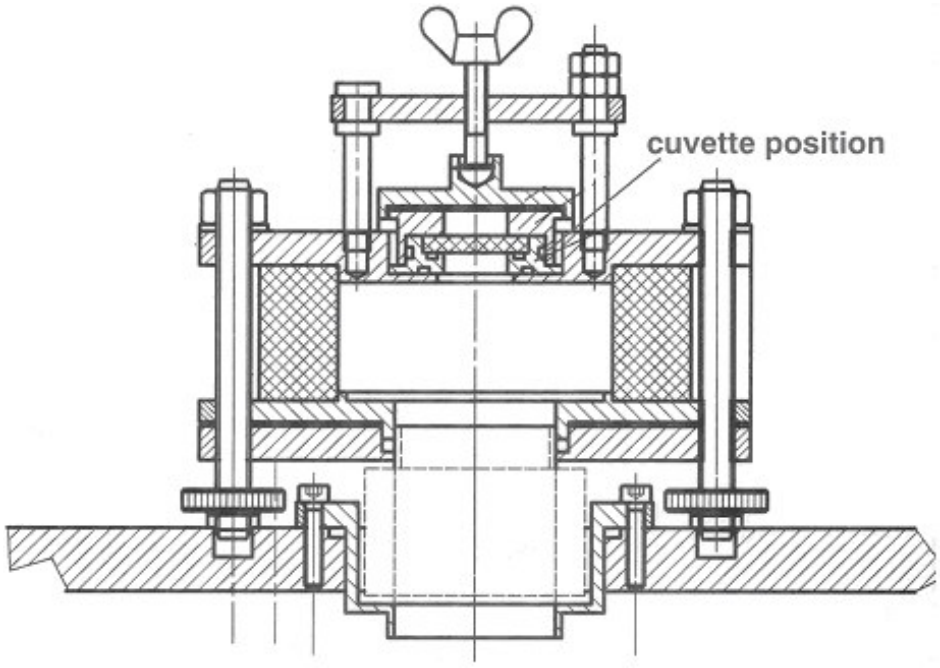

Fig. 3.7. Cuvette arrangement for Bruker IFS 113v.

3.5 Solid sample preparation

Amino acids were purchased as polycrystalline powder from Fluka and used without further purification. Proteins were purified in one of our labs. Powder samples can be used in measurements as pellets cast from concentrated water solutions. Pellets are easy to manipulate and mechanically stable. This method of sample preparation was previously used with success (**[Gen1983II]**, **[Has1983]**).

Sample preparation for amino acids required a 15 minutes grinding in order to reduce the scattering. After grinding, the crystals were of 1-2 μm size. The dry samples were further mixed with polyethylene powder in ratio 1:10 and pressed in pellets of 1 cm diameter. The pressing force was 7kN for each sample. A micrometer determined the thickness d of the resulting pellets: typically between 200 and 400 μm, for the low-frequency experiments even thicker. Despite this reduced thickness, the samples are not very transparent, showing a maximum transmission of ~70% on a reduced domain, at very low frequency, and decreasing to ~10% at higher frequencies.

3.6 Results analysis

Based on the recorded transmission spectra of the pellets (polycrystalline samples in polyethylene matrix), we calculated the absorbance *A* of the amino acids in the following way:

$$A = -\log(1/T_{AA}) \tag{3.6.1}$$

where the transmission of the amino acid is given by:

$$T_{AA} = T_{pellet}/T_{PET} \tag{3.6.2}$$

Here T_{pellet} is the transmission measured through the pellet. The transmission of the bare polyethylene matrix of the pellet is given by:

$$T_{PET} = (1-R_{PET})^2 \exp(-\alpha_{PET} \cdot d \cdot c) \tag{3.6.3}$$

Here R_{PET} indicates the reflectivity of the polyethylene, α_{PET} is the absorption coefficient of polyethylene, *d* is the thickness of the pellet, and *c* indicates the concentration of the polyethylene in the pellet. The absorption coefficient of polyethylene was calculated as

$$\alpha_{PET} = 4\pi k/\lambda \tag{3.6.4}$$

k is the extinction coefficient of polyethylene and was determined from fitting of transmission spectrum of a pellet of polyethylene. For the measurements in the range 50-650 cm^{-1} we used amino acid pellets with the mass ratio amino acid/PET of 1:10, while for the range 10-50 cm^{-1} the ratio was 1:1 or 1:4.

Chapter 4

AMINO ACIDS IN FIR

In this chapter, we present the absorbance spectra of 18 amino acids in the frequency range between 10 and 650 cm^{-1} and discuss the features they have in common. Our assignment of the observed vibrational bands is based on isotope replacement effects, calculations of the normal modes available in literature and comparison of the spectra of different amino acids. No systematic study is available to comprise all of the α-amino acids. Common infrared atlases do not present the complete far-infrared spectra **[Sch1989]**; in general, data below 400 cm^{-1} are missing.

Comparing spectra of different amino acids brings out some of the resemblance that is expected because of the similarity of the compounds. However, this resemblance is limited to a few general features. The individual features are sufficiently different to be used in identifying the compounds.
The results are presented starting with glycine and following the evolution of the spectra complexity, as the molecule is getting bigger and more complex.

4.1 Glycine

Glycine is the smallest of the amino acids: its side group is a plain hydrogen atom. It is also the first amino acid that was produced from hydrolysis of proteins[15]. According to the 3*N*-6 rule (with *N* the number of atoms) it has 24 normal modes: theoretically, all of them are infrared and Raman active **[Vij1992]**. The smallest of the amino acids has also a simple spectrum.

[15] **[Bra1820]**

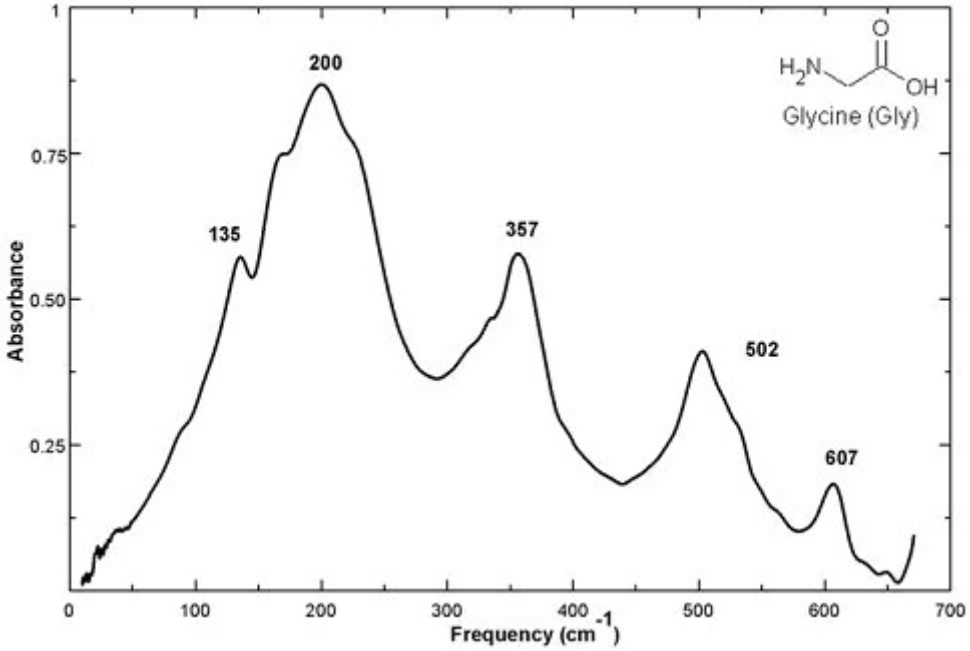

Fig. 4.1. Absorbance spectra of glycine.

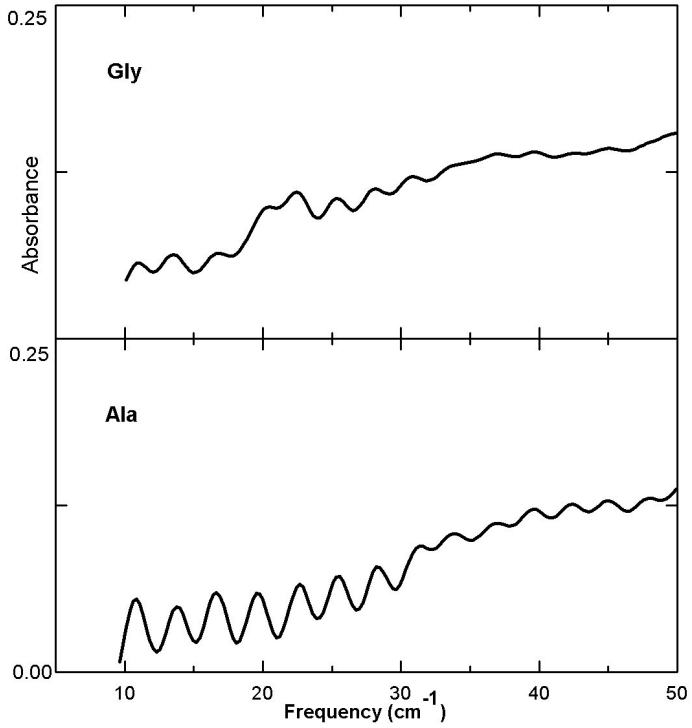

Fig. 4.2. Low frequency absorbance spectra of glycine.

There are four strong peaks between 200 and 650 cm^{-1} (Fig. 4.1 - 4.7): at 200, 357, 502, and 607 cm^{-1}. Beside these, there are some other features of weak intensity: at 233, 318, and 526 cm^{-1}. Many attempts have been made to assign the modes found in the solid glycine spectrum (**[Ste1998]**, **[Vij1992]**, **[Tsu1958]**[16], **[Suz1963]**[17], **[Gre1972]**[18], **[Gen1983]**).

At 607 cm^{-1} is visible a C=O bending, as it was earlier described **[Tsu1958]**. From DFT calculations, it was expected to appear at 624 cm^{-1} in gaseous glycine **[Ste1998]**. At 502 cm^{-1} a strong COO^- mode is observed **[Tsu1958]**. This peak is asymmetric with a shoulder toward higher frequency (526 cm^{-1}). This hidden mode represents a NH_3^+ torsion (**[Des1971]**, **[Ket1989]**). It is interesting that it was not predicted by recent calculations (**[Ste1998]**, **[Vij1992]**), although it was evidenced **[Des1971]**. One reason is its low intensity, which makes it difficult to observation. Another possible reason is the "anomaly" in the frequency shift produced by isotope replacement.

At 356 cm^{-1}, there is a strong peak in the spectrum due to the $CC^{\alpha}N$ bending **[Mac1977]**.

The far-infrared absorbance of glycine is dominated by a broad band centred at 200 cm^{-1}, which exhibits a series of peaks on its low-frequency wing. These excitations have more than just one contribution: hydrogen bond deformations, skeletal modes, lattice vibrations, and other modes of the COO^- and NH_3^+ groups **[Ban1983]**. We identify weak modes at 59, 68, 77, 85 cm^{-1} (τCC **[Vij1992]**), 135 cm^{-1} (NH•••OC stretching **[Fan1973]**, **[Ban1983]**), and 164 cm^{-1}.

The lowest lying modes have been identified performing a Lorentzian fit of the spectrum. They appear at 22, 37, and 52.4 cm^{-1}. In Fig. 4.2 is presented the absorbance of glycine below 50 cm^{-1}. There is no mode at 29 cm^{-1}, as it was predicted in **[Mac1977]**. Other studies determined the existence of a mode at

[16] **[Tsu1958]** in Annex A, table 3, page 148

[17] **[Suz1963]** in Annex A, tables 4, page 148

[18] **[Gre1972]** in Annex A, table 14, page 153

33 cm^{-1} **[Pow1979]**. There are no assignments for any of these low-lying modes.

Measurements at low temperatures and measurements using isotope-labelled glycine bring more information about the type of vibrations that appear in definite regions. The vibrational mode frequency depends on the masses of the atoms, the geometry of the molecule and the force constants. Substituting an atom with an isotope will determine a change of the mode frequency in which the atom is involved. The geometry and the force constants do not change. The shift in frequency following an isotope substitution is useful in making vibrational assignments.

In the simplest model the frequency of a mode is given by:

$$\nu = \frac{1}{2\pi}\sqrt{\frac{k}{m}} \tag{4.1}$$

where m is the mass of the oscillating unit, and k is the force constant. The frequency shift can be determined from the ratio ν_1/ν_2:

$$\frac{\nu_2}{\nu_1} = \sqrt{\frac{m_1}{m_2}} \tag{4.2}$$

where ν_1 is the original frequency, ν_2 is the frequency modified by the isotope substitution, m_1, m_2, is the mass of the oscillating unit before and, respectively after isotope replacement.

We performed measurements with Gly-^{15}N and Gly-^{14}N, looking for frequency shift that indicates the modes where N is involved. The expected shift in frequency is determined as:

$$\nu_2 - \nu_1 = \nu_1\left(\sqrt{\frac{m_2}{m_1}} - 1\right) \tag{4.3}$$

with ν_2 frequency corresponding to Gly -^{15}N and ν_1 the frequency for Gly-^{14}N. Experimental, there is no frequency shift, neither at 300 K, nor at 5 K. From (4.3), with m_1 and m_2 given by:

$$m_1 = \frac{m(^{14}NH_3)m(CH_2COO)}{m(^{14}NH_3) + m(CH_2COO)} \tag{4.4}$$

and

$$m_2 = \frac{m(^{15}NH_3)m(CH_2COO)}{m(^{15}NH_3) + m(CH_2COO)} \tag{4.5}$$

the expected variation in frequency for the mode at 526 cm^{-1} is 11 cm^{-1}. In order to determine the correct shift, which is zero, one has to take into account at least two other modes: the stretching r(CH_2) and the out-of-plane bending γ(COO^-). With these considerations, it was proved that there is no shift for the mode at 526 cm^{-1}, at 300 K or 5K **[Gre1972]**.

For the peak at 356 cm^{-1} a shift in frequency of ~5 cm^{-1} is for Gly -^{15}N expected. This is indeed observed.

The differences between Gly-^{14}N and Gly-^{15}N spectra are small, both at 300K and 10K. There are two modes for which the variation in frequency is consistent: at 357 cm^{-1} for Gly-^{14}N (364 cm^{-1} at 5 K) compared with 352 cm^{-1} for Gly-^{15}N (359 cm^{-1} at 5 K), and 502 cm^{-1} for Gly-^{14}N (506 cm^{-1} at 5 K) compared with 499 cm^{-1} for Gly-^{15}N (501 cm^{-1} at 5 K).

In the case of ^{13}C replacement, the vibration at 607 cm^{-1} moves toward lowers frequencies in Gly-2-^{13}C. This is one more piece of evidence this vibration involves the COO^- group. In addition, the mode at 85 cm^{-1}, considered to have mainly the contribution of CC torsion, is moving to 88 cm^{-1} following the ^{13}C change. When the same measurements are made at 5K, the details in the spectra become visible. Thus the vibration at ~360 cm^{-1} in Gly-^{14}N, shifts to lower frequency in ^{15}N-Gly. This proves this is the region where the NCC deformations appear. Comparing the measurements of the same sample at different temperatures, one can see that new features develop, as the temperature is decreasing.

The decrease in temperature has as effect a noise reduction; in consequence, the spectral features become sharper. The reason for this behaviour is the stimulated emission effect **[Xie1999]**: as the temperature is increasing, stimulated emission from the excited states would tend to decrease the observed absorbance, because the emitted photons would tend to counterbalance the absorbance. Since the excited states are depopulated at lower temperatures, the emission is lower at low temperatures and the absorbance higher than they are at higher temperatures. These excited state effects likely govern much of the behaviour of low-frequency modes in all biomolecules.

At low temperature the absorbance, bands become narrower and the difference in resonant frequency is more visible.

At 5 K, the shoulder seen at 526 cm^{-1} at 300 K develops into a strong peak toward higher frequency (546 cm^{-1}, Fig. 4.5 – 4.7 and **[Hus1984]**).

The broad maximum seen at 300 K at 200 cm^{-1} together with its side wings at 164 and 233 cm^{-1}, develops into three distinct peaks at 5 K.: 180, 214, and 238 cm^{-1}. For both Gly-^{14}N and Gly-^{15}N, they have the same frequency.

Below 200 cm^{-1}, one can distinguish three peaks that are increasing in intensity and are shifting toward higher frequency as the temperature is decreased. There frequencies are: 85 (92 at 5K), 135 (147 at 5 K), and 164 (180 at 5 K) cm^{-1}. These modes are related with the lattice modes.

The features of weak intensity from 233, 318, and 526 cm^{-1} have different behaviour with the temperature evolution. Whereas the features from 526 and 233 cm^{-1} turn into strong peaks, the other one disappears.

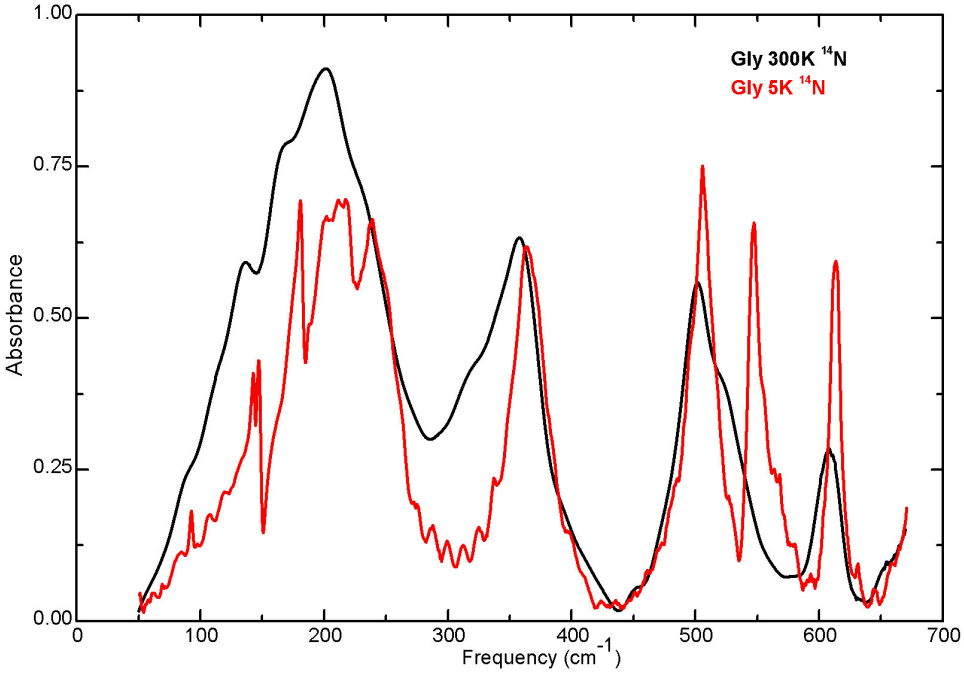

Fig. 4.3 Absorbance spectra of Gly at 5K and 300K.

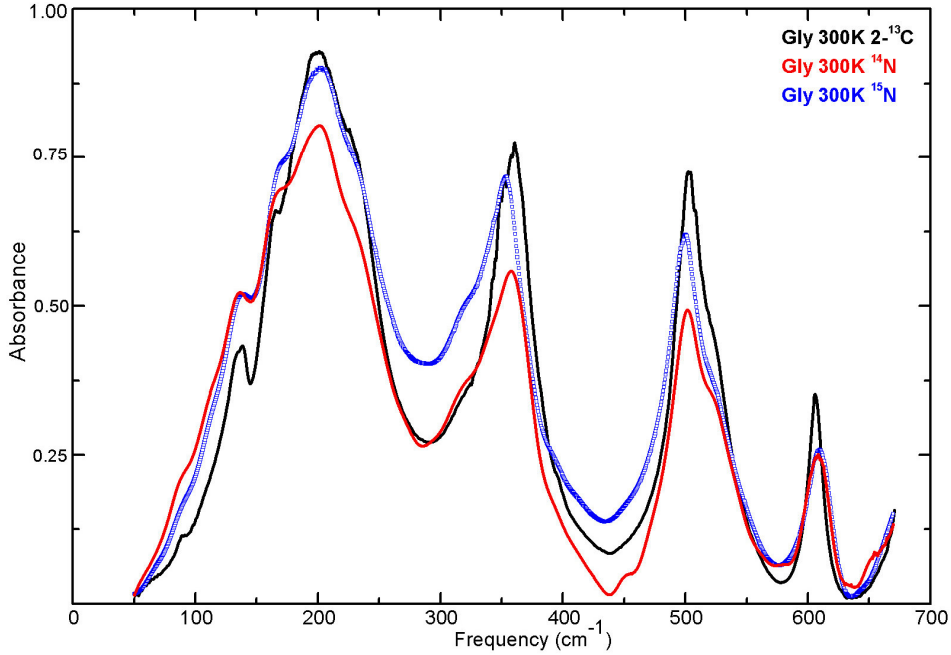

Fig. 4.4 Absorbance spectra of Gly and isotope-labelled Gly (Gly ^{15}N and Gly-2-^{13}C) at 300K.

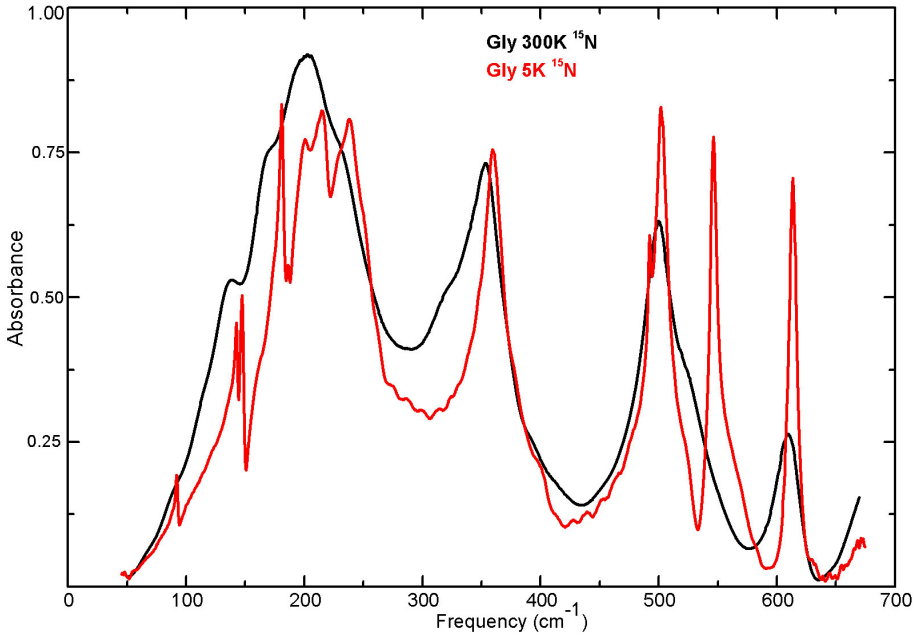

Fig. 4.5. Absorbance spectra of ^{15}N-Gly at 300K and 5K.

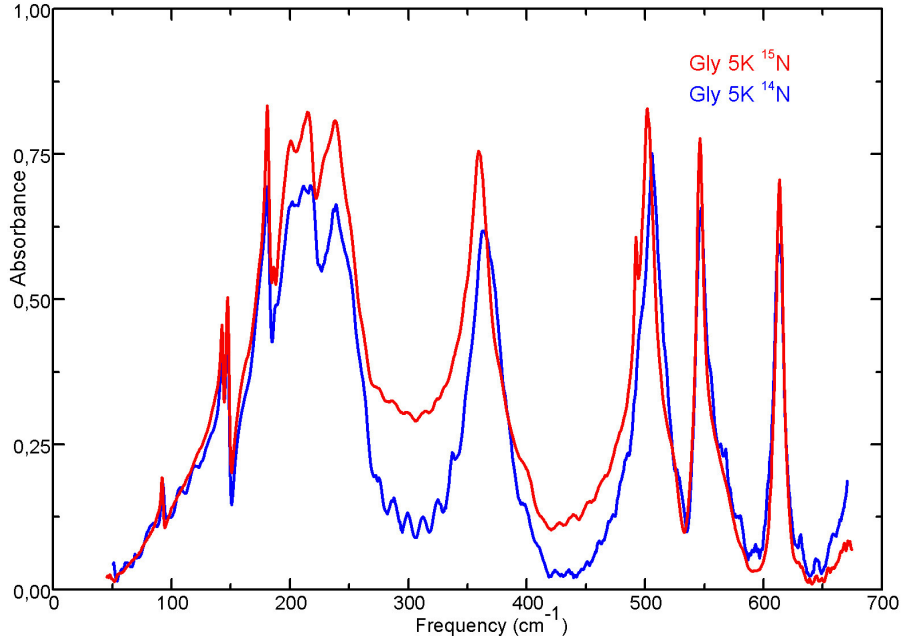

Fig. 4.6 Absorbance spectra of ^{15}N-Gly and ^{14}N-Gly at 5K.

4.2 Alanine

The other simple amino acid, alanine, crystallizes in an orthorhombic form with space group symmetry $P2_12_12_1$ **[Sim1966]**; it is expected that all the 33 fundamental internal vibrations of the molecule are both Raman and FIR active **[Hus1984]**. Going from glycine to alanine the increasing number of modes becomes immediately obvious (Fig. 4.7). The reason is that by introducing the CH_3 group, the overall symmetry of the crystal is lowering **[Wan1971]**.

Different models have been proposed for determining the vibrational frequencies. In **[Fuk1959]** alanine was considered a seven-body molecule, taking the CH_3 and NH_3^+ as dynamical units. The skeletal vibrations have been calculated along with the CH bending motion, which is considered to couple closely with the skeletal vibrations. The model does not reproduce the reality, and the calculated frequencies have lower values than the results we present here. The same model applied to deuterated alanine **[Suz1959]** was able to identify two vibrations of the molecule: the COO^- out of plane vibration at 599 cm^{-1} and a CCN skeletal deformation at 232 cm^{-1}.

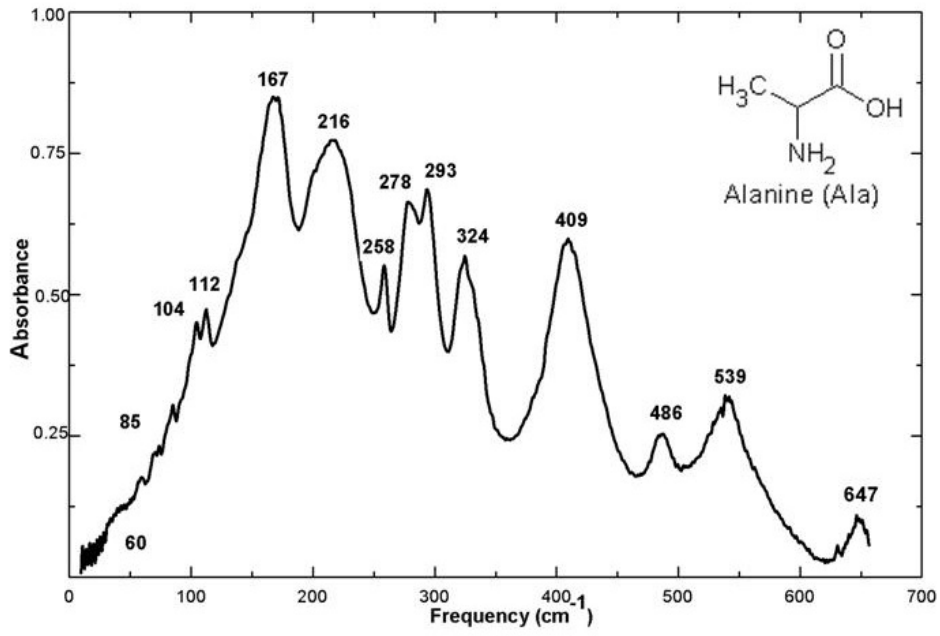

Fig. 4.7 Absorbance spectra of alanine.

Temperature-dependent spectra gave insights into bands due to hydrogen bonds **[Ban1983]**[19]. Below 100 cm^{-1}, the authors observed two such bands: at 73 and 85 cm^{-1}, that were considered to represent a combination of hydrogen bond bending NH•••OC, COO^- torsions and CCN deformations. We have been able to detect one more band under 100 cm^{-1}, that was predicted but not observed by **[Ban1983]** namely at 60 cm^{-1} (Fig. 4.7). This band has the same origin as the two mentioned above.

As the temperature is decreasing, some of the absorbance frequencies shift to lower values, the bands are getting sharper, and sometime, they even split **[Hus1984]**. The bands between 100 and 140 cm^{-1} become sharper as the temperature decreases, indicating the contribution of lattice modes. As it was shown in **[Gen1983]**, band at 324 cm^{-1}, which is assigned to skeletal deformation modes, splits in two bands at low temperature. One of the bands stays at 324 cm^{-1}, while the new one shifts up to 351 cm^{-1} at 6K. This behaviour could not be explained. The NH_3^+ torsional band is splitting too **[Bar2002]**, for temperatures below 220K.

Raman measurements **[Wan1971]**[20] revealed the lattice and internal modes of L-alanine single crystal. The lattice modes are considered to appear below 190 cm^{-1}.

4.3 Glycine and Alanine

Because glycine is the simplest amino acids, one would expect that the features from its spectra would be characteristic for the class of molecules. In consequence, all the other amino acids should display these features. In this section, glycine spectrum will be compared with alanine spectrum, observvng how the vibrational features change due to the different side chain.

[19] **[Ban1983]** in Annex A, table 22, page 159

[20] **[Wan1971]** in Annex A, table 16, page 154

If we compare glycine with alanine (Fig. 4.8 - 4.10), we see that there are features that both spectra share.

In the alanine absorbance spectrum, the COO^- modes are shifted to higher frequencies compared to glycine: the COO^- rocking mode appears at 647 cm^{-1} and the COO^- rocking/bending/wagging mode is observed at 538 cm^{-1} (see also Table 4.1). In glycine, these vibrations appear as a single peak, the one around 607 cm^{-1}.

For alanine, the NH_3^+ torsion peak is very distinct compared with glycine, and is located at 486 cm^{-1} (481 cm^{-1} in **[Ada1972]**[21], 473 cm^{-1} in **[Fuk1959]**). Raman and incoherent inelastic neutron scattering (IINS) investigations showed that the NH_3^+ torsional band is splitting too, for temperatures below 220K. The temperature dependence was explained in terms of hydrogen bonds of unequal strength **[Bar2002]**.

Four peaks of medium to strong intensity are found in alanine between 278 cm^{-1} and 409 cm^{-1} and all of them have their origin in the $CC^{\alpha}N$ deformation and CH_3 torsion **[Wan1971]**. In the glycine spectrum the equivalent to those modes is the peak at 357 cm^{-1}, which represents the $CC^{\alpha}N$ bending.

The shoulder present in glycine at 233 cm^{-1} is not visible in the spectrum of alanine. Instead of it, there is a maximum developing at 216 cm^{-1}, described as COO^- torsion **[Ban1983]**. The same assignment is given to the peak in alanine at 258 cm^{-1}.

Below 200 cm^{-1}, alanine spectrum is richer in features than glycine, all the peaks indicating hydrogen bonds (H-bonds) deformations coupled with other modes. The strong peak that dominates the spectrum of glycine at 200 cm^{-1} is displaced in alanine towards lower values, at 167 cm^{-1}. This is assigned as a H-bond stretch **[Bar2002]**. This band shifts to higher wavenumbers as the temperature is decreased **[Ban1983]**, which is an unexpected behaviour,

[21] **[Ada1972]** in Annex A, Table 15, page 153

considering that the hydrogen bond potential function used in calculations had no temperature dependence.

At 112, 104, 86, and 59 cm^{-1} are H-bonds coupled with COO^- torsion, at 112 cm^{-1} with NH_3^+ torsion and at 60 cm^{-1} with $CC^{\alpha}N$ deformation **[Ban1983]**. We could not observe any absorbance maximum under 50 cm^{-1} (Fig. 4.8), although there are expected to appear modes that represent $CC^{\alpha}N$ deformation, H-bond deformations, and COO^- and NH_3^+ torsions. In alanine, also CH_3 modes contribute to the absorbance below 200 cm^{-1}. We were able to detect for both amino acids an absorbance peak at 59 cm^{-1}, which was not previously observed. This finding is in agreement with DFT calculations **[Ste1998]** that predict the existence of a band of $NC^{\alpha}C$ torsion at 62 cm^{-1}.

Gly	Ala	Assignment
22 w		Hydrogen bond modes
37 vw		
52 vw		
59 w	60 w	
68 w		
77 w	73 w	
87 w	86 w	
	104 w	
	112 w	
135 w		
164 w	167 s	
200 s		
233 w	216 s	
	258 w	COO^- vibrations
	278 w	
	293 w	$CC^{\alpha}N$ deformations
	324 m	
356 s		
	409 s	NH_3^+ modes
526 sh	486 w	
502 s	539 w	COO^- rock/bend/wag vibrations
607 s		
	647 w	

Table 4.1. Absorbance frequencies for glycine and alanine.

It can be observed that alanine spectrum presents more absorbance peaks than glycine, which is surprising if we consider that the structural difference between the two molecules is only a methyl group, which, by itself, does not show many specific absorbance lines.

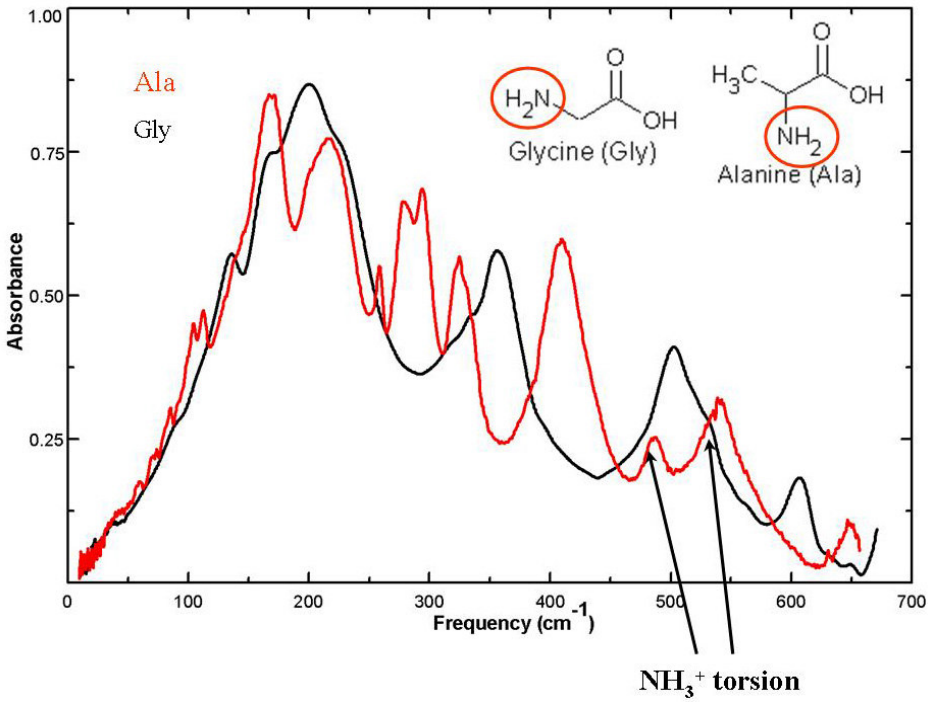

Fig. 4.8 Glycine compared with alanine – the NH_3 group torsion.

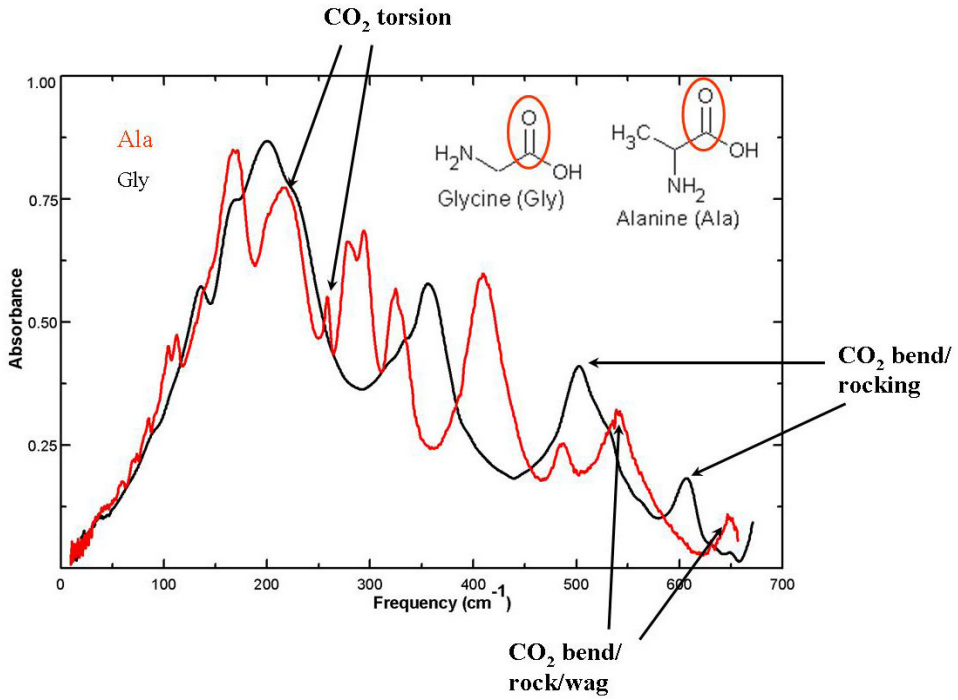

Fig. 4.9 Glycine compared with alanine – the CO_2 group modes.

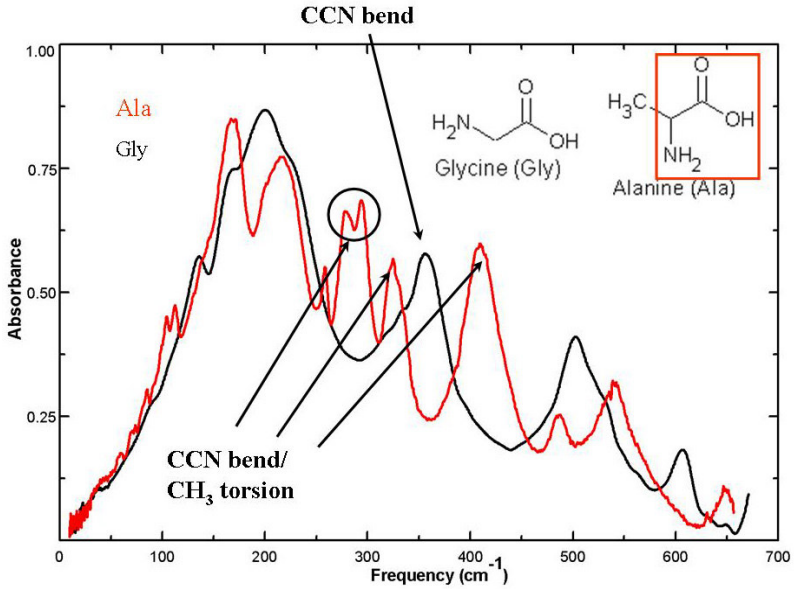

Fig. 4.10 Glycine compared with alanine – the CH_3 group torsion and the CCN bend.

4.4 Phenylalanine

The vibrational spectrum of Phe is presented in Fig. 4.11. The spectrum has a few strong features, at 195, 365, and 525 cm^{-1}. The strongest peak in absorbance appears around 365 cm^{-1} and is considered a skeletal mode (CCN deformation). The details of the spectrum are discussed further, by comparing Phe with Ala and Tyr.

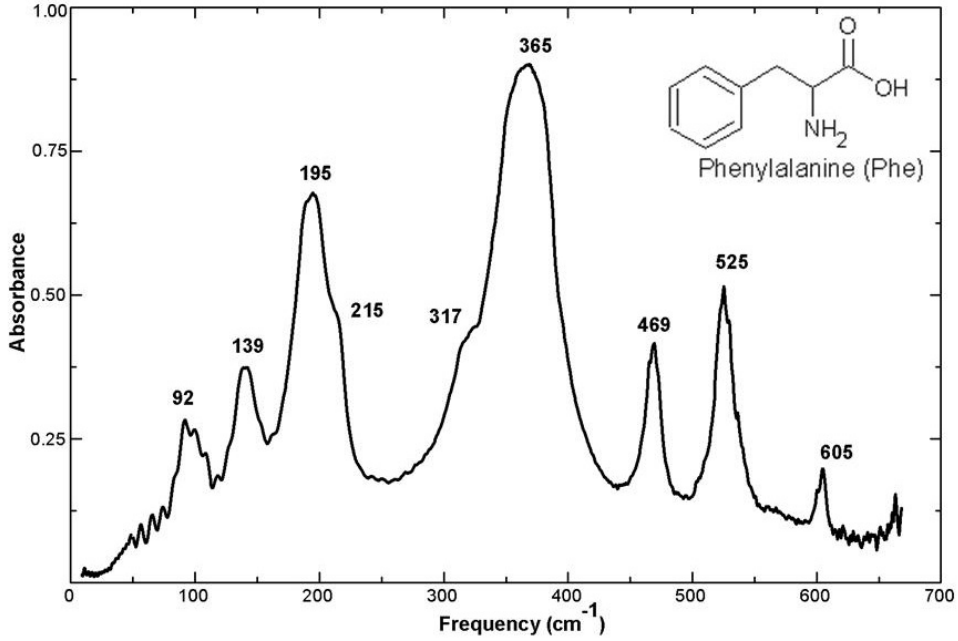

Fig. 4.11 Absorbance spectra of phenylalanine.

4.5 Alanine and Phenylalanine

Phenylalanine is alanine that has a phenyl group replacing a hydrogen atom. Because of this substitution, the vibrational spectra are very much different (Fig. 4.12). The spectrum of alanine shows more features than phenylalanine, all of them having comparable medium to weak intensity. Phenylalanine has only four peaks above 200 cm^{-1}, the most prominent being at ~350 cm^{-1}, where alanine has a minimum of absorbance.

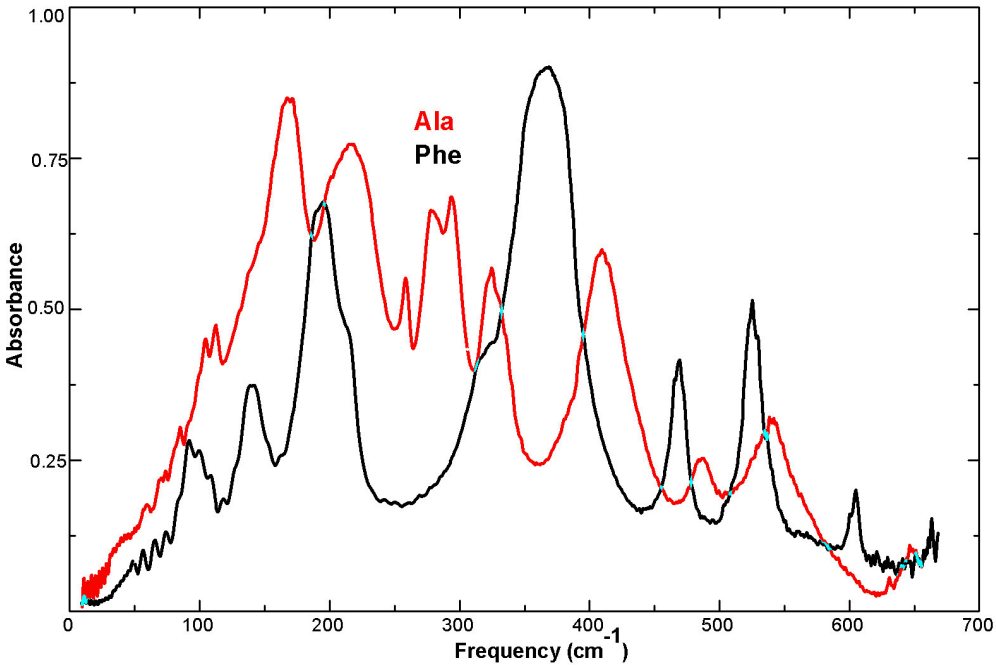

Fig. 4.12 Absorbance spectrum of alanine and phenylalanine.

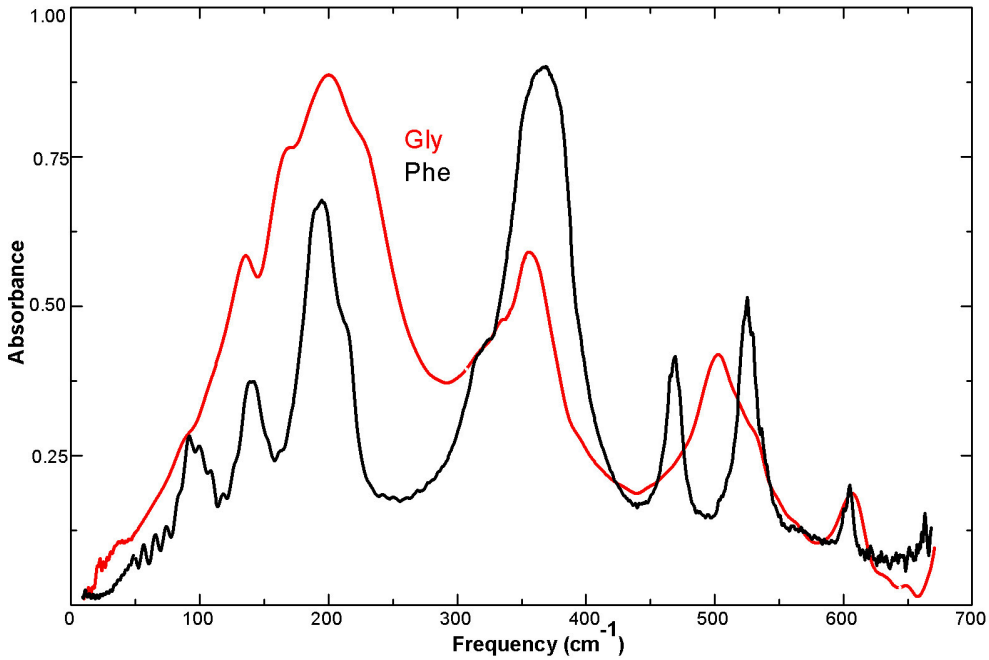

Fig. 4.13 Absorbance spectrum of glycine and phenylalanine.

The COO^- group vibrations appear in Phe displaced toward lower frequencies (525, 605 cm^{-1}) in comparison with Ala (539, 647 cm^{-1}). The same is

happening with the NH_3^+ vibration: in Phe is shifted down at 469 cm^{-1}, while in Ala is at 486 cm^{-1}.

The CCN mode in Phe is at 365 cm^{-1}, while Ala has three peaks around this value, and all of them represent CCN deformation (coupled with other modes).

From the point of view of band distribution, spectrum of Phe resembles more the spectrum of Gly (Fig. 4.13) than that of Ala. The CCN mode around 350 cm^{-1} is visible for both Phe and Gly, both samples have a strong peak at ~200 cm^{-1}, without splitting. In addition, both samples display a COO^- group mode at ~600 cm^{-1}.

4.6 Tyrosine and Phenylalanine

Tyrosine is an amino acid that has in the side chain a benzene ring and an OH group attached to it. In the next section, we will compare tyrosine spectrum (Fig. 4.14 & 4.15) with phenylalanine, in search of common features.

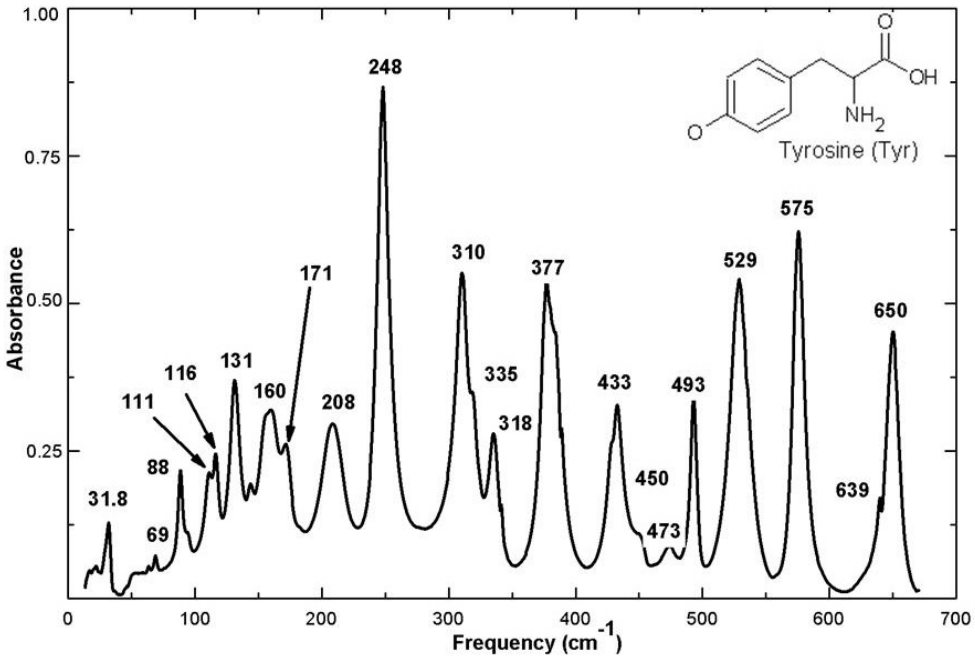

Fig. 4.14 Absorbance spectra of tyrosine.

Both amino acids have a benzyl group in the side chain. The only structural difference between them is that tyrosine has one hydroxyl group attached to the benzyl. The difference between the two is small, but not the same can be said about the difference in the vibrational spectra (Fig. 4.15 & 4.16). According to **[Gra2002]**, the benzene rings should be prevalent in the spectra, and the ring substituents could be treated as point masses. Watching the Fig. 4.15, we assume that this is a prediction for other region than FIR: the two amino acids do not share too many lines. There is no evidence that most of the lines are due to the benzene ring. We will first discuss common features.

<50 cm^{-1} region

One frequency region where Phe and Tyr absorb radiation unexpectedly different is between 10 and 50 cm^{-1}. We found a maximum of absorbance in Tyr at ~32 cm^{-1}, which was calculated in **[Fri1992]** and attributed to a torsion of the entire side chain about C-ring bond. This peak has no equivalent in Phe. The same data are reported in **[Miy2003]**, and cannot yet be explained.

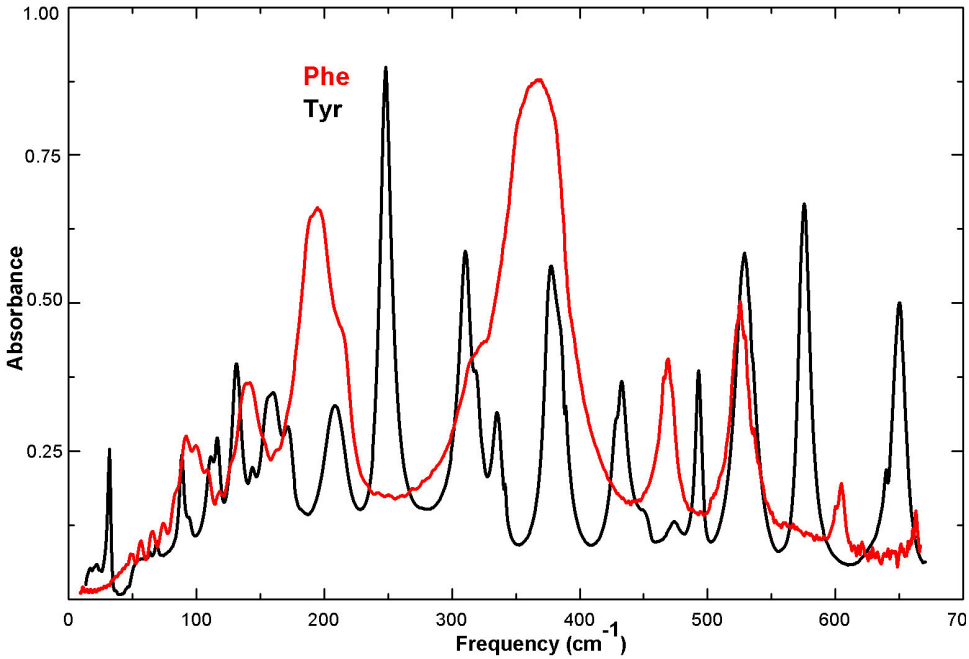

Fig. 4.15. Absorbance spectra of tyrosine and phenylalanine.

50-200 cm^{-1} region

Another feature that is common for both amino acids is the peak around 200 cm^{-1}. For Phe, this peak is situated a few wavenumbers under 200 cm^{-1}, while for Tyr is at a few wavenumbers above 200 cm^{-1}. As is already known, in this region of frequencies vibrate the hydrogen bonds and the CCN bonds (deformation). **[Xie1999]** overrules the possibility that these peaks could be the influence of the benzene ring. In this reference are presented the spectra of poly-L-phenylalanine as well as spectra of other homopeptides (poly-L-valine, poly-L-tryptophan, and poly-L-alanine). In the chains, the peak from 200 cm^{-1} is displaced to lower frequencies, at about 150 cm^{-1}, and it is found in all the samples, independent of the benzene's presence.

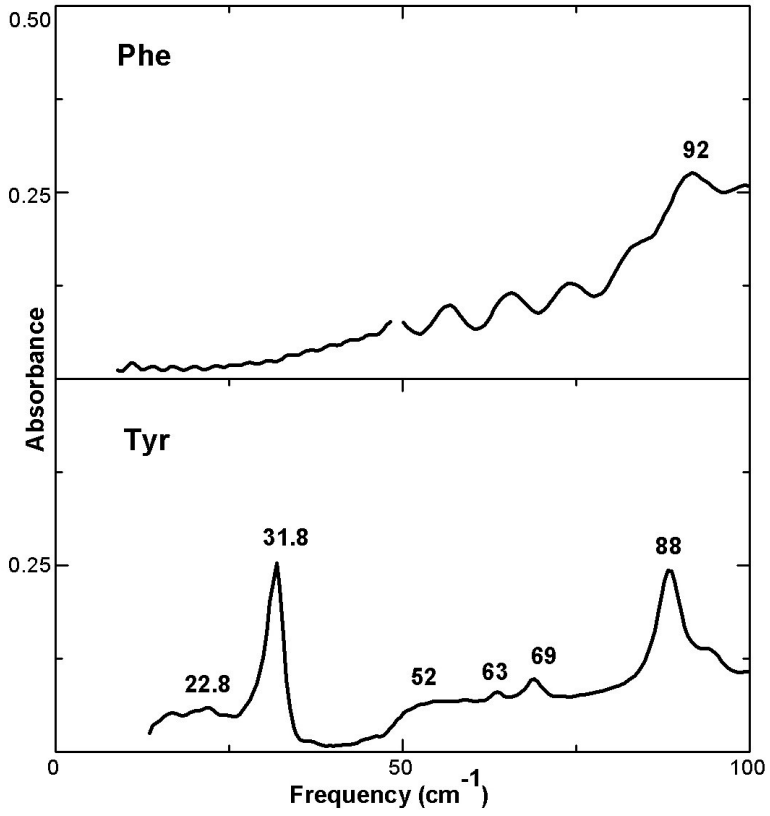

Fig. 4.16 Absorbance spectra of tyrosine and phenylalanine in the region below 50 cm^{-1}.

200-300 cm^{-1} region

Looking at the differences in this range, the first to be noticed is at 248 cm^{-1}. Tyr has here a very strong peak in absorbance, while Phe has a minimum. There is no assignment for this peak in literature.

[Gra2002] presents results of Raman investigations, and they report a line in Tyr at 255 cm^{-1}, which is assigned to the benzene-CH in plane bend. The same vibration was predicted to appear in IR at 325 cm^{-1} by **[Fri1992]**. We assume that this mode is visible in our spectra as a weak shoulder at 318 cm^{-1} in Tyr and at 317 cm^{-1} in Phe.

300-400 cm^{-1} region

There is a prominent peak in Phe, at ~365 cm^{-1}, that has as correspondent in Tyr three peaks of lower intensity, at 310, 335, and 377 cm^{-1}.

Calculations from **[Fri1992]** predicted these last three peaks to appear at slightly different positions. The assignment is the following: torsion ring-OH bond at 302 cm^{-1}, C-H in plane bend at 325 cm^{-1}, and NCC bend at 398 cm^{-1}.

From the prediction we consider that the peak in Phe is a NCC bend coupled with the in plane bend of chain-CH. In **[Xie1999]** is presented the spectrum of poly-L-phenylalanine, showing a strong band at ~350 cm^{-1}. We assume this peak as being the one that appears in Phe at 365 cm^{-1}. The shift in frequency must be due to the chain: the heavier it grows, the lower becomes the vibration frequency (Fig. 4.17).

>400 cm^{-1} region

The band observed in Tyr at 493 cm^{-1} calculated at 480 cm^{-1} in α-poly-L-tyrosine **[Bah1997]**, is a COO^- wag mode with contribution from the ring CCC bending. Its equivalent in Phe is probably the peak at 469 cm^{-1}.

Phe and Tyr have another common peak, situated around 525 cm^{-1} (in Phe at 525 cm^{-1} and in Tyr at 529 cm^{-1}). This is presented in **[Gra2002]** as appearing at 535 cm^{-1}, and is assigned as a benzene mode (16b). We consider that the peak shows also the influence of COO^- modes, like bending, rocking, and wagging, modes which appear in many amino acids, starting with Ala.

For the absorbance peak in Tyr at 650 cm^{-1}, no assignment has been made by now.

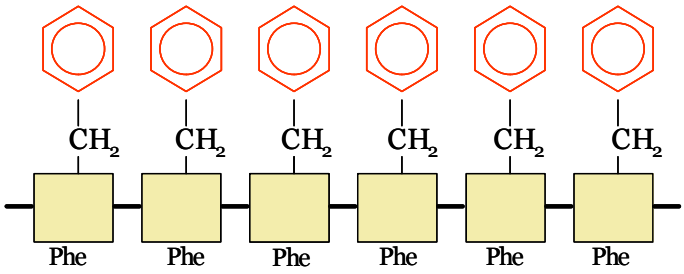

Fig. 4.17. In a phenylalanine chain, the stiffness of the newly formed CN bonds determines a shift of the CCN vibrations to lower frequencies. The yellow square represents the part common to all the amino acids: H_2N-$^{\alpha}$CH- COOH.

4.7 Leucine

Leucine spectrum (Fig. 4.18) presents strong absorbance peaks at 123, ~200, 333, 402, and 536 cm^{-1}. There are a few peaks below 100 cm^{-1}, at 21, 27, 55, and 71 cm^{-1}. They are connected with COO^- torsion, H-bonds deformations, and lattice modes. The band at 536 cm^{-1} is a COO^- rocking mode (**[Paw1996]**), that appears almost unshifted in poly-L-leucine (**[Ito1968]**, **[Ito1969]**). The CCN deformation modes appear between 333 and 444 cm^{-1}.

4.8 Isoleucine

Isoleucine (Fig. 4.19) is the isomer of leucine. It has the typical spectrum of an amino acid: COO^- modes at 538 and 557 cm^{-1}, NH_3^+ torsion at 490 cm^{-1}, CCN deformation modes between 294 and 443 cm^{-1}, and H bonds deformations at 167 cm^{-1}, like in alanine.

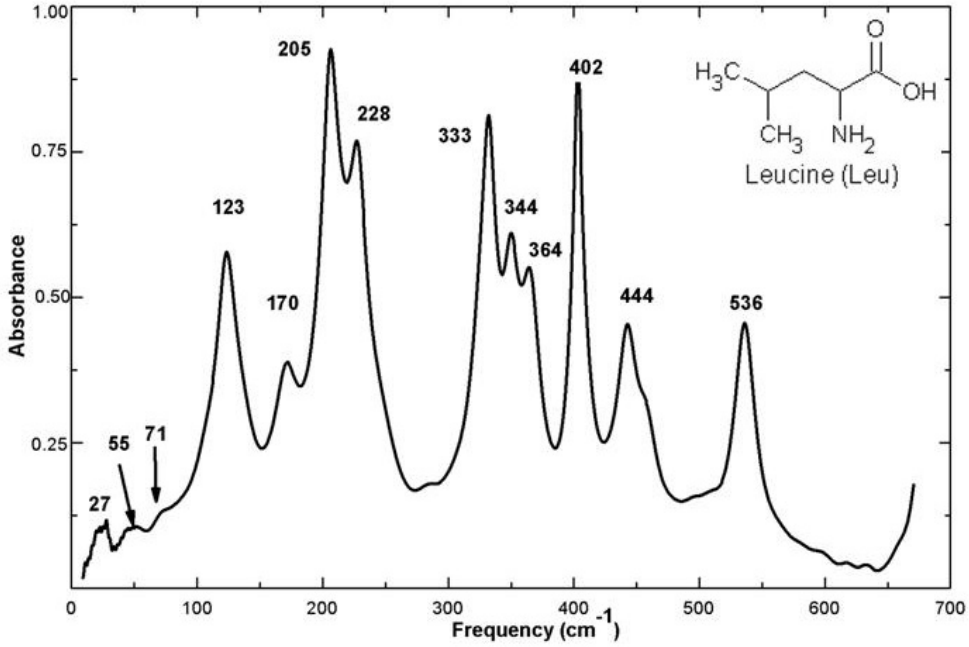

Fig. 4.18. Absorbance spectra of leucine.

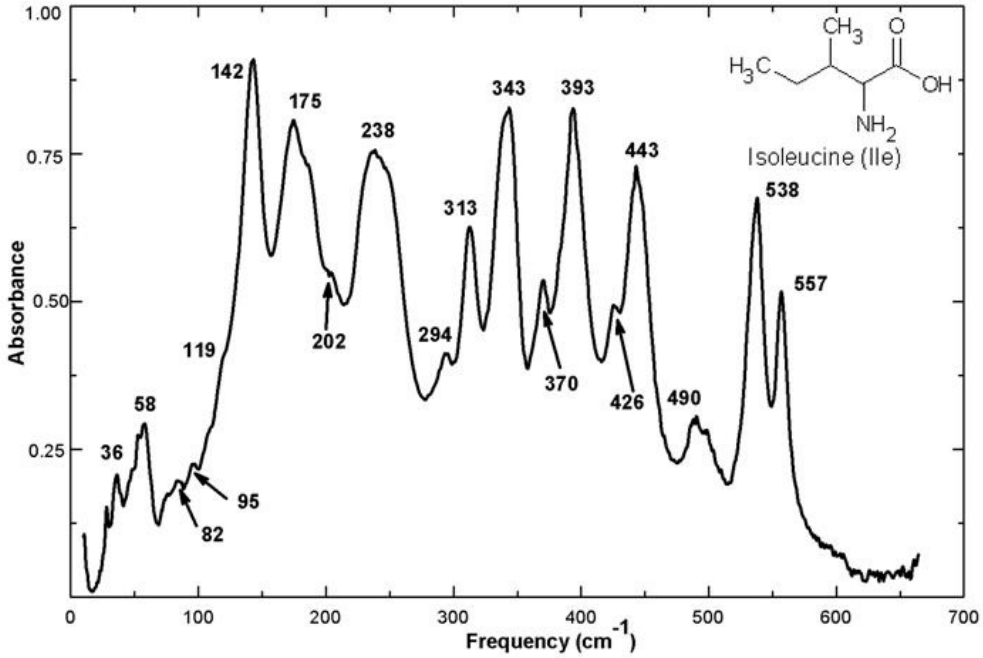

Fig. 4.19 Absorbance spectra of isoleucine.

4.9 Isoleucine and Leucine

One would expect that for two amino acids with similar structure, the absorbance spectra should be similar since they represent the characteristic vibrations of the molecules. This is in fact the case for the mid-infrared spectra of the amino acids. However, the situation is completely different when it comes to the far-infrared frequency range. Our FIR absorbance study reveals that the spectra of the amino acids are very particular and, in fact, they can serve as fingerprints for the molecules. Starting from the established assignment of the bands for glycine and alanine, we can now assign some bands in the spectra of the other amino acids, even if normal mode calculations have not been performed.

Leucine and isoleucine (Fig. 4.20) have four methyl groups in their side chain. Their spectra show some similarities in absorbance not only between them, but also compared with glycine and alanine. Isoleucine has the bands slightly

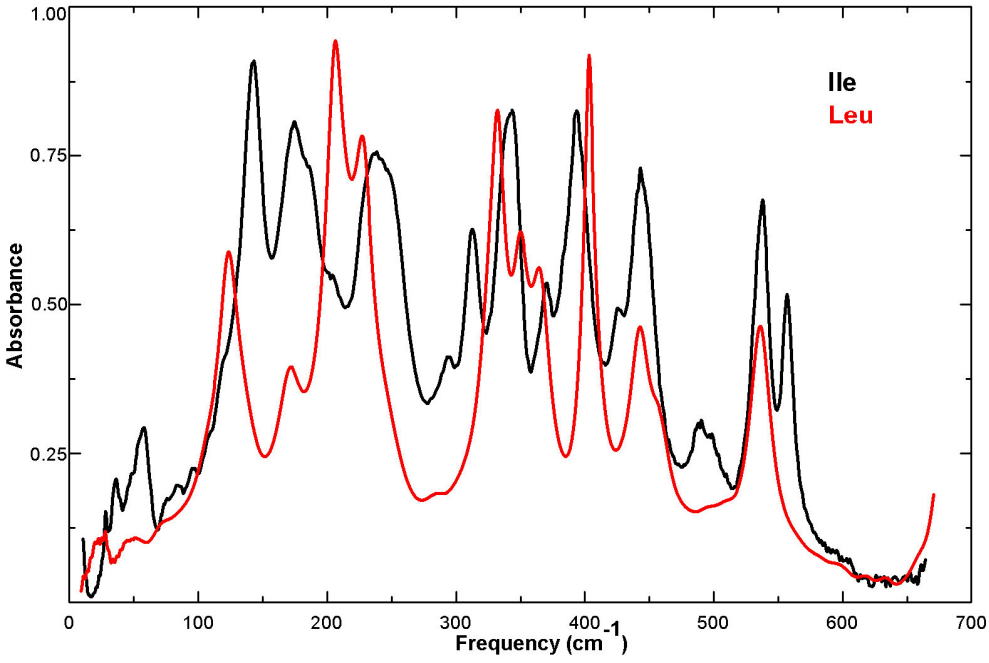

Fig. 4.20 Absorbance spectra of leucine and isoleucine.

displaced to higher frequency, compared with leucine. The shift is bigger below 300 cm^{-1}.

The NH_3^+ torsion mode is not visible in leucine, while it appears very clear in isoleucine at 490 cm^{-1}. The shoulder seen at ~450 cm^{-1} in leucine may be connected to the NH_3^+ torsion.

The three bands of medium intensity in the 300–400 cm^{-1} region in Ile and Leu belong to $CC^{\alpha}N$ and CCC deformations. For both amino acids, the CCN deformations modes appear between 300 and 450 cm^{-1}, as three bands of medium intensity.

Between 200 and 300 cm^{-1} are observed torsions of CH, CH_2, and CH_3 groups (**[Paw1995]**, **[Paw1996]**, **[Paw1997]**). The low-lying strong bands of intramolecular vibrations shift to lower frequencies as the molecule size increases in this group of amino acids; they are found at 142 cm^{-1} for isoleucine and at 123 cm^{-1} for leucine. These absorbance features are assigned to an overlap of hydrogen bond deformations, $CC^{\alpha}N$ deformations, and lattice vibrations.

The pronounced 539 cm^{-1} peak in alanine becomes a doublet at 538 cm^{-1} (rocking mode of COO^-) and 557 cm^{-1} (wagging mode of COO^-) in the isoleucine spectrum, and a band at 536 cm^{-1} in the case of leucine; they are assigned from IINS measurements as COO^- rocking/wagging modes.

4.10 Valine and Isoleucine

Isoleucine is valine with a hydrogen atom replaced by a CH_3 group. The spectra of the two are very much alike (Fig. 4.21 - 4.23, Table 4.2). The CH_3 group behaves as a heavier atom, leaving the valine spectrum almost unchanged.

Absorbance maxima at low frequencies appear in Val and Ile at about the same positions: 40, 55, 75, 95 cm^{-1} in Val, and 49, 58, 82, 95 cm^{-1} in Ile. They have been described as lattice modes in **[Paw1995]**, **[Paw1996]**, **[Paw1997]**.

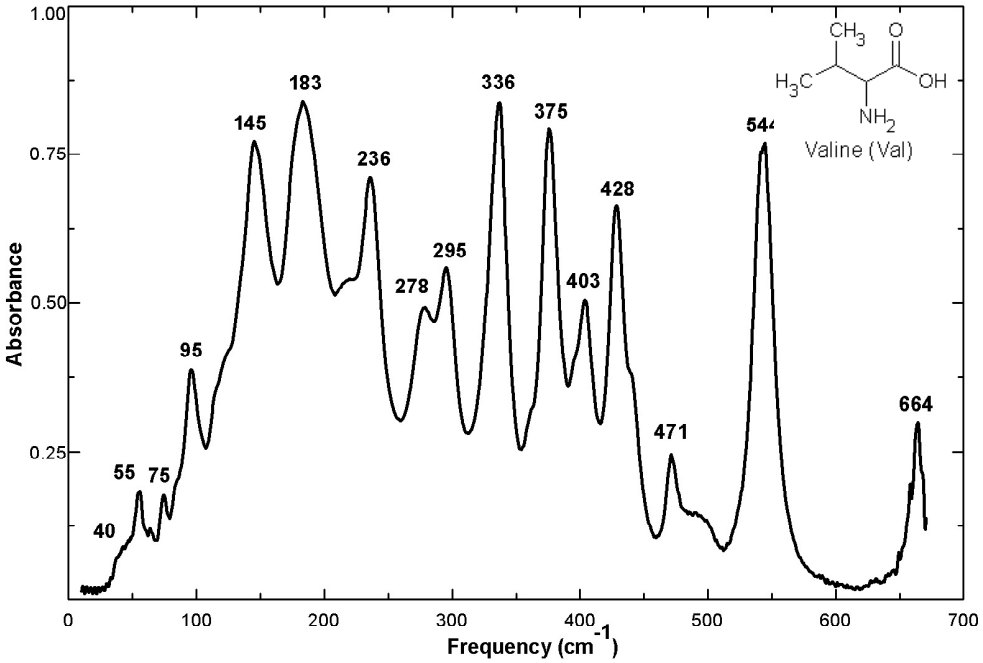

Fig. 4.21 Absorbance spectra of valine.

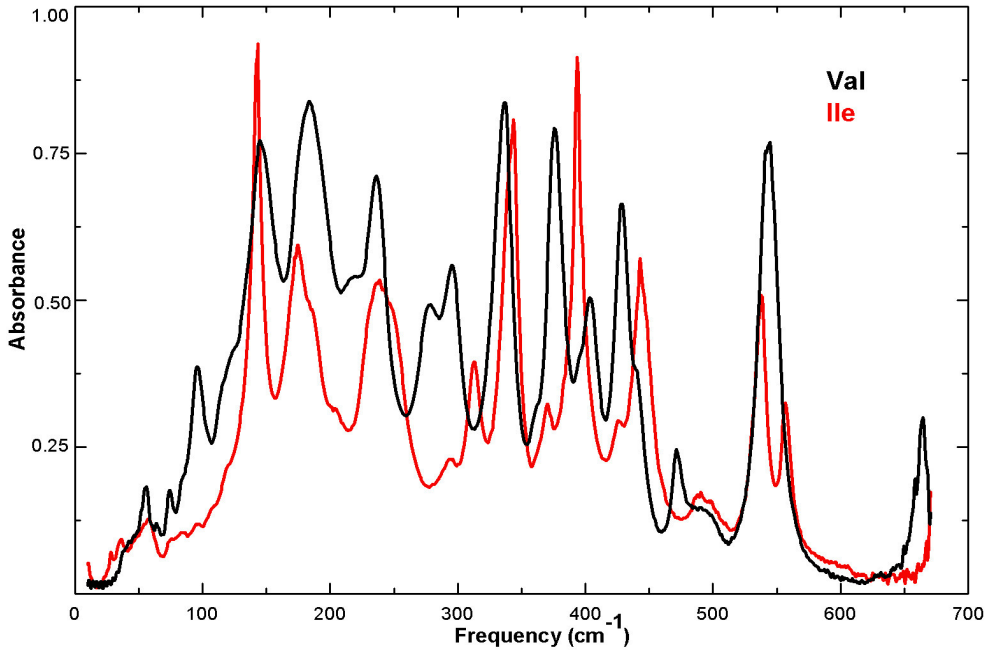

Fig. 4.22 Absorbance spectrum of isoleucine and valine.

Table 4.2 Absorbance frequencies for leucine, isoleucine, and valine.

Leu	Ile	Val	Assignment
21 vw	10 w		Hydrogen bond modes
27 w	28 w		
	36 w		
45 vw	49 w	40 w	
55 w	58 w	55 w	
71 w	82 w	75 w	
	95 w	95 w	
123 s	119 w		
	142 s	145 s	
170 w	175 s	183 s	COO^- torsion
205 s	202 vw		$CH/CH_2/CH_3$ torsion
228 w	238 s	236 s	
		278 w	
	294 w	295 w	
	313 m		$CC^{\alpha}N$ deformations
333 w		336 s	
344 s	344 s		
364 w	370 w	375 s	
402 s	393 s	403 w	
	426 w	428 s	
444 s	443 w		
	490 w	471 w	NH_3^+ torsion
536 s	538 s	544 s	COO^- rock/wag vibrations
		664 w	

Three strong absorbance peaks dominate the low frequency region: at 145 (H bond modes, lattice modes), 183 (COO^- torsion), and 236 (CH torsion) cm^{-1}, which correspond to those seen in Ile at 142, 175, and 238 cm^{-1}.

Torsion of the group COO^- is visible at 175 cm^{-1} in Ile and 183 cm^{-1} in Val.

In the second region of valine spectrum, there are four peaks at 336, 375, 403, and 428 cm^{-1} corresponding to those seen in isoleucine at 344, 370, 393, and 443 cm^{-1} and representing skeletal modes ($CC^{\alpha}N$ and CCC deformations).

The NH_3^+ torsion mode appears in valine at 471 cm^{-1}, displaced to lower frequency compared with isoleucine (490 cm^{-1}).

In the region 500-650 cm^{-1}, there is a peak of high intensity in valine at 544 cm^{-1}. In isoleucine, this last peak is split in two peaks of lower intensity at 538 and 557 cm^{-1}.

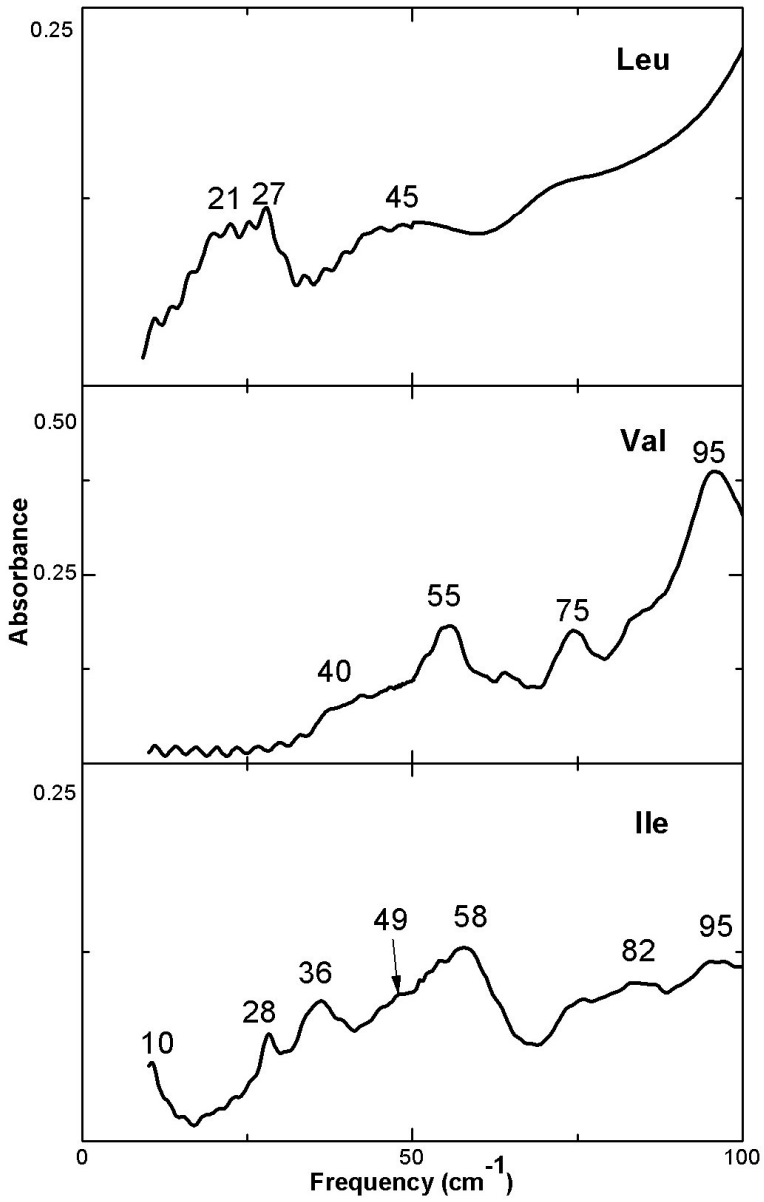

Fig 3.23 Low frequency absorbance of valine, leucine, and isoleucine.

4.11 Phenylalanine, Tyrosine, Histidine, and Tryptophan

This subgroup of amino acids includes the molecules, which have a phenyl ring as a part of the side group (Fig. 4.16, 4.24 - 4.26, Table 4.3).

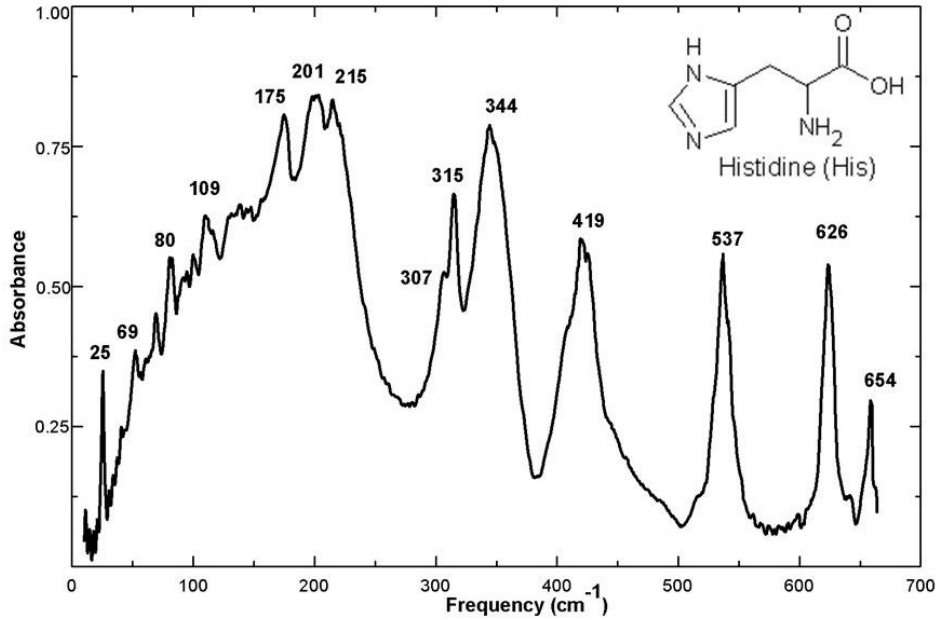

Fig. 4.24 Absorbance spectra of histidine.

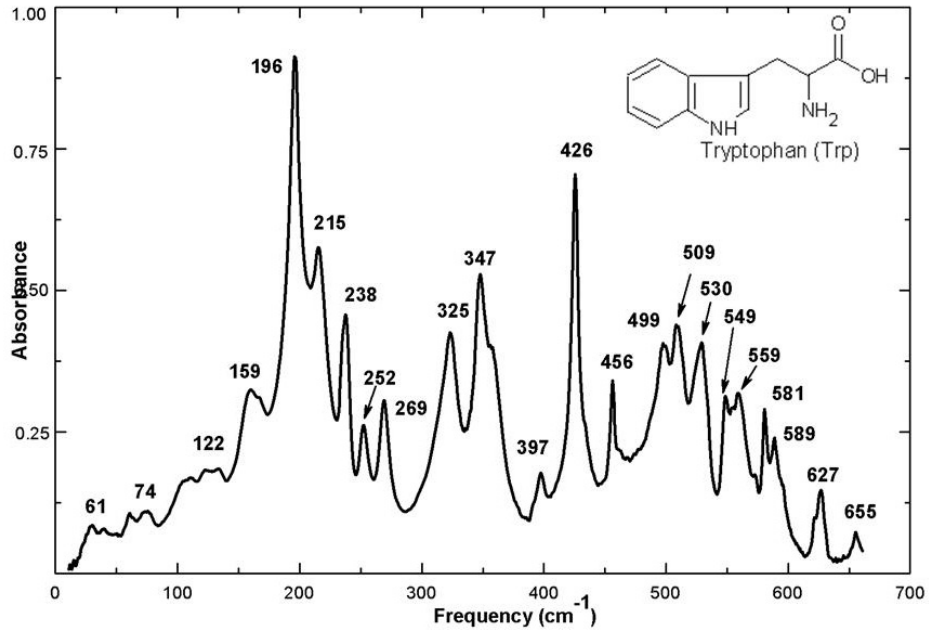

Fig. 4.25 Absorbance spectra of tryptophan.

His	Tyr	Phe	Trp	Assignment
	22.8w			-
25.5 s	31.8 s		28 w	Torsion of entire side chain about C-ring bond
			40.6 w	Hydrogen bond modes
	52 vw		61 w	
69 w	69 w			
80 w	88 w	92 w	74 w	
	111 w			
129 w	116 w		122 w	
	131 w	139 w		
	160 w		159 w	
175 w	171 w			
201 s		195 s	196 s	
215 w	208 w		215 w	
			238 m	COO^- vibrations
	248 s		252 w	
			269 w	
307 w	310 s			$CC^{\alpha}N$ deformations
315 m		317 w	325 m	
344 s	335 w		347 s	
	377 s	365 s		
			397 w	NH_3^+ modes
419 s			426 s	
	433 m			
		469 m	456 w	
	473 w			
	493 m		499 w	COO^- rock/bend/wag vibrations
			509 w	
537 s	529 s	525 s	530 w	
			549 w	
			559 w	
	575 s		581 w	
			589 w	
		605 w		
626 s			627 w	
	639 vw			
654 w	650 s		655 w	

Table 4.3. Absorbance frequencies for tyrosine, tryptophan, phenylalanine, and histidine.

The simplest of them is phenylalanine; it is based on alanine with one H-atom in a side group substituted by a benzene ring.

The attachment of a big mass changes the vibrational spectra considerably. Nevertheless, the spectrum of phenylalanine is surprisingly simple: it exhibits only four peaks above 200 cm^{-1} and three significant maxima in the spectral range below.

Normal modes calculations **[Bah1997]** predicted that there is a band in poly-L-tyrosine at 624 cm^{-1}, which represents a ring mode. We could not identify this mode in tyrosine, but it can be seen in histidine and tryptophan spectra at 626 cm^{-1} and 627 cm^{-1} respectively.

In the low frequency range, three of the amino acids with a phenol group, Tyr, His, and Trp present spectral features under 50 cm^{-1} (Fig. 4.16 & 4.26): in tyrosine at 22.8 and 31.8 cm^{-1}, in tryptophan at 29.5 and 40.6 cm^{-1}, and in histidine at 25.5 cm^{-1}. We assume these minima in transmission as an effect of the phenol ring.

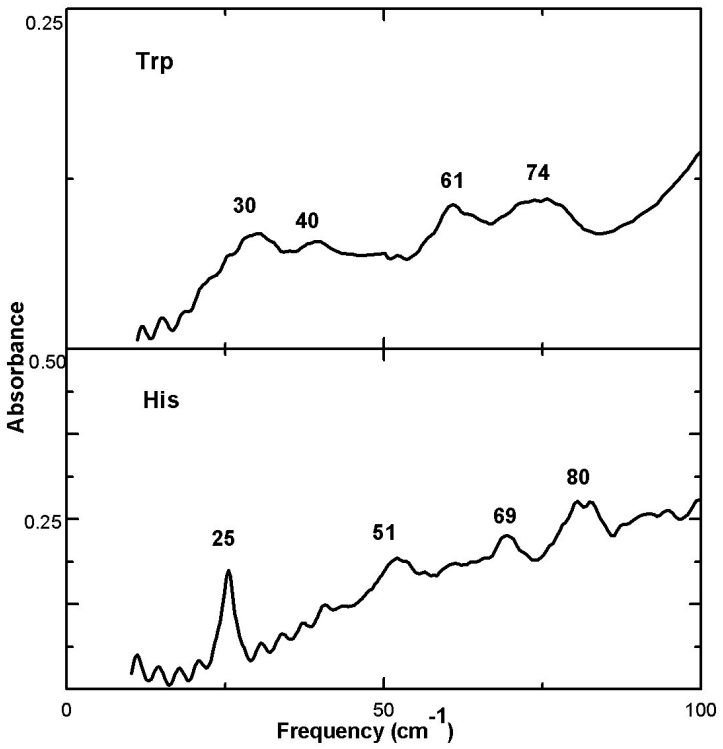

Fig. 4.26. Absorbance spectra below 50 cm^{-1} for His and Trp.

Although the structure and symmetry of phenylalanine and tyrosine are not so much different, the FIR spectra change completely. Tyrosine exhibits more than a dozen almost equally spaced absorbance peaks. From the amino acids of this group, a normal-mode calculation was performed for tyrosine **[Gra2002]**. In our study, we observed the predicted bands; these calculations are also helpful in an assignment of less complicated phenylalanine spectrum.

In Table 4.4, we compare the vibrational frequencies we have measured for tyrosine with the result of normal mode calculations **[Gra2002]**.

In general, the computed values are very close to those observed; this is in particular the case for the comparably strong mode detected at very low frequencies (32 cm^{-1}) and assigned to the torsion of the entire side group **[Gra2002]**. According to the calculations from **[Gra2002]**, the 208 cm^{-1} peak in tyrosine spectra is assigned to a contribution of the C-C-C (backbone) bending the same assignment can be proposed for the strong absorbance feature slightly below 200 cm^{-1} in phenylalanine spectra.

In the 300-400 cm^{-1} region, tyrosine is richer in spectral features than phenylalanine. In the case of phenylalanine, there is a prominent absorbance peak at around 365 cm^{-1}, which in tyrosine corresponds to three peaks of lower intensity, at 310, 335, and 377 cm^{-1}. Normal mode calculations **[Gra2002]** predict the positions of the respective absorbance bands: the torsion ring-OH bond at 302 cm^{-1}, the C-H in plane bend at 325 cm^{-1}, and the $CC^{\alpha}N$ bending at 398 cm^{-1}; the agreement is very good. We assume that the peak observed in phenylalanine is a $CC^{\alpha}N$ bend overlapping with the in-plane bending of the chain-CH; spectroscopic studies on poly-phenylalanine **[Xie1999]** prove an assignment of the 365 cm^{-1} band to the backbone bending vibration.

The only indication for the presence of the phenyl ring seems to be given by the weak shoulders observed at 318 cm^{-1} in tyrosine and at 317 cm^{-1} in phenylalanine. According to the predictions from **[Gra2002]**, we assign them to a phenyl-CH in-plane bend, which is expected at 325 cm^{-1}.

The COO^- group vibrations of phenylalanine are displaced toward lower frequencies compared to alanine (525 and 605 cm^{-1} in phenylalanine, 539, and 647 cm^{-1} in alanine). The same happens with the NH_3^+ vibration: it shifts down in frequency to 469 cm^{-1}.

ν, (cm^{-1}) measured	ν, (cm^{-1}) calculated	Mode
31.8 w	32.63	Torsion of entire side chain about C-ring bond
52 vw	52.72	Torsion of $HOOCNH_2HC$ about chain C-C-bond
63 w	-	-
69 w	68.02	C-H oop bend, in-phase (11)
88 w	87.76	COOH torsion
111 w	-	-
116 w	-	-
131 w	-	-
160 w	163.20	Amino torsion
171 w	-	-
-	199.07	Distal chain C-C-C bend
208 w	210.29	Proximal chain C-C-C bend
248 s	-	-
-	297.49	O=C-C and H_2N-C-C bends, in-phase
310 s	302.08	Ring OH torsion
335 w	325.39	C-H ip (trigonal) bend (15)
377 s	393.76	N-C-C bend (w/proximal C-C-pair)
433 m	434.79	C-H oop bend (C_6 libration) (10b)
473 w	461.25	C-H ip bend (9b)
493 m	483.98	C-C-C oop bend (16a)
529 s	518.73	Carboxyl HO-C-C bend
575 s	559.94	C-C-C ip bend (6a)
-	610.14	C-C-C oop bend (16b)
639 vwsh	627.90	Carboxyl OH torsion
650 s	-	-

Table 4.4. Absorbance frequencies for phenylalanine. The first column indicates our results; the second and the third column are from **[Gra2002]**.

4.12 Glutamic Acid and Aspartic Acid

The overall-shape of the glutamic acid spectrum (Fig. 4.27 & 4.31) resembles that of glycine. It also consists of four wide bands, which fall in the same spectral regions: one at 100–250 cm^{-1} with a maximum at 227 cm^{-1}, the second one between 300 and 450 cm^{-1} with a maximum at 376 cm^{-1}, and finally two bands located at 503 and 536 cm^{-1}. The absorbance bands observed in glutamic acid (Fig. 4.27, Table 4.5) are in general wider and have some structure, in contrast to the glycine spectrum. The low-lying band has the same origin as in glycine, i.e. it is governed by hydrogen bonds, but there is much more structure on the low-frequency side. A very pronounced mode is observed at 39 cm^{-1} which is a COO^- torsion coupled with a CC torsion **[Ram1995]**. The same type of vibrations is found at 55 cm^{-1}. Following the results from **[Nav1994I]** we consider the wide band with a maximum at around 400 cm^{-1} as due to the backbone deformation: a CC torsion at 416 cm^{-1}, at 402 cm^{-1} a bending of CCC group. The same type of vibrations appears around the point 500 cm^{-1}: CC torsion at 511 cm^{-1} and CCC bending at 503 cm^{-1}.

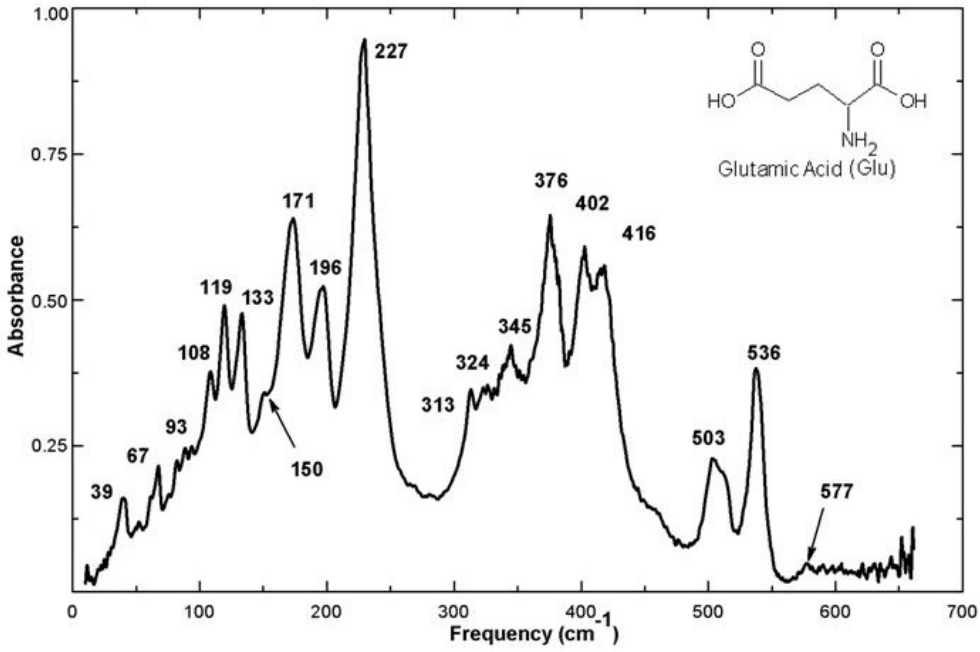

Fig. 4.27 Absorbance spectra of glutamic acid.

The absorbance peak at 503 cm^{-1} was lately **[Ram1995]** assigned as an OH torsion following normal mode calculations. We incline not to believe this result, as this mode does not appear either in aspartic acid or in glutamine and asparagine. According to our assignments above, these bands above 500 cm^{-1} represent deformations of the COO^- group: in plane bending of COO^- at 577 cm^{-1}, at 539 COOH out of plane bending **[Nav1994]**.

The NH_3^+ torsion mode common for all amino acids is visible at 463 cm^{-1}.

The absorbance spectrum of aspartic acid (Fig. 4.28 & 4.31) exhibits similar features: three well-defined bands, which have a certain structure. We can safely assume that these wide bands have the same origin like in glutamic acid. The NH_3^+ torsion mode appears in aspartic acid at 449 cm^{-1}. Bands measured at 657, 553 are identified as COOH in plane bending **[Nav1994II]**. The same reference assigns the 599 cm^{-1} peak as a COO^- bending vibration. The COO^- modes are not very stable in amino acids, and they can appear at quite different frequencies, as in the case of glycine (502 cm^{-1}). The COO^- torsion mode appears in Raman at 187 cm^{-1} **[Nav1994II]** and in IR at 177 cm^{-1}. Between 214 and 414 cm^{-1} are dominating the torsions and deformations of the CCN group.

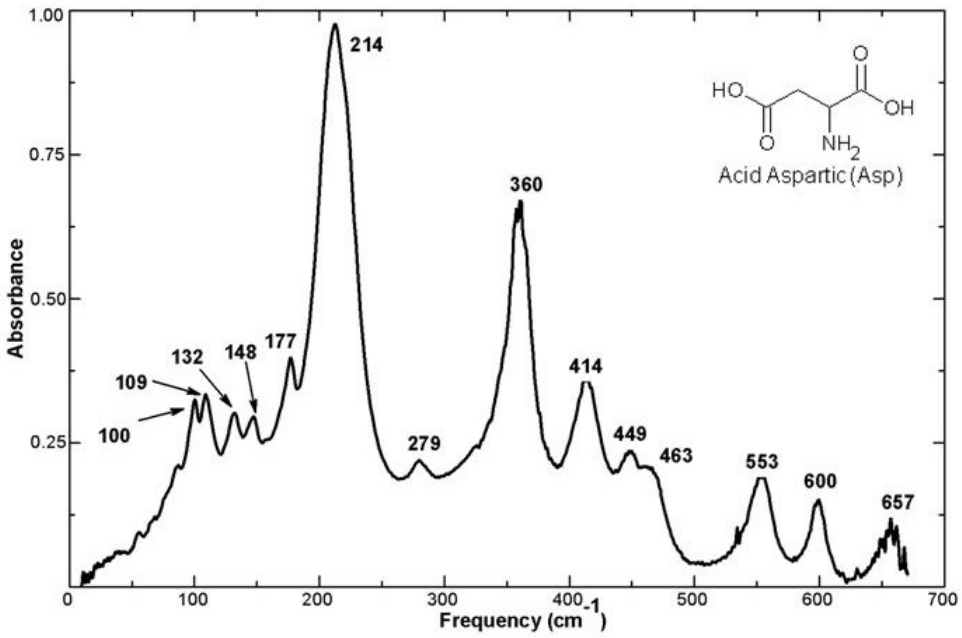

Fig. 4.28 Absorbance spectra of aspartic acid.

4.13 Glutamine and Asparagine

Asparagine and glutamine (Fig. 4.29 - 4.31) present a common feature at about 539 cm^{-1}. This absorbance peak was by now assigned to a NH_3^+ torsion **[Cas1995]**. One of the reasons for such an assumption was that both amino acids have a NH_3^+ group in the side chain. However, this feature appears in glutamic acid at almost the same point, 536 cm^{-1}, and in aspartic acid at a little higher frequency (553 cm^{-1}). We cannot decide if this is only a NH_3^+ torsion or if we deal with a COO^- vibrational mode, of the same type like in glycine **[Tsu1958]**. It is reasonable to assume that it is an overlapping of both.

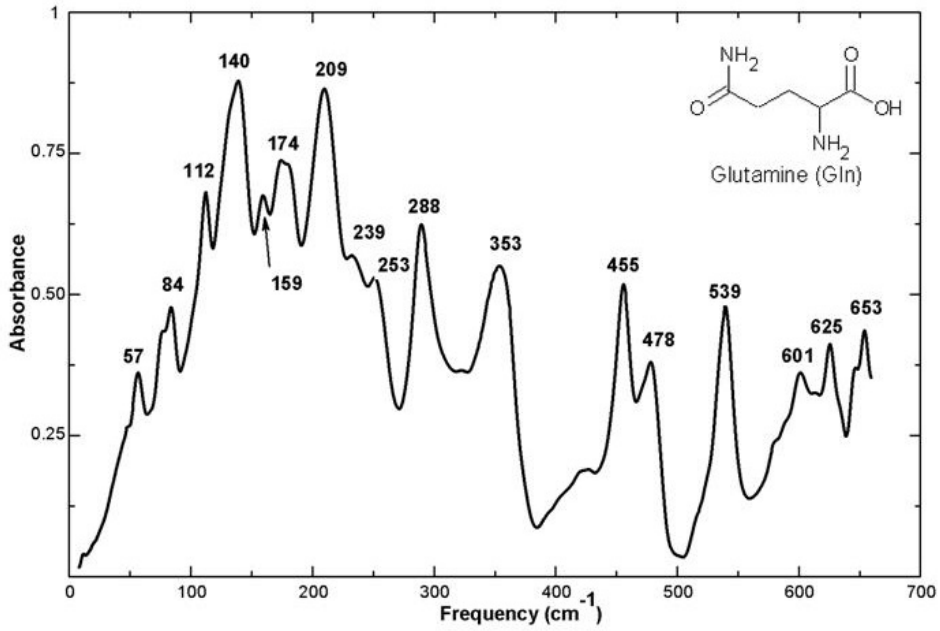

Fig. 4.29 Absorbance spectra of glutamine.

The NH_3^+ torsion mode appears in glutamine at 455 cm^{-1}, and at 456 cm^{-1} in asparagine. The assignment was made following previous results obtained for alanine (NH_3^+ torsion mode at 477 cm^{-1} **[Bel1975]**) and cysteine (NH_3^+ torsion mode at 498 cm^{-1} **[Sus1983]**).

Between 550 and 660 cm^{-1} there are three peaks assigned as follows: at 653 cm^{-1} a CCN out-of-plane bending, at 625 cm^{-1} a COO^- bending, and at 601

cm^{-1} a NH_3^+ bending **[Dha1993]**, **[Bel1975]**. In the same region the glutamic acid spectrum shows no feature.

Other modes are assigned as follows: NH_3^+ torsion at 537 cm^{-1}, NH_3^+ torsion at 477 cm^{-1}, and skeletal bending at 455 cm^{-1} **[Dha1993].**

At lower frequencies, the spectra become more specific for each molecule and only a few general features can be extracted. As a rule, a strong absorbance maximum due to a backbone deformation, probably coupled with other molecular vibrations is present in the 300-400 cm^{-1} range. A wide intensive band with a maximum at about 200 cm^{-1} is also observed in all of the four spectra. It is formed by an overlap of vibrations of H-bonds and complicated molecular vibrations involving COO^- torsion, NH_3 torsion $CC^{\alpha}N$ deformation. With increasing size of a molecule, the bands split into a larger number of small peaks.

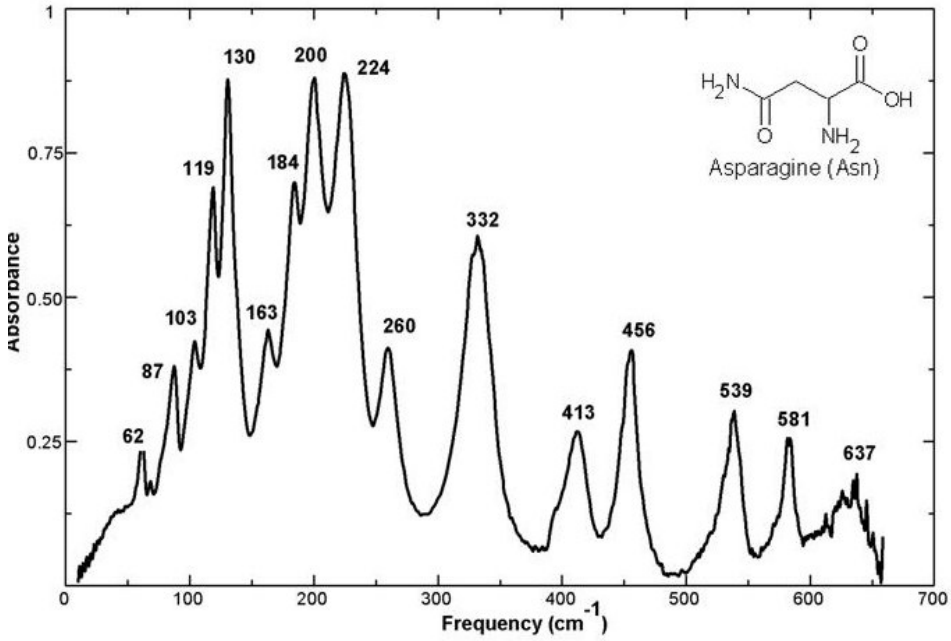

Fig. 4.30 Absorbance spectra of asparagine.

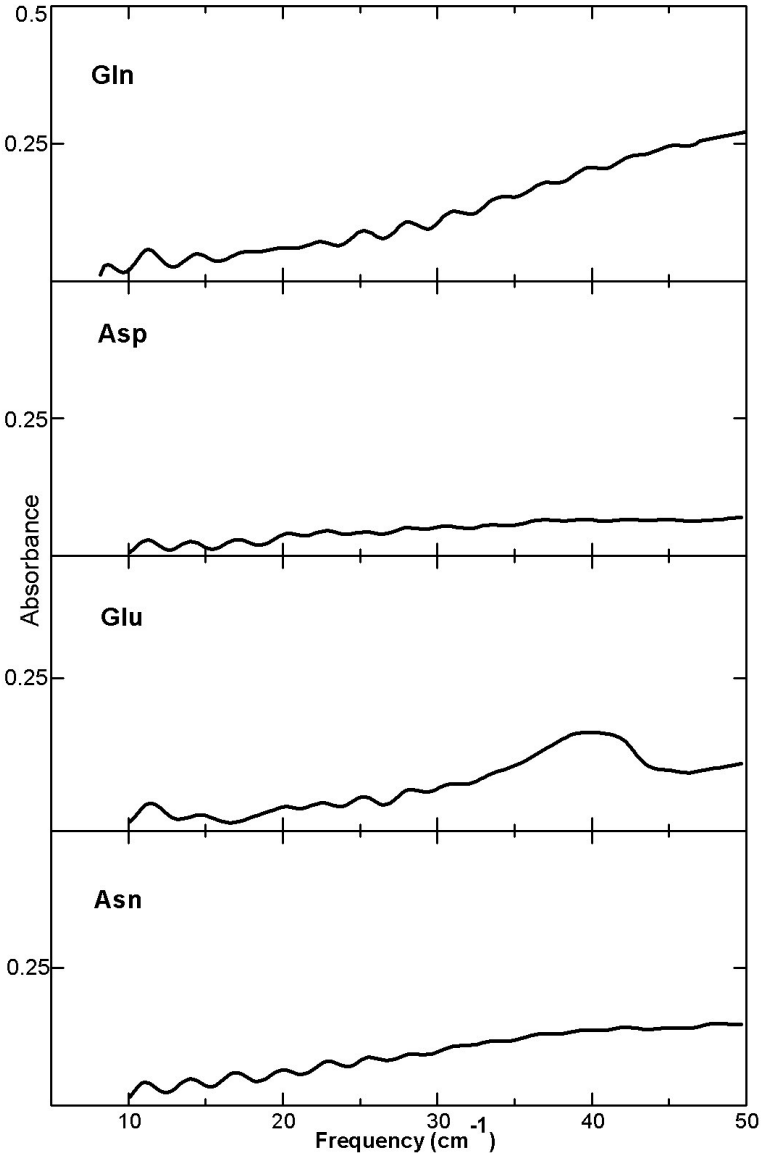

Fig. 4.31 Low frequency spectra for glutamine, asparagine, glutamic acid, and asparagine.

Asp	Glu	Gln	Asn	Assignment
	11 w			-
	39 w			COO^- torsion + CC torsion
57 w	55 w	57 w		CC torsion + COO^- torsion
	67 w		62 w	Hydrogen bond modes
	82 w	76 w	87 w	
	89 w	84 w		
	93 w			CC torsion
100 w			103 w	Hydrogen bond modes
109 w	108 w	112 w		
	119 s		119 w	
132 w	133 w	140 s	130 s	
148 w				
	150 w	159 w	163 w	
177 w	171 s	174 w	184 w	CCC bending + CC torsion + NH_3^+ torsion
	196 w	209 s	200 s	CCC bending + NH_3^+ torsion
214 s	227 s	239 w	224 w	CCC bending + NH_3^+ torsion + CC torsion
279 w		253 w	260 w	COO^- vibrations
	313 w	288 s		$CC^{\alpha}N$ bending + CCC bending CC torsion
	324 w			
	345 w		332 s	
360 s	376 s	353 s		
414 m	402 w			
	416 w			
			413 w	NH_3^+ torsion
449 w	463 w	455 s	456 s	
		477 w		
	503 m			OH torsion
553 w	537 s	537 s	539 m	COO^- vibrations
	577 w		581 m	
600 w		601 m	637 w	NH_3^+ bending
657 w				COO^- bending
		625 m		
		653 m		$CC^{\alpha}N$ out-of-plane bending

Table 4.5. Vibrational frequencies for asparagine, aspartic acid, glutamine, and glutamic acid in the frequency range 10-650 cm^{-1}.

4.14 Threonine

Making use of the knowledge about the previous amino acids, one can make assignment for methionine, serine, and threonine as well. The vibrational frequencies of these three amino acids are presented in the Table 4.6.

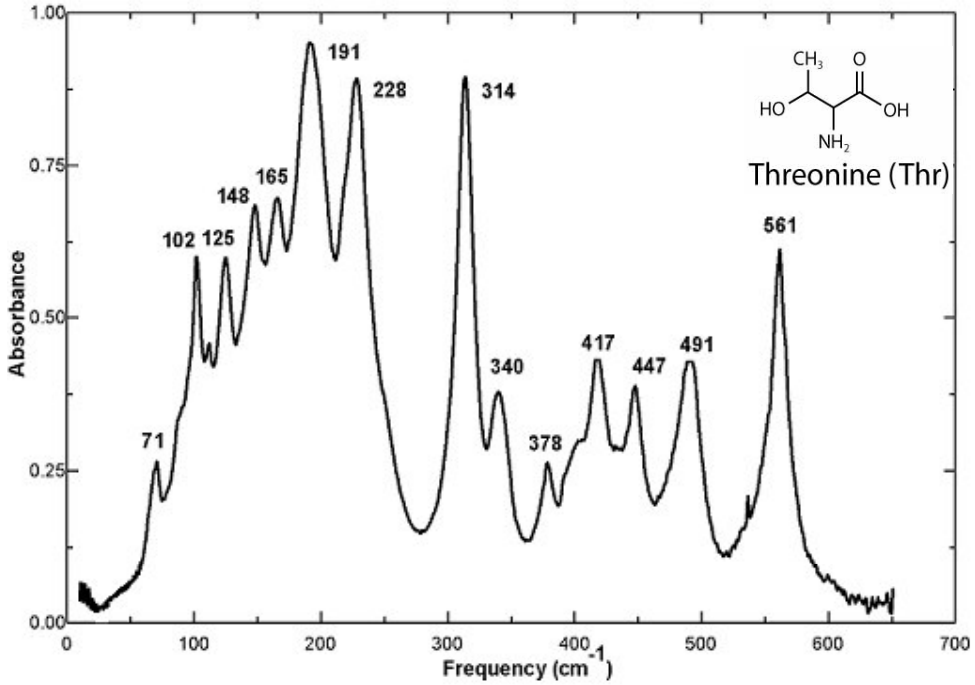

Fig. 4.32 Absorbance spectra of threonine.

For threonine (Fig. 4.32 & 4.33), two COO^- torsion modes have been calculated at ~50 and ~80 cm^{-1} **[Paw2001]**. In the present measurements one of these modes is visible at 71 cm^{-1}. The neighbour peaks at 191 and 228 cm^{-1} have been calculated as CCC bending modes. At ~230 cm^{-1} a CH_3 torsion mode is expected in **[Paw2001]**, but does not appear in the measurement. The modes between 314 - 417 cm^{-1} represent mainly deformations of the backbone group, but also contributions from the OH torsion. The band situated at 417 cm^{-1} represents torsion of the $CC^{\alpha}N$ structure. The torsional mode of NH_3^+ appears at 447 cm^{-1}. The rocking of COO^- appears at 561 cm^{-1}. The wagging of the COO^- group appears at higher frequency **[Sil1998]**.

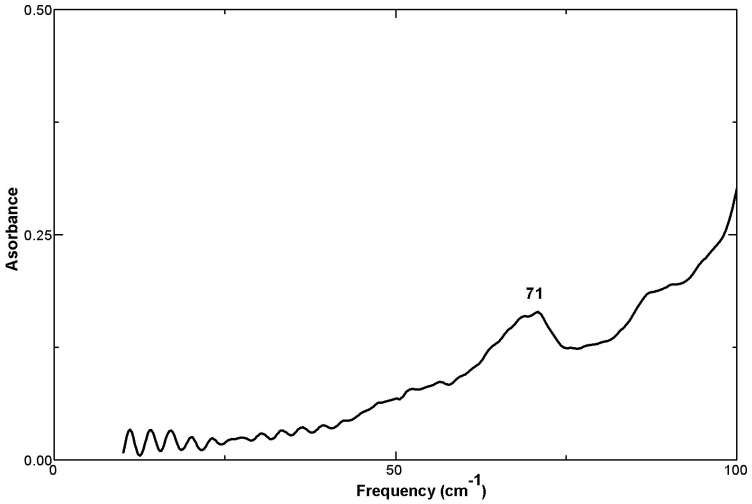

Fig. 4.33 Absorbance spectra of threonine at low frequency.

Met	Thr	Ser	Assignment
37.4 w		38 w	Hydrogen bond modes
	71 w	64 s	
	102 m	140 s	
	125 w		
	148 w		
129 w	165 w		
160 w	191 s	172 w	
203 s			
	228 s		COO^- vibrations
		251 s	
284 m	314 s	299 s	$CC^{\alpha}N$ deformations
335 w	340 m		
364 w		366 s	
	378 w		
417 s	417 m		
448 w		431w	NH_3^+ modes
	447 w		
	491 s		COO^- rock/bend/wag vibrations
546 s		524 m	
	561 s	563 w	
		605 m	
643 w		638 w	
654 w			

Table 4.6. Vibrational frequencies for methionine, threonine, and serine in the frequency range 10-650 cm^{-1}.

4.15 Methionine

For the experimental assignment for methionine (Fig. 4.34 & 4.35), we compared our data with previous results **[Gru1987]** above 400 cm^{-1}.

Some assignments were deduced from comparison of the spectra of different conformers of L-methionine with the spectra of the derivatives DL-methionine, C-D_3, and N-D_3. Accordingly, we consider the vibrations at 654, 643 cm^{-1}, and 546 cm^{-1} to be COO^- modes, the one at 448 cm^{-1} as NH_3^+ torsion, and a $CC^{\alpha}N$ at 417 cm^{-1}. Moreover, we incline to believe that the absorbance maxima at 364 and 335 cm^{-1} represent also the behaviour of the $CC^{\alpha}N$ group.

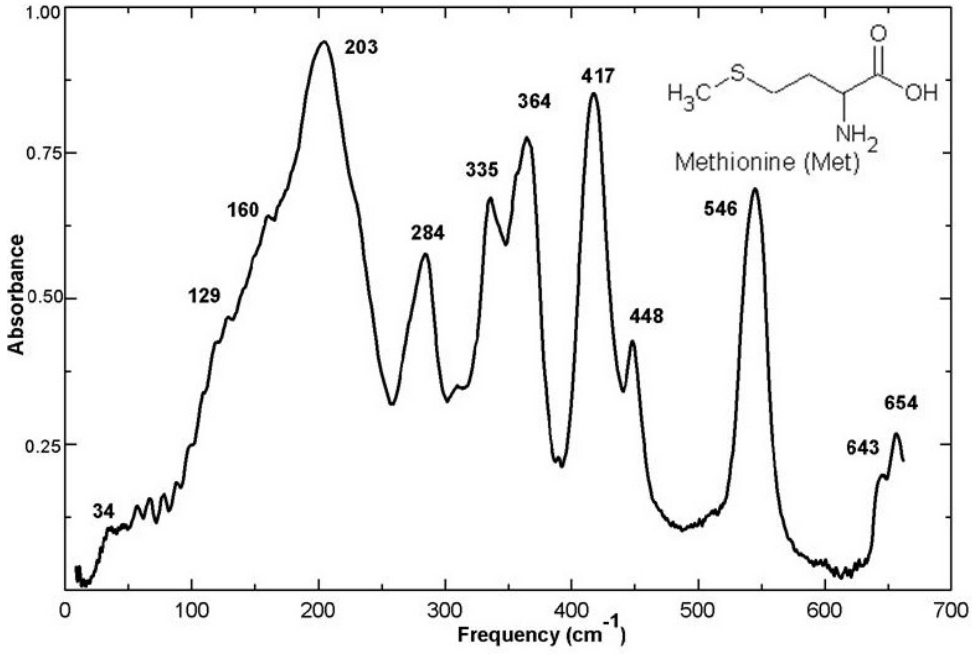

Fig. 4.34 Absorbance spectra of methionine.

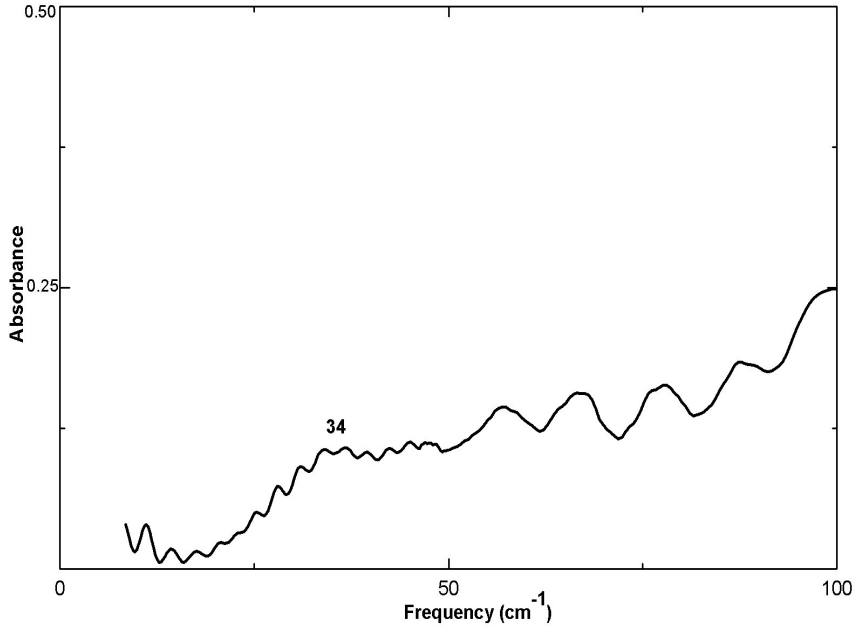

Fig. 4.35 Absorbance spectra of methionine at low frequencies.

4.16 Serine

In the case of serine (Fig. 4.36 & 4.37), theoretical studies as well as experimental do not always agree with each other. In Table 4.7 are compared the results from different references with those that we obtained.

In **[Tak1995]**, for example, are evaluated the vibrational frequencies for serine at 300, 369, 525, and 608 cm^{-1} only, which makes for a rather incomplete result.

In **[Mac1979]**, an OH torsion is calculated at 295 cm^{-1}, but the authors fail to detect it in IR measurements. Our measurements are more successful from this point of view, and we observe an absorbance peak at 299 cm^{-1}. However, there is a problem arising: which is the correct assignment for this value? According with a more recent study **[Paw2002]** at 299 cm^{-1} is visible a CCC bending. The reason for this assignment is that the peaks in the IINS spectrum of L-serine in the range from 200 to 700 cm^{-1} are much stronger than those appearing in the spectrum of deuterated L-serine. In particular, the intensities at 193, 261, 299, and 362 cm^{-1} reduce drastically when hydrogen is

replaced with deuterium, which is an indication for the large contribution of amino group vibrations. The authors conclude that in this region are visible the deformation vibrations of CCC, CCN, NCC and COO^- groups mixed with torsional vibrations of the carboxylic and amino groups. Our assumption is that to the peak at 299 cm^{-1} corresponds not only the vibration of the CCN backbone that is omnipresent in amino acids, but also OH torsion from the side chain. To our knowledge, the absorbance peak from 299 cm^{-1} (295 cm^{-1} in calculations, 299 cm^{-1} in IINS) is for the first time reported in an IR measurement.

In the case of serine the lattice vibrations are observed at lower frequencies than those of glycine and alanine. The highest lattice vibration is calculated to appear in DL-serine at 138 cm^{-1} **[Mac1979]** (Table 4.7). We could not detect the NH_3^+ torsion at 430 cm^{-1}.

In this study, we managed to observe for the first time in an IR experiment the OH torsion at 430 cm^{-1}, which is coupled with a hydrogen bond torsion **[Paw2002]**.

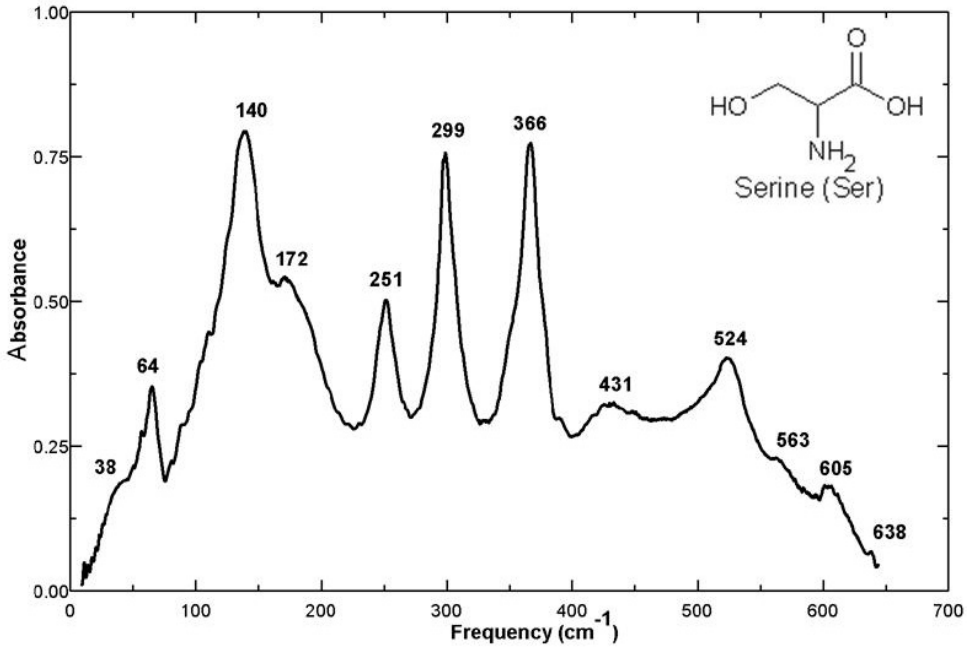

Fig. 4.36 Absorbance spectra of serine.

Exp. data	Assignment [Mac1979]	IR exp. [Mac1979]	IR calculated [Mac1979]	IR DL-serine [Wri1939]	IR exp. [Sus1983]	IR calc. [Sus1983]	Assignment [Sus1983]	IINS [Paw2002]	Assignment [Paw2002]
638 w	CO_2 bend.	617	641	620	618	622	CO_2 bend.	620	CO_2 bend.
604 m	-	-	-	-	-	-	-	-	-
564 w	CCO def.	559	573	567	566	560	-	576	CO_2 wagg.
-	-	-	-	561	-	-	-	-	-
524 w	CO_2 rock.	525	527	528	525	530	-	521	CO_2 rock.
-	NH_3 tor.	499	495	502	499	487	NH_3 tor.	-	-
-	-	-	-	-	-	-	-	494	NH•••O torsion
-	-	-	-	-	-	-	-	475	NH•••O torsion
430 w	-	-	-	-	-	-	-	442	OH tor. + NH•••O torsion
366 s	CCN def.	383 324	374 342	-	-	370	-	362	NCC bend.
299 s	OH tor.	-	295	-	-	-	-	299	CCC bend.
251 s	CCC def.	228	228	-	-	-	-	261	CCN bend.
172 w	CO_2 tor.	-	202	-	-	-	-	193	CCO bend.
140 s	CH_2OH tor.	-	142	-	-	-	-	100	CC torsion
64 s	-	-	-	-	-	-	-	55	CO_2 tor.
38.6 w	-	-	-	-	-	-	-	-	-

Table 4.7. Experimental and theoretical data for serine absorbance.

In our measurements, there are only two lattice vibrations visible: at 38 and 64 cm^{-1}. Another distinct characteristic of the serine spectrum is the CH_2OH torsion that was predicted by above mentioned calculations to appear at 142 cm^{-1} and can be observed in our measurements (for the first time) at 140 cm^{-1}. Considering that the lattice modes in amino acids appear below 200 cm^{-1}, we think that the mode at 140 cm^{-1} could represent also an external vibration.

Another torsion of the OH group appears at 564 cm^{-1}. This peak was calculated for poly-L-serine at 563 cm^{-1} **[Gup1997]**, which is the range of the OH wagging mode in other polymers, like poly(vinyl alcohol) **[Zbi1969]**. The CCC deformation expected at 228 cm^{-1} in DL-serine appears in our measurements at 251 cm^{-1}.

We assign the peak from 172 cm^{-1} to be a COO^- torsion, which was expected to appear at 202 cm^{-1} **[Mac1979]**. Other spectral features present in our measurements and typical for amino acids are: CCC deformation at 251 cm^{-1}, CCN deformation at 366 cm^{-1}, COO^- rocking at 524 cm^{-1}, COO^- rocking at 604 cm^{-1}, and COO^- bending at 638 cm^{-1}.

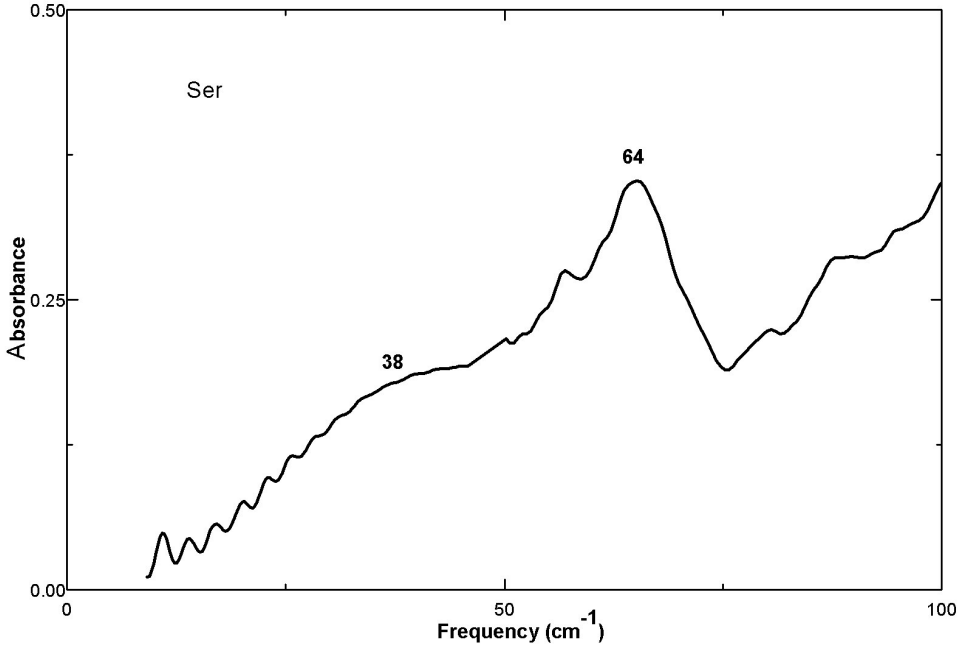

Fig. 4.37 Absorbance spectra of serine at low frequency.

4.17 Proline

Proline is an atypical amino acid, because it has a cyclic form, where the side chain binds to the NH_3^+ group. In the circumstances, not all of the regular vibrational modes for amino acids will appear in the spectrum (Fig. 4.38 & 4.39). We will compare proline spectrum with that of alanine (Fig. 4.11), the first amino acid that shows distinct all the COO^- modes.

A ring torsion mode has been calculated **[Gup1977]** for proline oligomers $(L\text{-}Pro)_n$, with n = 2, 3, 4, 5, 6, 8) between 527 and 550 cm^{-1}. Proline spectrum has a single band between 500 and 600 cm^{-1} that can be associated with the ring mode mentioned above.

One can see that the COO^- rocking/ bending/ wagging that are present in Ala, are also visible in Pro, at 644 cm^{-1} **[Rev1994]**. We believe that the bands at 205 and 246 cm^{-1} are the COO^- torsion that appears in Ala at 216 and 258 cm^{-1}.

At 454 cm^{-1} is visible a ring out-of-plane bending **[Rev1994]**.

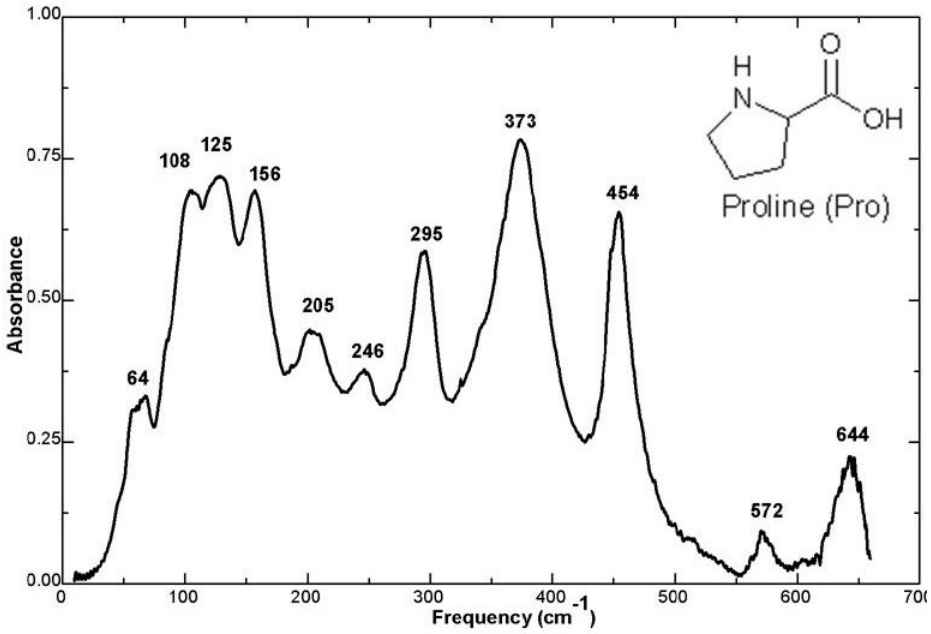

Fig. 4.38 Absorbance spectra of proline.

Below 100 cm^{-1}, proline shows absorbance maxima at 42, 56, and 65 cm^{-1}.

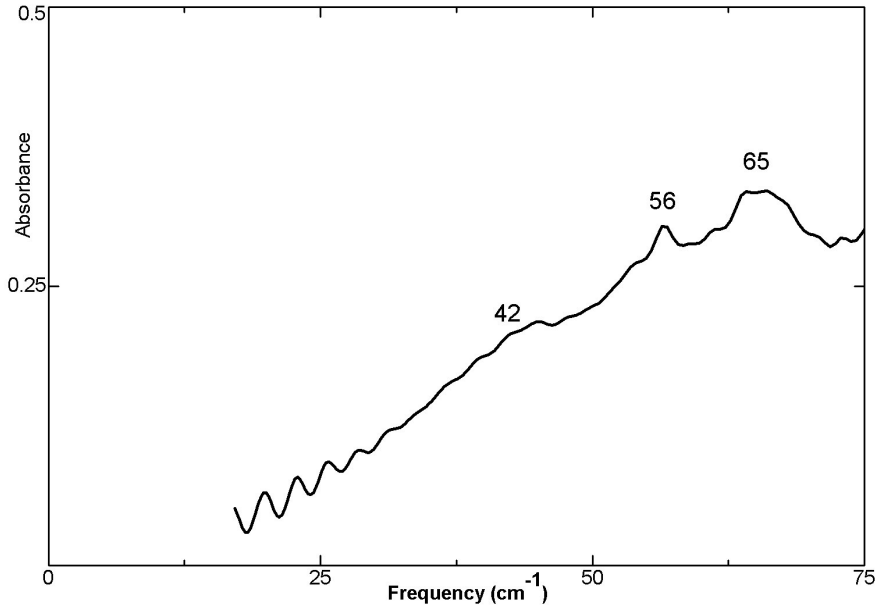

Fig. 4.39 Absorbance spectra of proline at low frequency

4.18 Lysine

Lysine has the longest side chain of all the amino acids.

Its absorbance spectrum is dominated by the strong and broad peak at 225 cm^{-1} (Fig. 4.40 & 4.41, Table 4.8).

Below 50 cm^{-1}, there are three absorbance maxima: at 22, 28, and 36 cm^{-1}.

Using the information from the other amino acids, we assign the peaks in absorbance at 322 and 356 cm^{-1} as backbone modes, the peak at 483 cm^{-1} as NH_3^+ torsion mode, and the one at 551 cm^{-1} as a COO^- mode.

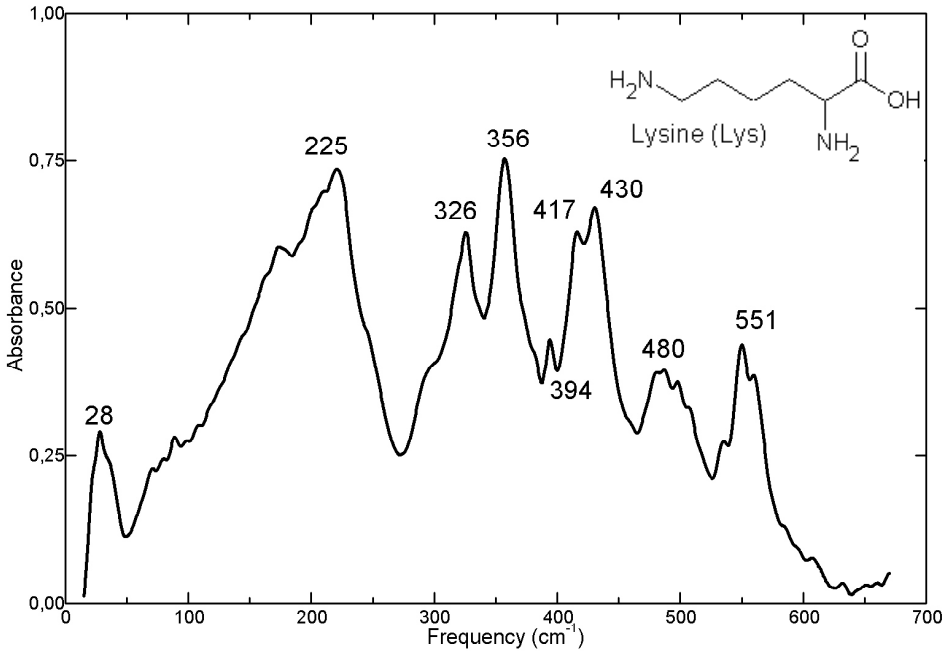

Fig. 4.40 Absorbance spectra of lysine.

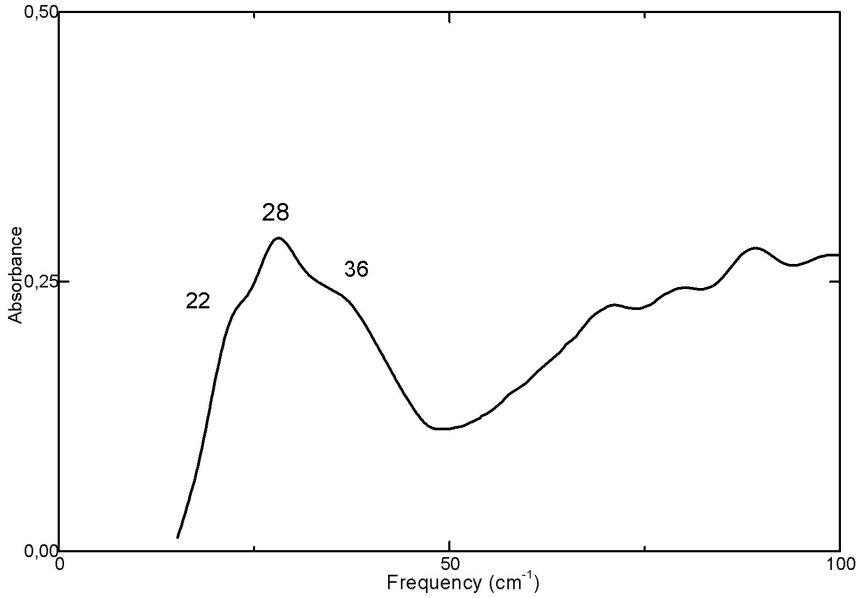

Fig. 4.41 Absorbance spectra of lysine at low frequency.

Pro	Lys	Assignment
	22 w	Hydrogen bond modes
	28 w	
	36 w	
42 w		
56 w		
65 w		
108 w		
125 s		
156 w		
	225 s	
205 w		COO^- vibrations
246 w		
	326 m	$CC^{\alpha}N$ deformations
	356 s	
	394 w	
	417 w	NH_3^+ modes
454 s	430 s	
	480 w	
	551 w	COO^- rock/bend/wag vibrations
572 w		
644 w		

Table 4.8 Vibrational frequencies for proline and lysine in the frequency range 10-650 cm^{-1}.

4.19 The statistics

After looking at all the spectra, one can conclude upon the absorbance bands that these amino acids have in common. There are four categories of vibrational modes that are present in all amino acids: the H bond, CCN, NH_3^+, and COO^- modes. Figure 4.42 shows at which frequencies is more probable to have strong absorbance in the spectrum of an amino acid. The frequency domain is divided in a few regions, one for each category of predominant vibration. Each bar spans 20 wavenumbers. The height of a bar is a measure for the number of peaks that appear in the region[22].

[22] This does not mean that a peak in the region 270-380, for example, comes only from a CCN deformation. Usually there are more contributions to an absorbance maximum.

The region below 200 cm^{-1} belongs to the H bond modes. They are not always very pronounced at room temperature, but become more visible as the temperature is decreased (ex. **[Ban1983]** for alanine).

Other vibrations appear here as well: the lattice vibrations, the backbone deformations, and the vibrations of the ending groups NH_3^+ and COO^-. These are less intense than the hydrogen bonds. However, the question "what is the lowest frequency where the H bonds appear ?" is still open.

Around 270 – 380 cm^{-1} the most visible vibrations are the CCN deformations. The NH_3^+ modes appear around 380-480 cm^{-1}, and the COO^- modes – at frequencies above 480 cm^{-1}, as well as between 220 and 300 cm^{-1}.

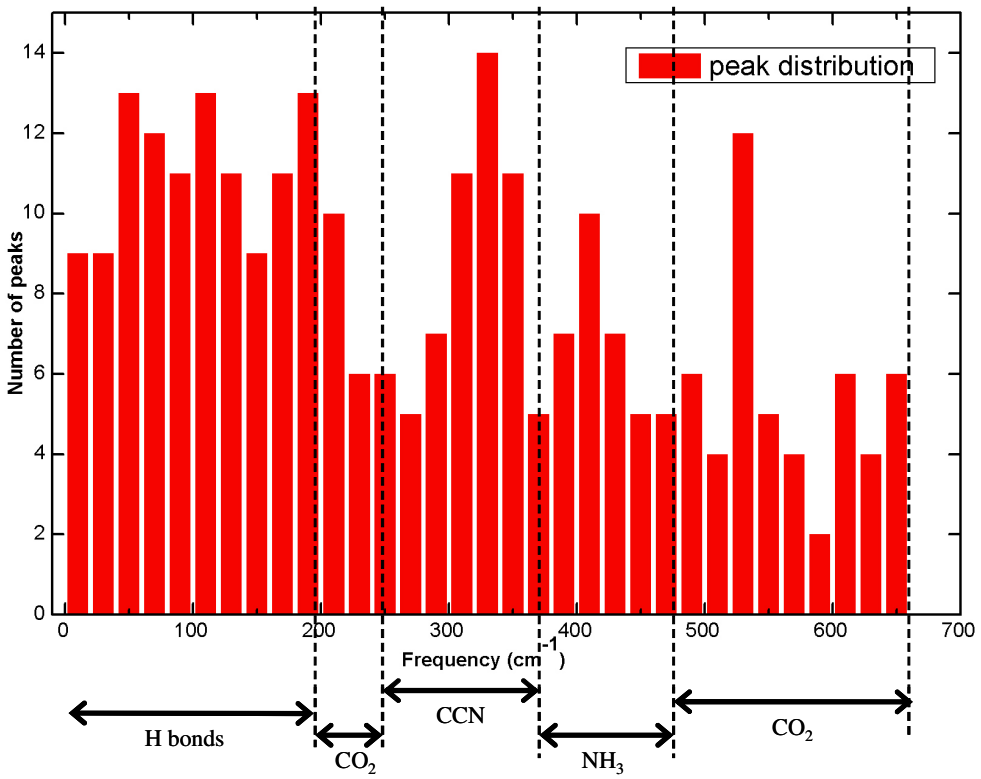

Fig. 4.42 The peak statistic in amino acids.

Chapter 5

RESULTS AMINO ACIDS CHAINS

Intermolecular forces that appear in polymer crystals can have several effects on the IR spectra of a crystalline polymer. It can happen that the bands of the free molecule only shift slightly in frequency, or each band of the free molecule splits into closely spaced components (into a number equal to the number of molecules from the primitive cell), or new bands appear at low frequency **[Gup1972]**.

As normal coordinate calculations have shown, intramolecular and intermolecular modes are expected to appear in the frequency region 0-500 cm^{-1} (**[Ito1969]**, **[Ito1970]**, **[Sma1970]**, **[Sin1971]**, **[Abe1972]**, **and [Fan1971]**). Torsions about the skeletal bonds, skeletal angle deformations, as well as intermolecular bonds involving the hydrogen bond and the side-groups interactions are assumed visible in the low-frequency side of the IR spectrum.

Infrared spectroscopic studies on polypeptides have been mainly concerned with correlating the vibrational frequencies with polymer conformation **[Sma1970]**.

In the far infrared region, the normal modes consist mainly of skeletal bending, torsions, internal rotation and hydrogen bonds deformations. Skeletal torsional modes, especially those about the peptide bond, involve large displacements of the α-carbon. It was expected **[Fan1973]** that these modes have frequencies dependent on conformation, which means that, from the spectra, it is possible to make assumptions about the secondary structure of the chain. Skeletal vibrations involve displacements of large numbers of atoms, which makes them sensitive not only to secondary structure, but also

to the tertiary structure. Infrared absorption was proved often to be a good tool in identifying the secondary structure of short length peptides.

Oligomers of alanine (n = 3-6) assume β-form **[Qia1991]**, **[Sho1974]**. This conclusion is determined by the presence of the bands either at 250 or 440 cm^{-1} (both characteristic for β-conformation) simultaneously with the absence of the band at 365 cm^{-1} (characteristic for α-helix). The amide V band (NH out-of-plane bend + CN torsion) shifts toward higher frequencies in chains with more than three amino acids (**[Moo1976II]**, **[Ito1972]**, and **[Sut1970]**). This displacement from 630-640 cm^{-1} in the case of n^{23} = 2-3 to 700 cm^{-1} for n >3 was initially attributed to the β-structure. However, the amide V band behaviour cannot be discussed only in terms of secondary structure, being influenced by the properties of the CONH group **[Fill1976]**.

The modes below 200 cm^{-1} could also help to determine the secondary structure of polypeptides. Lattice calculations of polypeptide structures (**[Abe1972]**, **[Fan1972]**) showed that all modes in the range 0-200 cm^{-1} are affected by interchain hydrogen bonding. It is also known from the experiments that below 200 cm^{-1} the lattice modes become visible: they shift to higher frequency at lower temperature **[Xie1999]**, while, in the same conditions, the peaks above 200 cm^{-1} shift less.

From the comparison of frequencies assigned to skeletal deformations and torsions in polyglycine I, II and α-poly-L-alanine it becomes clear that certain bands are indicative of chain conformation. Bands at 371 cm^{-1} (infrared absorption, α-poly-L-alanine) and 378 cm^{-1} (Raman, α-poly-L-alanine) are characteristic for α-helix conformation. Bands at 442 cm^{-1} (infrared absorption, β-poly-L-alanine **[Ito1968]**) and 410 cm^{-1} (calculated, polyglycine I) indicate β form. Beside these two, the bands at 363 cm-1 (infrared absorption, polglycine II) and 340 cm-1 (Raman, polglycine II) describe the collagen like conformation.

[23] Number of repeat units.

5.1 Glycylglycine

We investigated glycine oligomers (Fig. 5.1, Table 5.1), observing how the spectra evolve from monomer up to hexamer.

In the progression toward longer Gly oligomers the crystal structure becomes less and less precisely defined because of the difficulty of forming crystals. One consequence of this is that the absorption lines at low frequency broaden and shift to lower frequencies in the progression toward longer oligomer chains. For a polypeptide, is rather impossible to distinguish the amino acids within, as the spectrum becomes broad in the same manner the water spectrum does.

Table 5.1. Experimental absorption frequencies, in cm^{-1}, for glycine, glycine oligomers, and polyglycine. The cells marked with blue, red, violet, yellow, and pink are indicating the frequencies characteristic for β-form.

Glycine	Di-gly	Tri-gly	Tetra-gly	Penta-gly	Hexa-gly	Polyglycine
22	40	54	**84**	**83**	**83**	**87**
37	51	**81**	100	**129**	**130**	**129**
52	65	92	**125**	170	169	**215**
59	**84**	**120**	173	**219**	**220**	
68	91	161	**220**	258	251	
77	116	185	247	268	279	
85	138	**224**	277	283	294	
135	149	267	293	322	305	
165	199	298	319	340	324	
200	**225**	317	331	377	353	
233	314	343	351	**467**	361	
318	404	366	412	533	428	
357	448	**466**	**468**	555	**467**	
502	531	550	514	568	491	
524	590	**572**	**578**	570	515	
607	668	**606**	**605**	**580**	547	
		648	**639**	590	**583**	
				602	**606**	
				610	**634**	
				629	657	
				636		
				646		

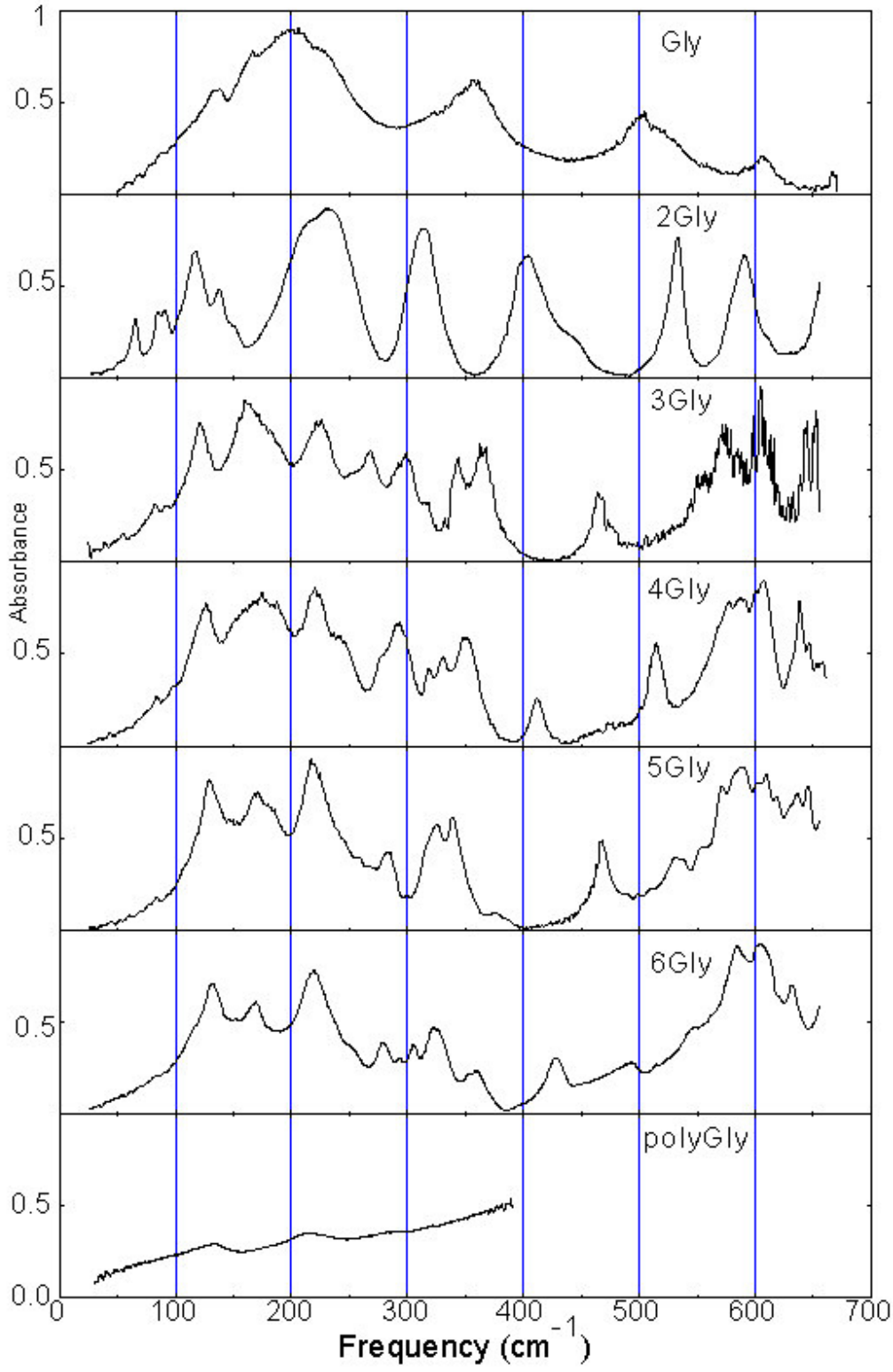

Fig. 5.1 Glycine chains of one to six molecules length.

The main behaviour to be seen is the hindered motion of hydrogen bonds.
Compared with glycine, the glycylglycine molecule shows a NH_3^+ torsion mode displaced toward higher frequencies: 532 cm^{-1} in our measurement, 528 cm^{-1} in **[Dwi1972]** (Table 5.3) compared with 504 cm^{-1} in Gly. In Glygly, there is a COO^- twist visible at 400 cm^{-1} that cannot be seen in glycine.
We have been able to identify in the dimer the typical features of an amino acid: amide VI (C=O out-of-plane deformation) at 590 cm^{-1}, $C^{\alpha}N$ torsion at 448 cm^{-1}, and skeletal deformations at 225, 314, and 404 cm^{-1} in agreement with earlier calculations **[Lag1983]**. According with the fitting, there seems to be a vibrational mode at 668 cm^{-1}. This has been described as amide IV (C=O in plane bending) **[Dwi1972]**, and calculated for 680 cm^{-1}. The value is situated slightly out of the detection limit, and the simple presence of this absorption maximum in the spectrum is questionable.
Below 200 cm^{-1}, the calculations predicted COO^- torsion, N-C^{β} torsion, and C^{α}-C at 189, 168, and 146 cm^{-1}, respectively **[Lag1983]**; we found bands at 138, 149, and 199 cm^{-1} that we assume to be the equivalent of these modes. Beside them, we observed other bands as well at lower frequencies: at 40, 51, 65, 84, 91, and 116 cm^{-1}. The first three of them, 40, 51, and 65 cm^{-1} have not been reported by now. The modes at 84, 91, and 116 cm^{1} have been associated with in-plane/out-of-plane bending and torsions of the backbone.

5.2 Alanyl-glycine and Glycyl-leucine

One step further on the complexity scale, between amino acids and proteins is represented by the co-peptides. Here we observed the modifications of amino acids spectra when put in a heterodimer. Figures 5.2-5.4 shows the absorption spectra of dimers AlaGly and GlyLeu, and GlyGly. Just like the amino acids, the dimers exist in zwitterionic form.
We fit these spectra so that we can closely follow the frequencies shift or stability. The values obtained from the fit are presented in Fig. 5.2-5.4 and Table 5.2, together with the assignments from **[Dwi1973]**. One question in

FIR is "can it be used to identify mixtures of amino acids, in the case when we don't know a priori what is in the mixture, and we have no entry of this mixture in a database?". For this purpose, we can follow a few fingerprint modes of amino acids, like NH_3^+ torsion and COO^- modes.

Some of these modes shift to higher frequencies in dimers compared with single amino acids, some of them toward lower frequency. AlaGly and GlyGly have the NH_3^+ torsion at a higher value than in alanine: 540 cm^{-1} in AlaGly, 532 in GlyGly, and 486 cm^{-1} in alanine. The COO^- wagging mode appears also at higher frequencies in AlaGly and GlyGly compared with Gly or Ala: 650 cm^{-1} in AlaGly, 668 cm^{-1} in GlyGly, 647 cm^{-1} in Ala, and 607 cm^{-1} in Gly. The COO^- rocking mode is shifted to lower frequency in the dimers compared with the single amino acids: 453 cm^{-1} in AlaGly, 490 cm^{-1} in GlyGly (**[Dwi1972]**), 539 cm^{-1} in alanine, and 504 cm^{-1} in glycine.

Table 5.2 NH_3^+, COO^-, and skeletal frequencies (in cm^{-1}) of alanine, glycine, alanyl-glycine, glycyl-glycine, and glycyl-leucine ([1]**[Dwi1972]**, **[Dwi1973]**, **[Lag1983]**).

	L-Ala[1]	L-Ala	Gly[1]	Gly	AlaGly[1]	AlaGly	GlyGly[1]	GlyGly	GlyLeu
NH_3^+ torsion	485	486	515	504-548	535	540	528	532	504
COO^- wag	650	647	605	607	680	650	658	668	-
COO^- rock	540	539	503	504	445	453	490	-	457
Amide VI (C=O) op def					599	589	588	590	582
N-C^α-C bend		293		357	343	343	348	-	360
C-N-C^α bend		324			107	119	117	116	124
N- C^α torsion					93	100	79	84	85

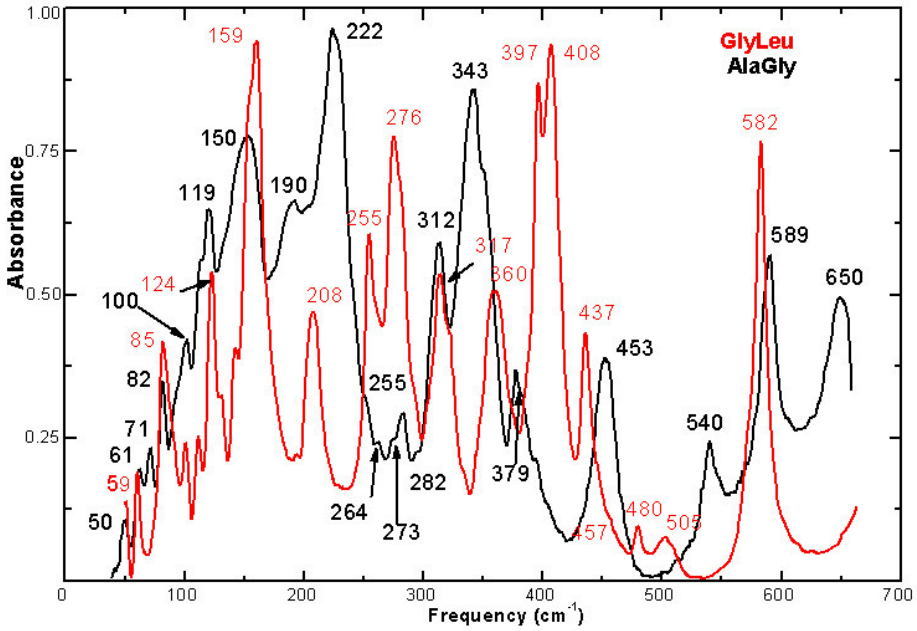

Fig. 5.2 Absorption spectra of alanyl-glycine and glycyl-leucine.

In the range 100-350 cm^{-1} the dimers show more features in spectra. In AlaGly and GlyGly there are more backbone modes visible than in alanine or glycine. In alanine they appear at 293 and 324 cm^{-1}, in glycine at 357 cm^{-1}, in AlaGly at 100, 119, 343 cm^{-1}, and in GlyGly at 84, 94 and 116 cm^{-1}.

Compared with the amino acids Gly and Leu, the dimer GlyLeu shows more structure in the spectrum. The Gly and Leu spectra can be divided in three frequency regions where the absorption maxima appear: 0-280 cm^{-1}, 280-460 cm^{-1}, and 460-650 cm^{-1}. For GlyLeu this arbitrary division is meaningless: the maxima are uniform distributed along the whole frequency range. Most of the individual peaks that appear in amino acids are displaced in the dimer (COO^- mode at 582 cm^{-1} in dimer), have different absorption intensity (at ~200 cm^{-1}), or are not present at all (as is the case of the mode from 170 cm^{-1}, present in Gly and in Leu, but absent in the dimer). In analogy with Glygly, we can identify in the dimer typical features of amino acids: amide VI (C=O out-of-plane deformation) at 582 cm^{-1} **[Ohs1995]**, NH_3^+ torsion at 504 cm^{-1}, $C^{\alpha}N$ torsion at 437 cm^{-1}, and skeletal deformations at 85, 124, and 360 cm^{-1}.

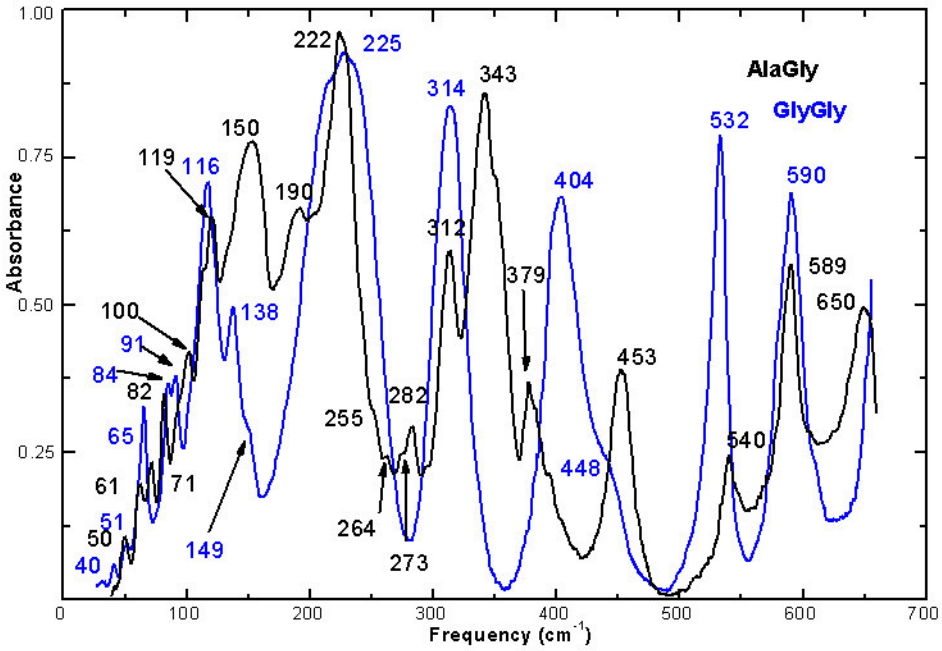

Fig. 5.3 Absorption of alanyl-glycine and glycyl-glycine.

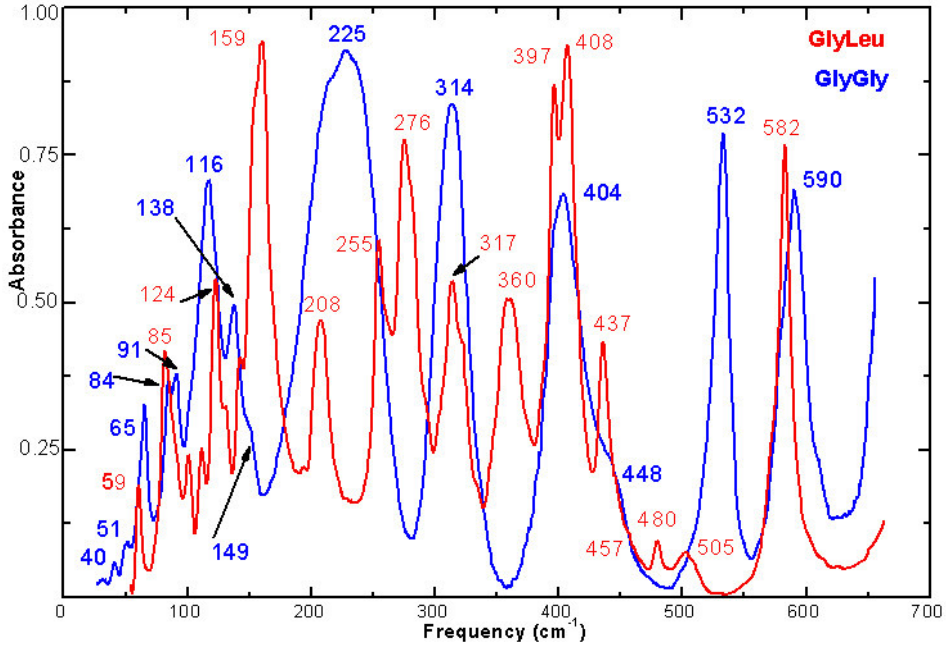

Fig. 5.4 Absorption of glycyl-glycine and glycyl-leucine.

Calculated [Dwi1972]	IR [Dwi1972]	INS [Dwi1972]	Assignments [Dwi1972]	Gly-gly (from fit)	Ala-gly (from fit)	IR [Dwi1973]	Calculated [Dwi1973]	Assignment [Dwi1973]
-	-	-	-	40	-	-	22	$t(C_\alpha\text{-}C)$
-	-	-	-	51	50	-	49	-
-	-	-	-	65	61	-	-	$t(C_\alpha\text{-}C)$
-	-	-	-	-	71	-	-	-
79	-	-	$t(N\text{-}C_\alpha)+t(C_\alpha\text{-}C)$	84	82	-	-	-
103	-	-	$t(C_\alpha\text{-}C)+t(N\text{-}C_\alpha)+ipb(C\text{-}N\text{-}C_\alpha)+ipb(N\text{-}C_\alpha\text{-}C)$	91	100	-	93	$t(N\text{-}C_\alpha)$
117	-	-	$ipb(C\text{-}N\text{-}C_\alpha)+ipb(N\text{-}C_\alpha\text{-}C)+t(C\text{-}C_\alpha)+t(C\text{-}N)$	116	119	-	107	$ipb(C\text{-}N\text{-}C_\alpha)+ipb(N\text{-}C_\alpha\text{-}C)+ipb(C_\alpha\text{-}C\text{-}N)$
-	-	-	-	138	-	-	-	-
-	-	-	-	149	150	-	-	-
194	216	210	$t(C\text{-}N)+t(C_\alpha\text{-}C)$ (Amide VII)	199	190	-	-	-
228	-	250	$ipb(N\text{-}C_\alpha\text{-}C)+ipb(N^+\text{-}C_\alpha\text{-}C)$	225	222	-	211	$ipb(CH_3\text{-}C_\alpha\text{-}C)+t(C\text{-}N)$
-	-	-	-	-	255	-	-	-
-	-	-	-	-	264	262	253	$t(CH_3)$
-	-	-	-	-	-	-	258	$t(CH_3)+t(C\text{-}N)$ (Amide VII)
272	308	300	$ipb(N^+\text{-}C_\alpha\text{-}C)+ipb(C\text{-}N\text{-}C_\alpha)+ipb(C_\alpha\text{-}C\text{-}O)$	-	273	-	-	-
-	-	-	-	-	282	-	283	-
-	-	-	-	-	293	-	-	-
-	-	-	-	314	312	312	-	$t(C\text{-}N)+ipb(CH_3\text{-}C_\alpha\text{-}C)+ipb(N\text{-}C_\alpha\text{-}C)$
331	348	380	$ipb(C\text{-}C_\alpha\text{-}O)+ipb(N^+\text{-}C_\alpha\text{-}C)+ipb(C_\alpha\text{-}C\text{-}N)$	-	343	343	338	$ipb(N^+\text{-}C_\alpha\text{-}C)+ipb(C_\alpha\text{-}C\text{=}O)+t(C_\alpha\text{-}C)$
-	-	-	-	-	379	375	382	$ipb(N^+\text{-}C_\alpha\text{-}CH_3)$
404	400	435	COO^- twist	404	-	-	-	-
-	-	-	-	448	-	-	440	COO^- twist
471	490	-	COO^- rock	-	453	445	447	COO^- rock
522	528	505	NH_3^+ torsion	532	540	535	480	NH_3^+ torsion
580	588	590	Amide VI	590	589	585	599	Amide VI (C=O out of plane deformation)
613	615	-	Amide IV	-	-	-	-	-
660	658	-	COO^- wag	-	650	650	651	Amide IV (C=O in plane deformation)

Table 5.3. Vibrational frequencies (in cm^{-1}) for alanylglycine and glycylglycine.

The dimer GlyLeu shows a less intense absorption intensity at ~200 cm^{-1}. This frequency region is mainly associated with H-bond absorption and there is no trivial explanation why the absorption is decreasing in intensity, considering that, in dimers, all the three protons of NH_3^+ participate in hydrogen bonding with the oxygen atoms of carbonyl **[Dwi1973]**.
The strong peak present in Leu at 402 cm^{-1} appears also in GlyLeu, although split in two components, at 397 and 408 cm^{-1}.

5.3 Triglycine, tetraglycine, pentaglycine, and hexaglycine

Oligopeptides of three amino acids length can already form a secondary structure. This was seen in the case of alanine **[Qia1991]** and is true also for glycine. The secondary structure of the glycine oligomers presented here, from trimer op to hexamer is not a priori known. Far infrared absorption can make the difference between the two forms.
Triglycine (or Gly_3) can assume a β-sheet as well as α-helix structure **[Hug1950]**, **[Yak1952]**, **[Len1932]**. The β form has been described in more detail **[Sun1989]** than the helix. It is not clear yet which are the factors that determine the occurence of one or another type of secondary structure. In **[Tag1997]** the authors reported that Gly_3 and Gly_4 exist only in the planar zigzag conformation because the terminal NH_3^+ is hindering the progression in the helical structure. Although the purpose of our study is not to decide what conditions determine the incidence of one or another type of secondary structure, we assume that the hydration level is one of the important factors.
Typical features of amino acids appear also in Gly_3. Amide V band composed of CN torsion and NH out-of-plane bending (ob) appears in Gly_3 at **[Sun1989]** at 550, 606, and 648 cm^{-1}. These values are in agreement with those previously calculated at 563, 609, and 643 cm^{-1}. A single COO^- mode is visible in FIR spectrum (at 572 cm^{-1}) from the two calculated (581 and 580 cm^{-1} in **[Sun1989]**).

As the figure 5.1 (Table 5.1) shows, the tetramer, pentamer and hexamer of glycine have absorption peaks in the same region where the amide V appears in trimer. It is reasonable to interpret this in terms of secondary structure, and to assume that the trimer up to hexamer have identical β-structure. The modes characteristic for this type of structure appear in our spectra at almost identical positions with those from previous studies **[Tag1997]**: 578, 605, 639 cm^{-1} in tetramer, 580, 602, 610, 636 cm^{-1} in pentamer, and 583, 606, 634 cm^{-1} in hexamer.

There are two more frequencies that these four oligomers share, and that are not present in glycine or glycyl-glycine: at ~120 cm^{-1}, and ~467 cm^{-1}. They are not described by now in literature, and we believe that are characteristic frequencies for the β-sheet.

Our spectra are the first to show the IR absorption of the oligomers down to 30 cm^{-1}. So comes that we can contradict previous statements like "Below the 900 cm^{-1} region, the spectral features of PG I are almost the same as those of Gly_5 and Gly_6" (**[Tag1997]**). The differences in spectra in this low frequency region are pretty obvious (Table 5.1).

Table 5.4. Observed bands in the IR spectra of glycine oligomers. All IR and values are in cm^{-1} **[Tag1997]**.

β-sheet					α-helix		
trimer	tetramer	pentamer	hexamer	PG I	pentamer	hexamer	PG II
578	582	581	588	593	567	572	572
606	606	607	605	603			
647	639	634	632	630			

5.4 Polyglycine

Polyglycine $(-CH_2CONH-)_n$ can assume two structural conformations, known as polyglycine I (PGI) and polyglycine II (PGII) **[Bun1947]**. X-ray studies have established that PGI contains fully extended linear zigzag chains (β-form) packed in an antiparallel arrangement (**[Ast1949]**, **[Bam1955]**) and

PGII is a left hand side 3_1-helix **[Cri1955]**. The helix chains are running parallel or antiparallel **[Pad1965]**, being H-bonded through N-H•••O=C and C-H•••O=C **[Sin1971]**, **[Gup1968]**. Detailed normal coordinate analysis of the vibrational spectrum of PGII **[Dwi1982]** supports the conclusion that that the 3_1-helical molecule crystallizes in antiparallel chain structure in which every third residue participates in a hydrogen bond C-H•••O=C. In the parallel chain arrangement, all CH_2 groups participate in hydrogen bonds of the type C-H•••O=C **[Dwi1982]**. In the case of antiparallel chains, the hydrogen bonds C-H•••O=C are very weak and only one third of the possible number of such bonds exist **[Ram1967]**. Neighbouring chains in β-form are hydrogen bonded via N-H•••O=C.

Neutron scattering experiments support the presence of C-H•••O=C bond, showing the peak corresponding to amide VII (C-N torsion) band in PG II has a lower intensity than its equivalent in PGI.

The two structures distinguish from each other in FIR also by other means: the amide VII band position appears in case of PG II at 340-367 cm^{-1}, while in PG I is visible at lower frequencies, around 215 cm^{-1} **[Gup1968]**.

Amide IV (C=O in plane deformation) is visible in PG II at 698 cm^{-1}, and in PG I at 628 cm^{-1}, while amide VI (C=O out of plane deformation) shifts from 573 cm^{-1} in PG II to 589 cm^{-1} in PG I **[Suz1966]**[24], **[Smi1969]**[25].

Early calculations of normal vibrations predicted more bands in the spectrum of PGI than could be found by experiments **[Fuk1963]**[26]. The vibrations at 176, 223, 278, and 541 cm^{-1} were all assigned to skeletal deformation vibrations. Experimental observations were completed with normal vibration calculations. In **[Moo1976I]**[27] is developed the analysis of the vibrational spectrum of glycine in β-form using a force field. The agreement with observed FIR and Raman bands was very good, and the force field was used

[24] **[Suz1966]** in Annex A, tables 6-8, page 149

[25] **[Smi1969]** in Annex A, table 11, page 151

[26] **[Fuk1963]** in Annex A, table 12, page 151

[27] **[Moo1976I]** in Annex A, table 19, page 156

in calculations of more complex molecules (β-poly-L-alanine and β-poly-L-alanylglycine **[Moo1976II]**[28]). Previous comparisons between the mid-infrared spectrum of PG I and the oligomers of glycine indicate that the oligomers up to pentamer may exist as antiparallel extended chains **[Smi1969]**[29]. In dodecaglycine, there is an absorption band at 365 cm^{-1} that can be considered the equivalent of the amide VII band from PG II spectrum. This indicates that between hexamer and dodecamer there is a chain of intermediate length for which the secondary structure changes from the planar zigzag structure to helix. Some authors are even considering the hexamer as the first step in the transition from β to α **[Gup1975]**. We cannot give a definitive statement about this, as we have no other means to determine the secondary structure, but the FIR spectrum. We incline to believe that hexamer has frequencies nearer to the PG I than to PG II and it cannot to be considered the "missing link" in the transition from β to α structure.

The secondary structure of the present polygylcine can be established from the spectral features visible below 400 cm^{-1}. Although the spectrum is noisy in the region beyond 400 cm^{-1}, which was more extensively characterized, the assignment is still possible.

The absorption maximum situated at 129 cm^{-1} was calculated for PG I at 133 cm^{-1} **[Fan1973]**. This is a lattice mode and represents stretching of the NH•••O hydrogen bond. The absorption peak at 215 cm^{-1} can be identified as amide VII mode (C-N torsion + C-O bend modes **[Dwi1982]**), calculated **[Gup1975]**, **[Dwi1982I]** for PG I at 217 cm^{-1}. Considering these three hints it can be assumed that the polyglycine studied here has a β-sheet structure. None of the vibrational frequencies characteristic for α-helix is present here, there is no band appearing at 113 or 365 cm^{-1}.

---

[28] **[Moo1976II]** in Annex A, table 20, page 157

[29] **[Smi1969]** in Annex A, table 11, page 151

In **[Fan1973]** is presented a calculated mode at 75 cm^{-1} in PGI, assigned as deformation of hydrogen bonds of the type NH•••O and C=O•••H.
In the measurements here presented, the equivalent for this peak can be the one that appears at 87 cm^{-1}.

5.5 Conclusions

We investigated glycine oligomers observing how the spectra evolutes from monomer up to hexamer. In the progression toward longer Gly oligomers, the crystal structure becomes less and less precisely defined because of the difficulty of forming crystals. One consequence of this is that the absorption lines at low frequency broaden and shift to lower frequencies in the progression toward longer oligomer chains. For a polypeptide, is rather impossible to distinguish the amino acids within, as the spectrum becomes broad in the same manner the water spectrum does. This broadening is exemplified by the spectrum of polyglycine: there are only three spectral features in the frequency region 0 – 400 cm^{-1}.
For alanyl-glycine and glycyl-leucine the spectra are still made up of four regions, like it was discussed in the previous chapter, in case of amino acids. However, the features are not a sum of those from the individual amino acids, but they indicate a new sample.
In the frequency range 0-650 cm^{-1}, oligopeptides and polypeptides spectra show the intramolecular and intermolecular modes. These modes are: torsions about the skeletal bonds, skeletal bending, end group vibrations, and intermolecular bonds involving the hydrogen bond and the side-groups interactions.
The lattice modes are visible below 200 cm^{-1}. The samples from the glycine family that are studied here have a feature at ~85 cm^{-1} that could be associated with the H bond mode. This feature appears at 85 cm^{-1} in Gly, 84

cm^{-1} in Gly_2, 81 cm^{-1} in Gly_3, 84 cm^{-1} in Gly_4, 83 cm^{-1} in Gly_5, 83 cm^{-1} in Gly_6, and at 87 cm^{-1} in PG.

A skeletal torsional mode frequency depends on conformation, and so comes that the spectra can be used as indicators for conformation of the chain. Certain bands are indicative of chain conformation, like those at 442 cm^{-1} (infrared absorption, β-poly-L-alanine) and 410 cm^{-1} (calculated, polyglycine I) that indicate β form.

Just like in the case of alanine, glycine oligomers, starting with Gly_3 take the β-form. This conclusion is determined by the presence of four different bands that were previously presented and appear in our studies too. These are: 466, 572, 606, 648 cm^{-1} for Gly_3; 468, 578, 605, 639 cm^{-1} for Gly_4; 467, 580, 602, 610, 536 cm^{-1} for Gly_5; and 467, 583, 606, 634 cm^{-1} for Gly_6. Simultaneously, the α-helix characteristic band at 365 cm^{-1} is absent. The polyglycine spectrum became very noisy in the experimental conditions that were ideal for the oligomers. This adds some difficulty in identifying the structure of PG. The highest frequency value that is displayed in the spectrum is at 400 cm^{-1}, too low to observe the expected feature at 410 cm^{-1}, characteristic for β-form. However, the presence of absorption peaks at 129 and 215 cm^{-1}, similar with those previously seen in PG, can be used as an indication for β structure.

Chapter 6

PROTEINS IN FAR INFRARED

In the present study have been investigated three proteins with enzymatic activity: acylase, lipase, and β lactamase. Acylase is a hydrolithic enzyme. Lipase is an enzyme involved in the digestion of fats. Beta-lactamase is a type of enzyme responsible for bacterial resistance to penicillin-type antibiotics[30]. Acylase and lipase have 1:1 ratio of α-helix and β-sheet structure. In beta lactamase the α-helix is predominant. The three proteins share a few common spectral features (Fig. 6.1).

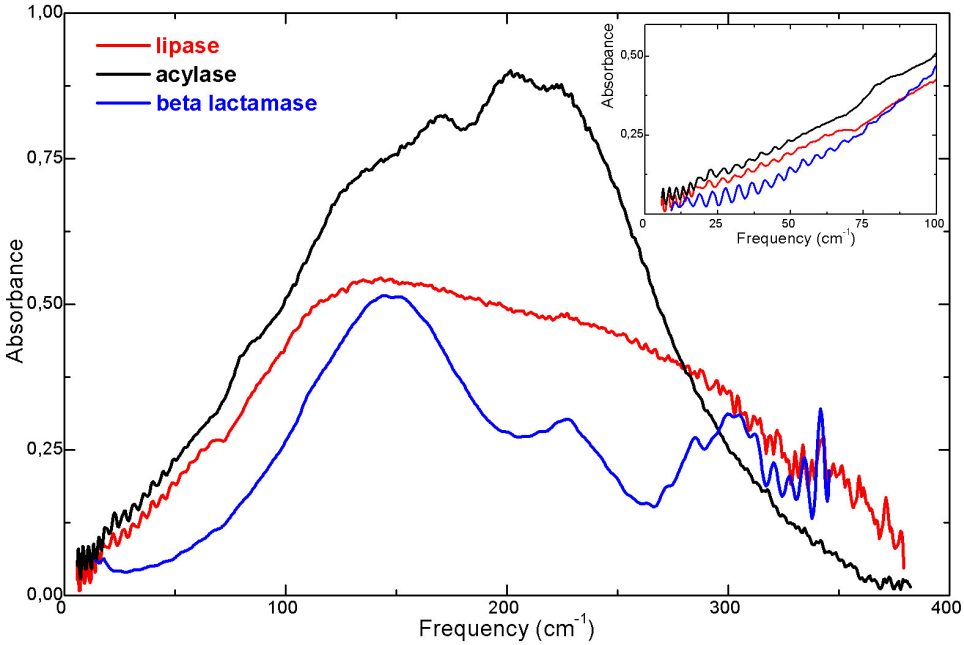

Fig. 6.1 Absorbance spectra of acylase, lipase, and beta lactamase. The inset shows the spectra at low frequency.

[30] Penicillin and related antibiotics have a four-atom ring in their structure, known as beta lactam. The lactamase enzyme breaks the ring and deactivate the molecule's antibiotic properties.

6.1 Secondary structure characteristics

As the figures 6.1 – 6.4 show, the protein absorption spectra are characterized by broad absorption features. The absorption frequencies are indicated also in Table 6.1.

Acylase	Lipase	Beta lactamase
25	22	148
80	135	229
143	264	306
169		
200		
222		

Table 6.1 Absorption frequencies for acylase, lipase, and beta-lactamase.

For acylase and lipase the dominant feature is an absorption band with the centre at ~ 200 cm^{-1}. Beta lactamase also shows a broad peak, at 148 cm^{-1}. This shift indicates the presence of different structures: whereas for beta lactamase the maximum at 148 cm^{-1} shows the vibrations of the hydrogen bonds responsible for the stability of the helix, in acylase and lipase, the absorption maximum indicates that the structure is more "diffuse". Vibrational modes from different secondary structures present in the two enzymes contribute to the absorption, so that there is no dominating oscillation, but a sum of oscillators of different frequencies. This determines the broadening of the band. A similar behaviour is seen in a very important hydrogen bonded system: the water (**[Pad2003]**, **[Pad2004]**).

The modes of acylase at 143 and 222 cm^{-1}, and those of lipase at 135 and 264 cm^{-1}, can be considered indicators for the presence of α-helix structure. In myoglobin were detected absorption maxima at 140 and 226 cm^{-1} **[Chi1973]** associated with the α-helix that disappear upon denaturatation. Myoglobin has

a mode at 380 cm^{-1}, identified from polypeptide chains as an α-helix indicator, which cannot be seen in any of the three proteins presented here because of the reduced frequency range. This is why an assignment in the here presented proteins is only tentative. As it was shown in **[Buo1971]**, **[Gen1983II]**, and **[Yam2002]** the FIR absorption is not the best indicator for the secondary structure of proteins.

Beta lactamase has three absorption maxima, at 148, 229, and 306 cm^{-1}. The first two are clear indicators for the presence of α-helix.

6.2 Low-lying spectral features

As it was discussed in Chapter 1, at low frequencies, proteins have a glassy behaviour and exhibit a boson peak. Molecular dynamics simulations **[Pac1998]**, **[Biz2000]** and neutron scattering experiments **[Pac1999]** showed the existence of an excess of low frequency vibration modes in the density of states of hydration water around plastocyanin.

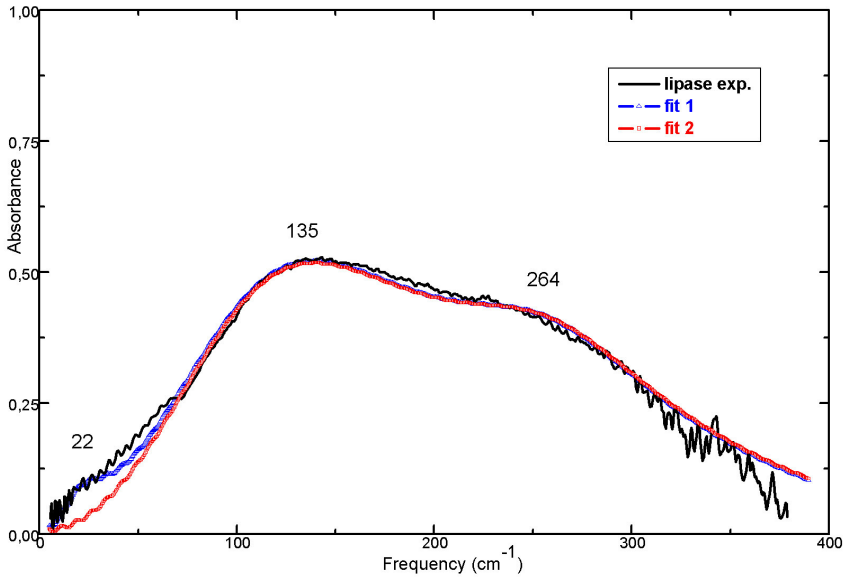

Fig. 6.2 Absorbance spectra of lipase.
The black line shows the experimental results, the blue line is the result of the lorentzian fit with a lorentzian oscillator at 22 cm^{-1}, and the red line represents the same fit, but without the low lying vibration.

Raman spectroscopy of lyophilized chymotripsin **[Pai1982]** revealed a broad absorption maximum at 30 cm^{-1}; neutron scattering experiments on polycrystalline lysozyme **[Gen1976]** confirmed the existence of a peak at 25 cm^{-1}.

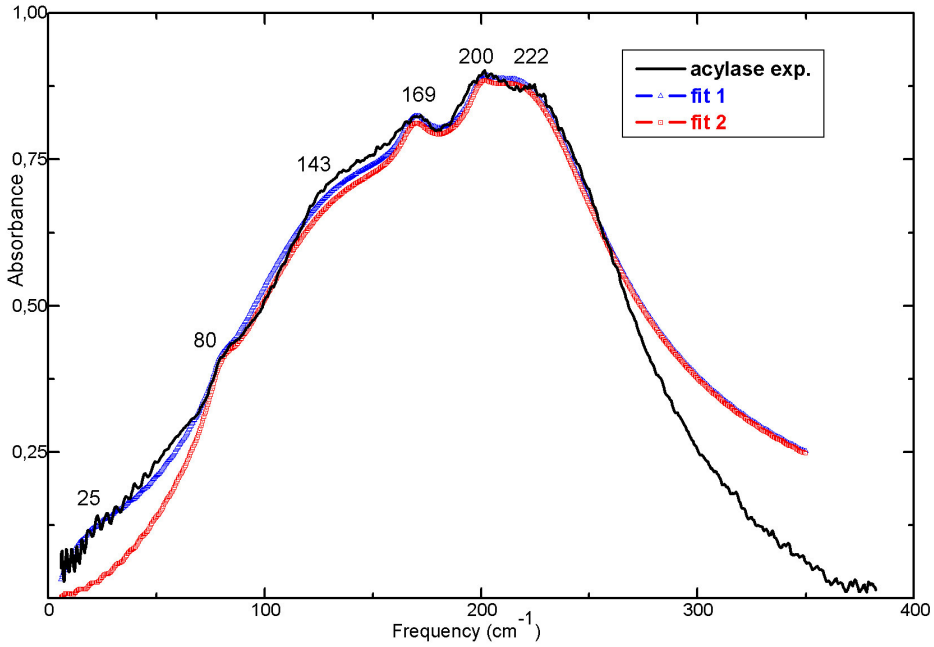

Fig. 6.3. Absorbance spectra of acylase.
The black line shows the experimental results, the blue line is the result of the lorentzian fit with a lorentzian oscillator at 25 cm^{-1}, and the red line represents the same fit, but without the low-lying vibration.

Low temperature inelastic neutron scattering of trypsin inhibitor, myoglobin, haemoglobin, lysozyme, and red blood cells **[Cus1989]**, **[Cus1990]**, and **[Dos1989]** showed a broad maximum in the incoherent dynamic structure factor at ~ 24 cm^{-1}.

The protein low frequency spectrum was interpreted in different ways. On one hand, it was suggested a connection between the low-frequency modes and the accordion-like modes of α-helical structure of the proteins; the latter modes were calculated in the range 19-30 cm^{-1} **[Cho1985]**. On the other

hand, in myoglobin it was recognized that the H-atoms from the side chains of the protein inner region contribute to the band at 24 cm^{-1} **[Mel1999]**.

The measurements were performed at room temperature, where the experimenters usually fail to observe the boson peak. However, in the present results low frequency modes are visible in lipase, at 22 cm^{-1} and acylase, at 25 cm^{-1}. There is no frequency mode in beta lactamase below 100 cm^{-1}

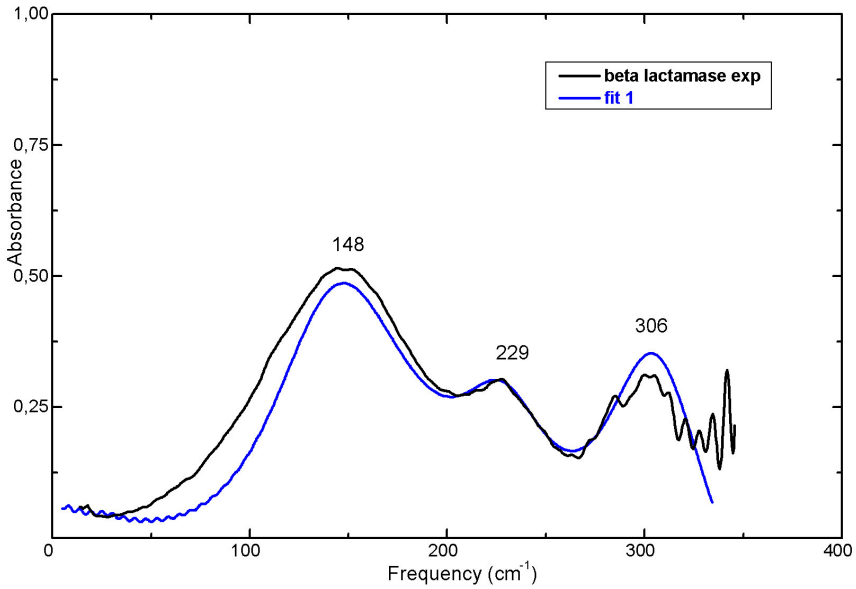

Fig. 6.4 Absorbance spectra of beta lactamase.
The black line shows the experimental data. The blue line represents the lorentzian fit. There is no absorption maximum below 100 cm^{-1}.

The intensities of the low-lying features in acylase and lipase are very low and they can be detected only from fitting the spectra. In this sense the figures 6.2 – 6.4 show three different curves: the experimental data, the fit that includes the low-lying mode, and the fit with the same parameters, without the questioned absorption maximum. We assume that these two features present in lipase and acylase represent the boson peak. For beta lactamase there is no such a feature present.

It is obvious by now that the spectrum of a protein does not keep the characteristics that are common among amino acids. The sharp features are

not at all present, and identifying a protein from the simple observation of its absorption, turns out to be a difficult task.

6.3 Conclusions

Three different proteins, acylase, lipase and beta lactamase, have been investigated in the frequency range 0 – 350 cm^{-1}.

For each of them, the polypeptide chain is arranged in a α-helix structure: for beta lactamase 80 % of the total length is twisted in helical form, for lipase and acylase only 50 %. The other 50 % of the lipase and acylase chain is arranged in β-sheet structure.

The absorption pattern that is characteristic for amino acids, is smeared out in proteins. The absorption spectra of the three proteins show only a few broad features. Acylase and lipase are characterized by a large absorption band with the centre at ~200 cm^{-1}. Beta lactamase also shows a broad peak, at 148 cm^{-1}.

This difference indicates the presence of different secondary structures: whereas for beta lactamase the maximum at 148 cm^{-1} shows the vibrations of the hydrogen bonds responsible for the stability of the helix, in acylase and lipase, the absorption maximum indicates the structure is less homogeneous. Vibrational modes from different secondary structures present in the two enzymes contribute to the absorption, so that the broad peak represents a sum of oscillators of different frequencies.

Considering former assignments, the modes of acylase at 143 and 222 cm^{-1}, and those of lipase at 135 and 264 cm^{-1}, can be considered indicators for the presence of α-helix structure. Beta lactamase has three absorption maxima, at 148, 229, and 306 cm^{-1}. The first two are indicate the presence of α-helix.

At low frequencies, below 50 cm^{-1}, proteins exhibit an absorption feature that is temperature independent. In glasses, this feature is called boson peak. Proteins that display such a peak are considered to have a "glassy behaviour". The origin of boson peak is not known.

Two of the three proteins show a low-lying feature that could be associated with the boson peak: acylase at 25 cm^{-1} and lipase at 22 cm^{-1}. These peaks have low intensity, and they can be distingushed only by fitting the spectra with a sum of lorentzians. The fittings are showed in figures 6.2 and 6.3. The blue fit includes the low–lying mode, while the red fit does not. In beta lactamase no such peak can be seen, as the figure 6.4 indicates.

It can be speculated about the origin of this low frequency behaviour. On one hand, maybe we deal with a boson peak. On the other hand, this feature could be connected with the secondary structure of the proteins. As lipase and acylase have 50% of their chain length in β-form, and they are the samples to disyplay such a peak, maybe there is a straightforward connection between the two facts; the peak could be either related to the hydrogen bonds the β-sheet forms, or with a specific amino acid, or with the hydration level of the proteins. However, these ideas are not supported yet by further measurements, but would make sense to follow them.

Chapter 7

HUMAN BLOOD SERUM

7.1 Setup and results

The results presented in this chapter have been discussed also in **[Mat2003]**. The liquid sample was purchased from Sigma Aldrich, under the name H4522. For measurements it was pipetted onto the silicon window, in a 55 µl volume, which was considered appropriate to fill the volume of the cell.
The measurements were performed in reflection, using a sample arrangement like in Fig. 7.1. The liquid sample was set on the Si window in a thick layer.
Because of silicon's high refractive index, the 2 mm thick window behaves as a Fabry-Perot resonator (Fig. 7.1).

Fabry-Perot resonator:
$\Delta\nu = 1/2nd$
d = 2 mm; n = 3.4; k = 0.006

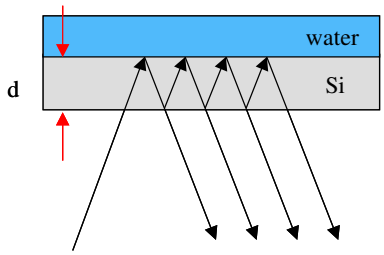

Fig. 7.1 Multiple reflection at the window.

The result is that the spectra will show fringes of 0.7 cm^{-1} spacing (Fig. 7.2). Multireflections within the window can be rigorously described by the Fresnel equations for the layer systems vacuum/Si window and silicon/serum/silicon. An accurate fit of the amplitude and position of fringes allows one to obtain information on the refractive index n and extinction coefficient k of the liquid sample under test.

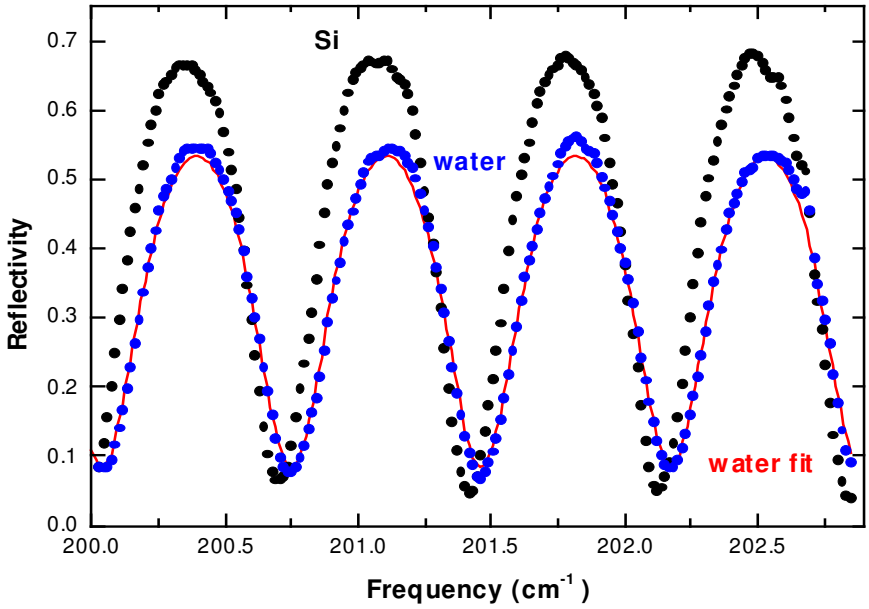

Fig. 7.2 Water spectra measured in reflexion.

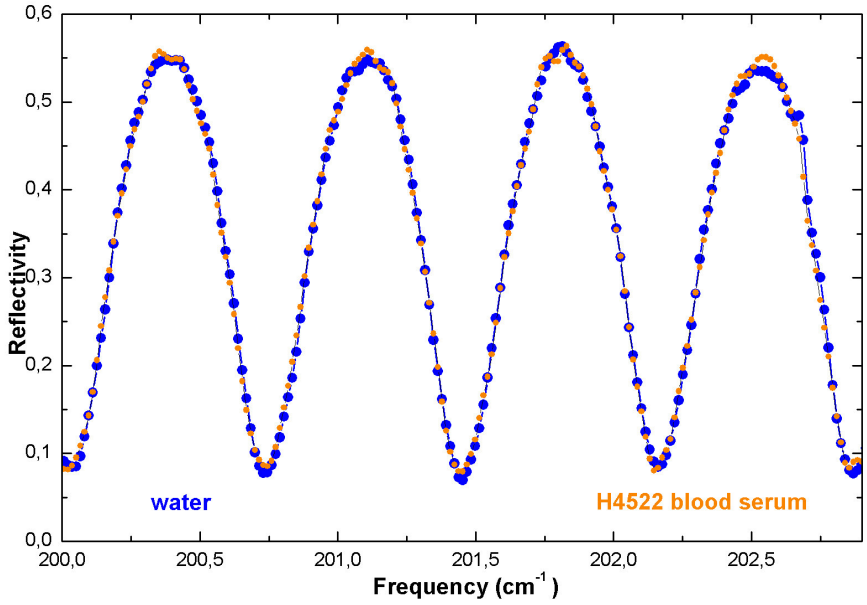

Fig. 7.3 The reflectivity of water and serum.

Fig 7.4 Refractive index *n* and extinction coefficient *k* for water and serum.

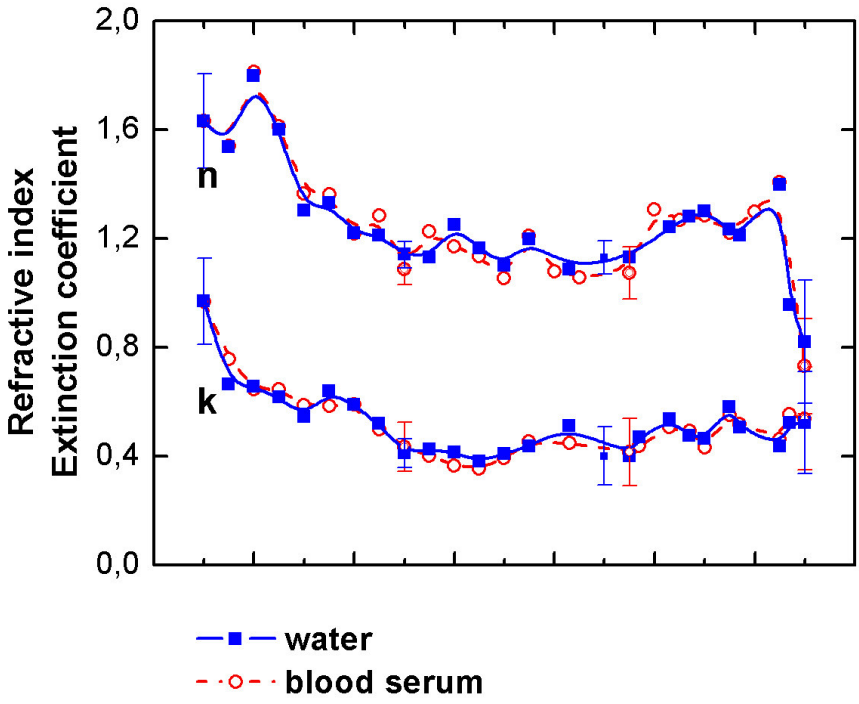

To analyze the reflectivity of blood serum, we first constructed a vacuum/silicon cuvette model, and determined the values ε_1 and ε_2 for this model over the entire frequency range. The next step was to introduce these values in the three layered system silicon/serum/silicon and to tune the ε_1 and ε_2 for H4522 so that the fitting curve describes the behaviour of the serum reflectivity. This allows an unequivocally determination of the optical parameters of the liquid ε_1 and ε_2, or *n* and *k*.

Due to the high water content, >90% the differences between serum and water spectra are extremely small (Fig. 7.4 and Fig. 7.5).

The absorption spectrum shows two broad maxima at 200 cm^{-1} and 450 cm^{-1}. This type of behaviour is very much water-like. In water there at 200 cm^{-1} are visible the intermolecular bonds vibrations, like hydrogen bond stretch. At ~400 cm^{-1} in water spectrum are seen the effects of librations, which are

hindered rotations of the molecules. We can conclude that the optical properties of serum are governed by water. We do not find any large deviations from the water spectrum and no strong features.

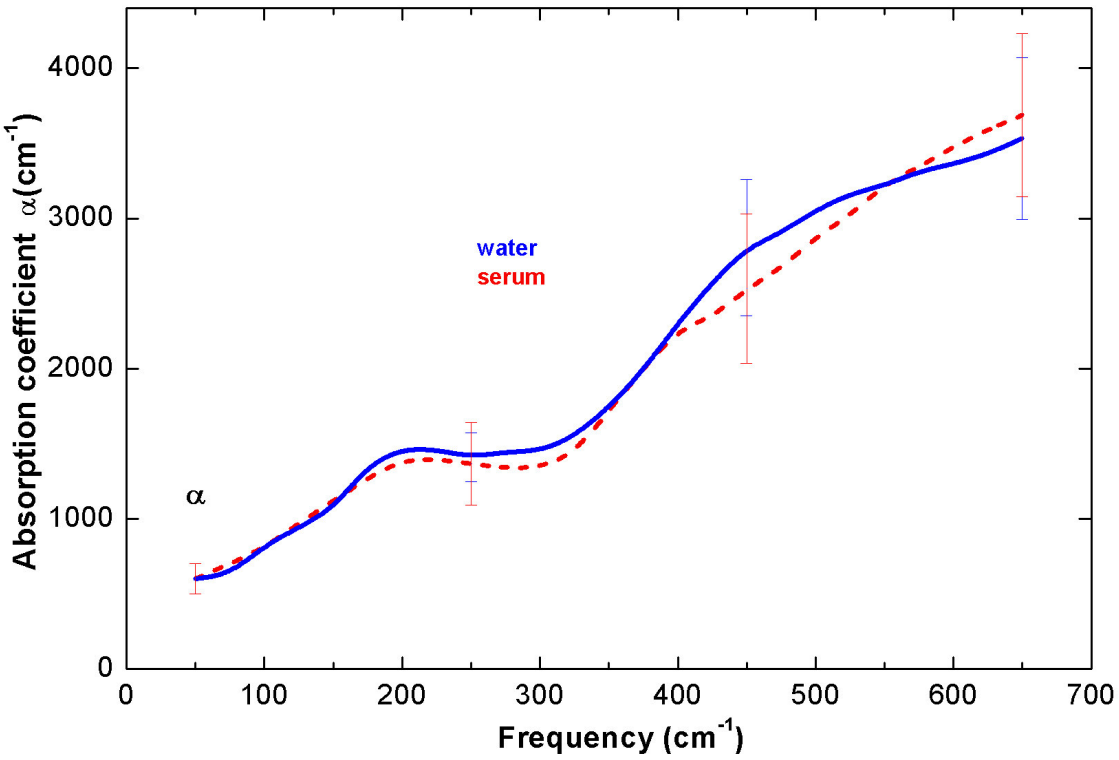

Fig. 7.5 Absorption coefficient for water and serum.

7.2 Conclusions

The optical properties of human blood serum have been measured in the far infrared frequency range. Due to its high water content (> 90%), the infrared properties of blood serum do not exhibit either sharp features or strong deviations compared to water.

We can conclude that the effect of the far infrared radiation on blood will be governed by the effects of water.

Chapter 8

CONCLUSIONS

8.1 Amino Acids

Since the first amino acids investigations in FIR, the absorption spectroscopy brought a lot of information about the behaviour of this type of molecules at low frequencies.

As they are the building blocks of the proteins, we expect that information about amino acids will help to understand the behaviour of proteins.

We looked for the properties of amino acids, those that they have in common and those that make them different from each other. In this respect, we recorded transmission spectra and determined the relative absorption.

Analyzing the graphs, we realized that there is a pattern in the absorption properties that is repeated for each amino acid. There are specific vibrational frequencies that can be observed in most of the amino acids. However, this pattern is not always stable, the same group of atoms vibrates at different frequency, depending on the amino acid.

Making a statistics for absorption frequencies, we can see that amino acids share common features, enough to make them a "class of molecules". On the other hand, they exhibit enough differences, to make each of them an individual. Analyzing its far infrared spectra can unequivocally identify each amino acid.

8.2 Amino acid chains

When the amino acids form oligomers, the absorption lines at low frequency shift and broaden to lower frequencies, as the oligomer chain is increasing. We investigated glycine oligomers observing how the spectra is changing from monomer up to hexamer. In the progression toward longer Gly oligomers, the crystal structure becomes less precisely defined because of the difficulty of forming crystals. In consequence, the absorption lines at low frequency broaden and shift to lower frequencies in the progression toward longer oligomer chains. For an amino acids chain, is rather impossible to distinguish the amino acids within, as the spectrum becomes broad in the same manner the water spectrum does. The spectrum of a polypeptide is broadening toward low frequencies in the same manner the water spectrum does. This is exemplified by the spectrum of polyglycine: there are only three spectral features in the frequency region 0 – 400 cm^{-1}.

For alanyl-glycine and glycyl-leucine the spectra are still made up of four regions, like it was discussed in the previous chapter, in case of amino acids. However, the features are not a sum of those from the individual amino acids, but they indicate a new sample.

In the frequency range 0 - 650 cm^{-1}, oligopeptides and polypeptides spectra show the intramolecular and intermolecular modes. These modes are: torsions about the skeletal bonds, skeletal bending, end group vibrations, and intermolecular bonds involving the hydrogen bond and the side-groups interactions.

The lattice modes are visible below 200 cm^{-1}. The samples from the glycine family that are studied here have a feature at ~85 cm^{-1} that could be associated with the H bond mode. This feature appears at 85 cm^{-1} in Gly, 84 cm^{-1} in Gly_2, 81 cm^{-1} in Gly_3, 84 cm^{-1} in Gly_4, 83 cm^{-1} in Gly_5, 83 cm^{-1} in Gly_6, and at 87 cm^{-1} in PG.

A skeletal torsional mode frequency depends on conformation, and so comes that the spectra can be used as indicators for conformation of the chain. Certain bands are indicative of chain conformation, like those at 442 cm^{-1} (infrared absorption, β-poly-L-alanine) and 410 cm^{-1} (calculated, polyglycine I) that indicate β form.

Just like in the case of alanine, glycine oligomers, starting with Gly_3 take the β-form. This conclusion is determined by the presence of four different bands that were previously presented and appear in our studies too. These are: 466, 572, 606, 648 cm^{-1} for Gly_3; 468, 578, 605, 639 cm^{-1} for Gly_4; 467, 580, 602, 610, 536 cm^{-1} for Gly_5; and 467, 583, 606, 634 cm^{-1} for Gly_6. Simultaneously, the α-helix characteristic band at 365 cm^{-1} is absent. The spectrum of polyglycine spans a shorter frequency range than the spectra of glycine oligomers. This adds some difficulty in identifying the structure of PG. The highest frequency value that is displayed in the spectrum is at 400 cm^{-1}, too low to observe the expected feature at 410 cm^{-1}, characteristic for β-form. However, the presence of absorption peaks at 129 and 215 cm^{-1}, similar with those previously seen in PG, can be used as an indication for β structure.

As the figure 8.1 indicates, the results presented here add information about the group frequencies characteristic for polymers at low frequencies. The red lines represent the regions where specific vibrational modes can be seen in oligomers of glycine and polyglycine.

The region below 200 cm^{-1} belongs mainly to the H bond stretching vibrations. The features are visible at room temperature, they have rather low intensity, but gain in intensity as the temperature is decreased (ex. **[Ban1983]** for alanine).

Other vibrations that appear here are the lattice vibrations, the backbone deformations, and the vibrations of the ending groups NH_3^+ and COO^-. Around 270 – 380 cm^{-1} the most visible vibrations are the CCN deformations. The NH_3^+ modes appear around 380-480 cm^{-1}, and the CO_2 modes – at frequencies above 480 cm^{-1}, as well as between 220 and 300 cm^{-1}.

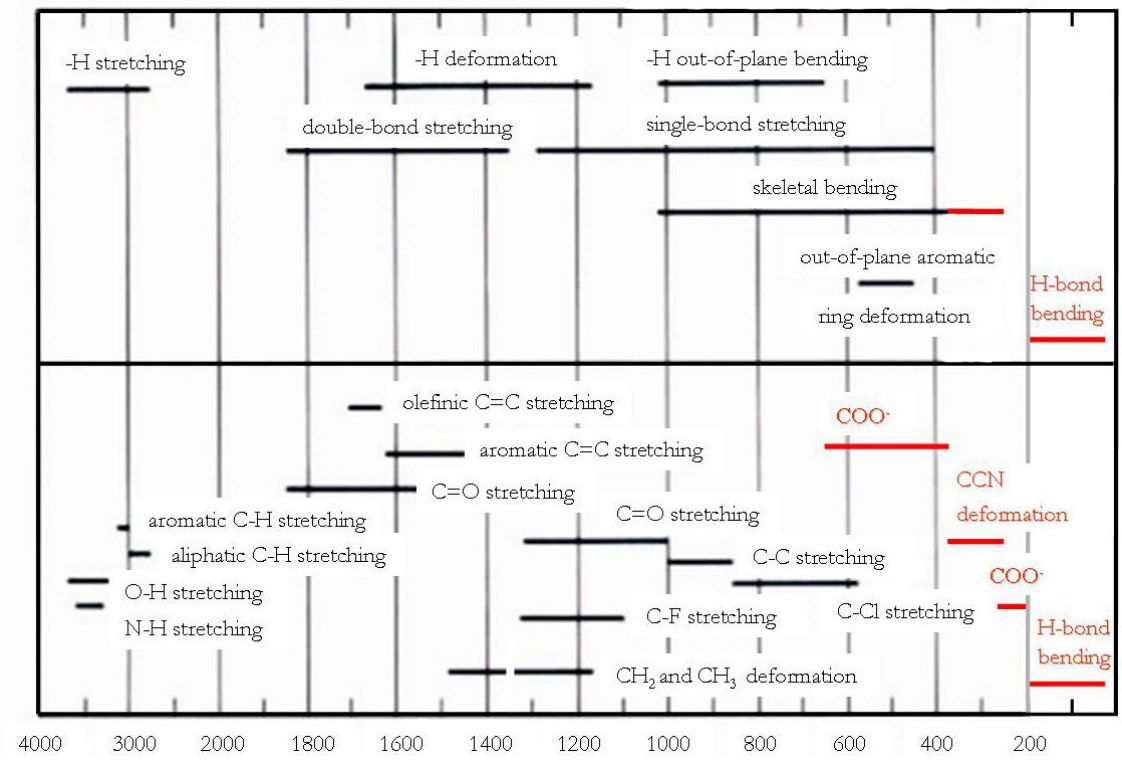

Fig. 8.1 Group frequencies present in polymers **[Bow1989]**. In the upper part of the diagram are visible the frequency regions with some general categories of vibrations. In the lower part are represented the more specific examples of these general types.

8.3 Proteins

In comparison with amino acids, proteins behave completely different in far infrared. The amino acids show definite features, most of them following some pattern, according with the group of atoms they represent. Proteins have broad spectra, where the features of amino acids are not retained. Moreover, protein spectra differ from those of homopeptides. Homoppeptides assume a secondary structure, just like proteins. There are studies that correlated secondary structure to the spectral features in

homopeptides as well as in proteins. Only that in proteins, this correlation is not always possible. Different studies have shown that proteins have almost identical spectra whether they are native or denaturated.

In our protein investigation we used three proteins with a high content of α-helix. Three different proteins, acylase, lipase and beta lactamase, have been investigated in the frequency range 0 – 350 cm^{-1}.

For each of them, the peptide chain is arranged in a α-helix structure: for beta lactamase 80 % of the total length is twisted in helical form, for lipase and acylase only 50 %. The other 50 % of the lipase and acylase chain is arranged in β-sheet structure.

The absorption pattern that is characteristic for amino acids, is smeared out in proteins: the absorption spectra of the three proteins show only a few broad features. Acylase and lipase are characterized by a large absorption band at ~200 cm^{-1}, beta lactamase by a broad peak, at 148 cm^{-1}.

This shift in frequency indicates the presence of different secondary structures: whereas for beta lactamase the maximum at 148 cm^{-1} shows the vibrations of the hydrogen bonds responsible for the stability of the helix, in acylase and lipase, the absorption maximum indicates the presence of more than one secondary structure.

The modes of acylase at 143 and 222 cm^{-1}, and those of lipase at 135 and 264 cm^{-1}, can be taken as indicators for the presence of α-helix structure. Beta lactamase has absorption maxima at 148, 229, and 306 cm^{-1}. The first two are indicators for the presence of α-helix.

At low frequencies, below 50 cm^{-1}, proteins exhibit an absorption feature that is temperature independent. In glasses, a similar feature, of unknown origin, is called boson peak. Proteins that display such a peak are considered to have a "glassy behaviour".

Two of the protein samples show a low-lying feature that could be associated with the boson peak: acylase at 25 cm^{-1} and lipase at 22 cm^{-1}. These peaks have low intensity, and they can be distingushed only by fitting the spectra with a sum of lorentzians.

The origin of this low frequency behaviour can be tentatively interpreted in two ways. On one hand, it can be the boson peak, on the other hand, the feature could be connected with the secondary structure of the proteins. As lipase and acylase have 50% of their chain length in β-form, and they are the samples to disyplay such a peak, maybe there is a straightforward connection between the two facts; the peak could be either related to the hydrogen bonds the β-sheet forms, or with a specific amino acid, or with the hydration level of the proteins. However, these ideas are not supported yet by further measurements, but would make sense to follow them.

8.4 Human blood serum

Due to the high water content (> 90%) the differences between serum and water spectra are extremely small. We do not find any large deviations from the water spectrum and no sharp features.
We can conclude that the optical properties of serum are governed by water, and that the effect of the radiation will manifest, first, in water.

The answer for the question from the Introduction, if one can identify an amino acid in a protein by means of FIR spectroscopy, is no. An amino acid is loosing its "identity" once is integrated in a protein. Already in a two amino acids-molecule is difficult to tell an amino acid from another.
But amino acids have clear, individual features in FIR. Their presence can be recognized in a sample as long as they have are not bonded with other molecules.

A. Amino acids absorption frequencies

Table 1& 2. Wavenumbers of infrared absorption bands **[Wri1939]**. Samples were observed in the form of thin, uniform layers of powdered crystals, containing about 1 mg/cm^2 area.

Table 1.

Gly	L - Ala	DL - Ala	L -Val	DL - Val	L - Leu	DL – Leu
				430	445	445
	486			476		
503	506	505				
527					516	521
	541	546	541	538	534	537
	583	583				581
609						
	648	647			649	649
			664			
				686		685
699						

Table 2.

L - Phe	DL - Phe	D - Glu	DL - Glu	L - Tyr	DL - Asp	DL - Ser
		438				
470	475	467		472	461	
				494		502
		514	512			
527	526			530		528
		536	538			
					554	561
			569			567
				575		
604	607				599	
		614				
		624			648	620
			642	651	657	
683	679	674	674			
	699					

Table 3. Assignment of observed frequencies (cm^{-1}) of glycine and glycine-D_3 in the low-frequency region **[Tsu1958]**. The samples were prepared as pellets with KBr matrix. s: strong; m: medium

α – Gly	α – Gly D_3	γ - Gly	γ - Gly D_3	Assignment
504 s	493 s	503 m	494 s	COO^- rock
516 m	-	557 m	-	NH_3 torsion
607 m	597 s	607 s	587 s	COO^- sym. bend.
694 s	667 s	686 s	659 s	COO^- wag

Table 4. Observed and calculated frequencies of the α-form crystal of glycine ($NH_3^+CH_2COO^-$), Gly-d_5 ($ND_3^+CD_2COO^-$), Gly-d_2 ($NH_3^+CD_2COO^-$), and Gly-d_3 ($ND_3^+CH_2COO^-$) **[Suz1963]**. IR absorptions of Gly and Gly - d_2 were observed in the forms of the KBr disks, and Gly - d_3 and Gly - d_5 in the form of Nujol and hexaclorobutadiene mulls. A normal coordinate treatment has been made as a seven-body problem of a Urey-Bradley type force field.

	Gly		Gly - d_5		Gly - d_2		Gly - d_3		Assignment
	Obs.	Calc.	Obs.	Calc.	Obs.	Calc.	Obs.	Calc.	
A´	355	308	334	297	357	305	-	-	CCN bend.
	503	508	461	487	461	496	-	-	CO_2 rock.
	698	702	646	661	668	669	-	-	CO_2 bend
A´´	-	135	-	119	-	119	-	135	C-C torsion
	516	-	702[31]	-	545	-	-	-	NH_3 torsion
	608	607	529	523	520	525	596	607	CO_2 wag

Table 5. Amide band frequencies in polymers **[Gup1968]**

Amide I	C=O stretching
Amide II	(N-H) in-plane bending + C-N stretching
Amide III	(N-H) in-plane bending + (C-M) stretching + (N-C) stretching
Amide IV	C=O in plane bending
Amide V	N-H out-of-plane bending
Amide VI	C=O out-of-plane bending
Amide VII	CO - NH torsion

[31] ND_3 torsion. In calculations ND_3^+ and NH_3^+ have been considered as a dynamical unit.

Table 6. Observed frequencies of Polyglycine II (α-form) and isotope substituted forms of it together with their assignments **[Suz1966]**

$(NHCH_2CO)_n$	$(NDCH_2CO)_n$	$(NHCD_2CO)_n$	$(NDCD_2CO)_n$	Assignment
363	356 s	374 s	345 s	Amide VII
-	520	-	534 m	Amide V´ (ND out of plane def.)
			497 s	Amide VI´ (C=O out of plane def.)
573 m	-	502 m	-	Amide VI
698 w	693 w	670 m	667 m	Amide IV

Table 7. Observed frequencies of Polyglycine I (β-form) prepared as pellets in KBr matrix **[Suz1966]**. The amounts of isotope shift are given not only by the frequency, Δν, but also by $\frac{\Delta\lambda}{\lambda^0} = \frac{\lambda(N^{15}) - \lambda(N^{14})}{\lambda(N^{14})}$ where $\lambda = 4\pi^2 c^2 \nu^2$, c being the velocity of light and ν the observed frequency (in cm^{-1}) at the maximum absorption.

$(NHCH_2CO)_n$	$(NDCH_2CO)_n$	$(NHCD_2CO)_n$	$(NDCD_2CO)_n$	Assignment
-	504	-	493	Amide V´
-	572	-	-	Amide VI´
589 m	-	534 m	-	Amide VI
614 m	614 w	564 m	554 m	Skel. Def.
628 w	625 w	610 m	605 m	Amide IV

Table 8. N^{15} isotope shifts in the vibrational frequencies of Polyglycine I and II **[Suz1966]**.

	Frequency (cm^{-1})		Shift		Assignment
	N^{14} species	N^{15} species	Δν, cm^{-1}	$\Delta\lambda/\lambda^0$	
Polyglycine I	614	611	-3	-0.009	Skel. Def.
	628	626	-2	-0.006	Amide IV
Polyglycine II	573	571	-2	-0.07	Amide VI
	698	695	-3	-0.09	Amide IV

Table 9. Calculated and observed spectra of polyglycine I **[Gup1968]**. The calculations are carried out according to Wilson`s GF matrix method **[Wil1939]**, as modified by Higgs **[Hig1953]** for an infinite chain. The methylene groups are treated as mass points (M). The molecule of polyglycine I belongs to the factor group C_{2v}.

	Calculated	Observed	Assignment
A_1	173	-	δ(N-M-C)-δ(C-N-M)
	220	-	δ(M-C-N)-δ(C-N-M)+δ(M-C-M)
A_2	91	inactive	τ(C-N), τ(N-M), τ(M-C)
	231	inactive	Amide VII
	618	inactive	Amide VI
	699	inactive	Amide V
B_1	277	-	δ(C-N-M)+δ(M-C-N)
	541	-	δ(N-M-C)+δ(M-C-M)
B_2	146	142	τ(C-N), τ(N-M), τ(M-C)
	410	413	Amide VII
	614		Amide VI

M: CH_2
δ, deformation mode
τ, torsional mode

Table. 10. The infrared and Raman frequencies for poly-L-alanine **[Koe1969]**. The samples were in the form of KBr disks.

Raman (cm^{-1})	Infrared (cm^{-1})	Calculated modes		Approximate group mode
		A	E	
294 w				Skeletal deformation
314 w		310		Skeletal deformation
	325 s		338	
375 s	368 s	361	368	Skeletal deformation
444 vw	445 m		474	Skeletal deformation
527 vs	528 s	524		
	595	592		N-H out of plane bending
610 w	615 w		612	C=O out of plane bending (amide VI)
662 w	655 m		655	N-H + C=O out of plane bending (amide V)
698 m	690 w-sh		695	
756 m		762		N-H and skeletal mode (amide V)
	770 vw		778	

Table 11. Vibrational frequencies of oligomeric and polymeric glycines **[Smi1969]**. The solid samples were in the form of KBr disks.

Frequency (cm^{-1})											
Diglycine (Raman)		Triglycine (Raman)		Tetraglycine		Pentaglycine		PG I	PG II		Assignment
Solid	Solution	Solid	Solution	Raman	IR	Raman	IR	IR	Raman	IR	
-	-	191 w	-	-	-	181 w	-	-	-		Skeletal modes
216 w	-	-	-	-	-	201 w	-	-	203 w		
-	-	-	-	212 w	-	-	-	-	-		
-	-	244 w	-	-	-	-	-	-	257 w		
298 w	-	302 w	-	285 m	-	281 w	-	-	-		
318 w	-	-	-	318 w	-	-	-	-	-		
-	-	-	-	-	-	326 w	-	-	-		
-	-	338 w	-	338 w	-	-	-	-	342 w		
-	379 m	-	-	-	-	363 w	-	-	-		
395 m	-	-	-	399 w	-	-	-	-	-		
-								-	-	363 s	Amide VII
452 w	-	468 w	472 m	-	-	468 w	-	-	-		-
-	-	-	-	516 m	-	-	-	-	-		-
536 w	-	-	-	-	-	-		-	-		-
-	-	-	-	564 m	-	-	-	-	-		-
-	-	-	-	-	-	-	-	-	568 w	573 s	Amide VI
-	-	-	-	-	579 s	-	-	-	-		-
-	-	580 m	-	-	-	-	585 s	-	-		Amide V
588 m	-	-	-	595 m	-	591 m	-	589 m	-		
-	-	603 m	-	-	605 s	-	609 s	-	-		-
-	-	-	-	-	-	-	-	614 m	-		-
-	-	-	-	-	636 m	-	633 m	628 w	-	698 s	Amide IV
663 w	-	-	-	-	700 s	-	695 s	-	-		-

Table 12. Calculated frequencies of polyglycine I **[Fuk1963]**. The calculations were carried out according to Wilson`s GF matrix method **[Wil1939]**. The methylene groups are treated as mass points (M). The aim of the calculations was the analysis of only skeletal vibrations and characteristic amide vibrations.

	Polyglycine I	N-deuterated polyglycine I
A_1	176	173
	223	221
	589	587
B_1	278	278
	541	518

223 cm^{-1} – antisymmetric skeletal deformation (M-C-N-M)
176 cm^{-1} – antisymmetric skeletal deformation (C-N-M-C)
278 cm^{-1} – symmetric deformation vibration of the C-N-M-C skeleton coupled with amide IV
541 cm^{-1} – symmetric deformation vibration of the N-M-C-N skeleton

Table 13. Infrared and Raman frequencies for alanine oligomers and polymer **[Sut1970]**. The samples for infrared measurements were all in the form of KBr pellets. The resolution was 4 cm^{-1}. Raman spectra had a resolution of 5 cm^{-1}.

Solid tri-L-Ala	Di-L-Ala	Tri-L-Ala	Randomlike solid di-L-Ala		β solid hexa-L-Ala		α solid poly-L-Ala		Tetra-L-Ala		Penta-L-Ala	
Raman	Solution (Raman)		Raman	IR	Raman	IR	Raman	IR	Raman	IR	Raman	IR
								120 s				
								167 m				
							187 w	190 m				
228 vw							212 m					
249 w			241 w						245 vw			
							257 w					
				296 vwsh			294 w	287 m				
306 m					306 m				306 m		306 m	
			316 w				314 w					
		326 w		329 s		328 s		325 s				
										355 w		
	375 m	377 m				373 s	375 s	368 s				
383 vw				381 m	388 vw					390 wsh		
403 vw			401 m	404 wsh								406 w
					438 m	433 s						
440 m	450 w	441 m					444 vw	445 m	440 m	439 m	440 m	445 m
466 wsh				466 s		457 wsh						452 wsh
			474 s							480 w		
						490 vw						
					502 vw							
528 w						530 vw	527 vs	528 s			524 w	521 m
			557 m	554 s					564 w	558 w		566 w
		587 m						595 w				
602 vw						605 w		615 w		607 w		610 w
										625 w		620 w
639 w				645 s	643 m				639 w		639 m	
								655				
			656 m				662 w		656 w	650 w		650 w

Table 14. Wave numbers and assignments of the observed bands for different isotopic species of glycine **[Gre1972]**

Molecules / Assignments	d_0 glycine	d_2 glycine	d_3 glycine	d_5 glycine
δ(CCN)	260	258	243	239
τ(CN)	313	312	243	239
δ(C-COO)	463	455	437	429
γ(C=O)	501	448	569.5	509
δ(C-COO)			527.5	512
	593	~500	532.5	
τ(CH_2)		~600		599
γ(O=H)	618	594		
	620	598	400	384

ν – stretching; γ - out of plane bending; δ – in plane bending; τ - torsion

Table 15. Assignment of the IR absorption bands of L-alanine **[Ada1972]**. For the measurements, single crystals of amino acid were grown by slow cooling of a saturated solution of L-alanine dissolved in 10% vol. aqueous acetic acid.

Frequency (cm^{-1})	Assignment
320 m	COO^- scissor
408 s	C_3C_2N scissor
481 m	NH_3^+ torsion
534 m	C_1C_2 symmetrical stretch
642 s	COO^- rock

Table 16. Vibration frequencies observed in Raman spectra of L-alanine grown crystals **[Wan1971]**.

	Frequency, cm^{-1}		Assignments
	300^0K	120^0K	
Lattice modes	42 s	40 s	
	50 m	48 m	
	75 m	75 m	
	88 m		
	101 m		
	107 s	107 s	
	115 s	117 s	
	131 w	132 w	
	141 m	143 m	
	160 w	165 w	
Internal modes	190 vw	200 vw	C-C torsion
	260-270 w	268 vw	CCNC deformation or twist
		281 w	
	287	286 w	
	290 m	291 vw	
	297 w	300 w	CH_3 torsion
	326 vw	326 w	CCNC deformation
	332 w	350 w	
	402 m	402 m	
	484 w	497 w	NH_3^+ torsion
	532 vs	534 vs	COO^- rock
	653 m	650 m	COO^- wag

Table 17. Raman and infrared frequencies for poly-L-leucine **[Koe1971]**. The polymers were pressed into disks in KBr matrix..

Raman (cm^{-1})	Infrared (cm^{-1})	Group	Tentative assignment
216 vw		Skeletal	τ(C-N) (amide VII)
249 vw		Skeletal	
	390 w	Skeletal	
452 w			
	471 s	Skeletal	
540 vw		Skeletal	
587 m	582 w	Skeletal	
	694 m	Skeletal	γ_{op}(N-H) (amide V)
	657 vw		
	614 m		

Table 18. Raman and infrared frequencies for poly-L-valine **[Koe1971]**

Raman (cm^{-1})	Infrared (cm^{-1})	Group	Tentative assignment
187		Residue	
228 vw		Skeletal	τ(C-N) (amide VII)
245 m		Residue	
310 m	390 w	Residue	
355 w			
	392 m	Skeletal	
407 m			
	436 m		
488 m	484 m	Residue	
	549 vw		
	606 w		
	709 s	Skeletal	γ_{op}(N-H) (amide V)

Table 19. Observed and calculated frequencies of crystalline polyglycine I **[Moo1976I]**

Observed		Calculated				Potential energy distribution
Raman	IR	A_g	A_u	B_g	B_u	
				29		NH•••O ipb(45), C=O•••H ipb(35), CN tor(11)
			34			NH•••O ipb(42), C=O•••H ipb(32), H•••O str(17)
				69		CαC tor(33), NCα tor(32), NH•••O ipb(17)
82 (87)		96				Hα••• Hα str(31), NCαC def(22), NH opb(15), H•••O str(14)
			110			NCαC def(38), CN tor(15), CαC tor(14)
112 (114)				110		H•••O str(79), CN tor(19)
		134				H•••O str(30), CN tor(23), NCαC def(12)
	140				145	H•••O str(52), CN tor(28), NH opb(24)
			179			NH opb(71), C=O opb(18)
170 (175)		181				NH opb(69), C=O opb(14)
211		217				CNCα def(75)
	217		230			CNCα def(67), C=O ipb(10)
					257	CNCα def(38), C=O ipb(27)
260				257		CNCα def(38), C=O ipb(35), NH opb(12)
		286				CαCN def(54), NCαC def(21), NCα str(12)
	285		290			CαCN def(58), NCαC def(18), NCα str(12)
	321				317	NCαC def(25), NH opb(23), C=O ipb(25)
327				318		NCαC def(25), NH opb(23), C=O ipb(25)
		12				NH tor(54), C=O tor(37)
589		584				C=O opb(40), C=O ipb(28), CαC str(12)
	589		585			C=O opb(39), C=O ipb(30), CαC str(12)
					585	CCαN def(45), C=O opb(18)
599				589		CCαN def(58)
				627		C=O opb(67), NH opb(19)
	614				618	C=O opb(52), CCαN def(18), NH opb(14), CH2 wag(10)
		628				C=O ipb(37), C=O opb(22), CH2 rock(11)
	628		629			C=O ipb(35), C=O opb(25), CH2 rock(11)

Table 20. Observed and calculated frequencies of β-poly-L-Ala **[Moo1976II]**.

Observed		Calculated				Potential energy distribution
Raman	IR	A_g	A_u	B_g	B_u	
			43			NH tor(29), C=O•••H ipb(18), NH opb(16), NH•••O ipb(10)
		35				NH tor(23), H•••O str(16), C=O tor(13), NH•••O ipb(13)
				31		NH•••O ipb(27), NH tor(21), C=O•••H ipb(19)
		25				NH tor(34), C=O•••H ipb(21), C=O tor(20)
				71		CαC tor(27), NCα tor(22), H•••O str(22), CN tor(12)
					89	H•••O str(36), CNCα def(18)
91		91				NH opb(22), Cβ bend 1(15), H•••O str(13)
					95	NH•••O ipb(29), CN tor(26), NH opb(16), CαC tor(14), C=O tor(12), NCα tor(10)
			103			NH•••O ipb(23), CN tor(20), NH opb(11)
	122			118		NCαC def(23), CNCα def(20), NCCα def(11)
135		139				NH opb(37), C=O opb(12), Cβ bend 1(12)
			140			NH opb(40), Cβ bend 1(13), C=O ipb(12)
					153	H•••O str(54), NCαC def(14), NH opb(10)
185		191				CNCα def(64)
			219			CNCα def(34), Cα Cβ tor(51), NCαC def(15)
					233	Cβ bend 2(46), Cα Cβ tor(15), CNCα def(10)
				231		Cβ bend 2(52), CNCα def(10)
					241	Cα Cβ tor(83), Cβ bend 2(10)
				240		Cα Cβ tor(89)
					699	CN tor(78), NH opb(34), NH•••O ipb(20)
698		703				C=O opb(55), CN tor(23), C^{β} bend 1(10)
	240		241			C^{α} C^{β} tor(51), $NC^{\alpha}C$ def(15)
235		240				Cα Cβ tor(69), NCαC def(11)
			287			NCCα def(43), Cα Cβ tor(16), H•••O str(10)
266		276				NCCα def(44), Cα Cβ tor(20), NCαC def(15)
					298	C=O ipb(36), NCαC def(16), CNCα def(14), Cβ bend 2(14)
300				300		C=O ipb(35), NCαC def(16), CNCα def(15), Cβ bend 2(13)
	326		325			NCαC def(32)
332		323				NCαC def(29)
375	372					α-helical structure
	445			436	437	C^{β} bend 1(50), NH opb(18)
	432		426			Cβ bend 2(66), NCαC def(10)
437		425				Cβ bend 2(67), NCαC def(11)
531	528					α-helical structure
					621	NCCα def(41), C=O opb(18), NCαC def(11)
	613			624		NCCα def(40), C=O opb(19), NCαC def(11)
	622		620			C=O ipb(57), CαC str(15)
		626				C=O ipb(56), CαC str(15)
					682	C=O opb(53), NCCα def(12)
				682		C=O opb(50), NCCα def(13)
			697			CN tor(51), C=O opb(35)

Table 21. Observed and calculated frequencies (in cm^{-1}) of β-poly-L-alanylglycine **[Moo1976II]**.

Observed		Calculated		Potential energy distribution
Raman	IR	A'	A"	
		25		C=O•••H opb(53), NH•••O opb(30)
			33	NH•••O opb(43), C=O•••H ipb(30)
		34		NH•••O opb(56), C=O•••H ipb(27)
			54	NH•••O opb(32), NH opb(15)
			72	CαC tor(27), NCα tor(24), H•••O str(16), NH opb(13), CN tor(11), NH•••O opb(10)
		90		H•••O str(16), NH opb(15), CαC tor(11)
		99		NH•••O opb(23), CN tor(24), NH opb(19), CαC tor(11)
	110		107	CN tor(19), NH•••O opb(23)
		129		H•••O str(74)
			150	NH opb(10), C=O opb(16)
		151		NH opb(43), C=O opb(16)
		187		CNCα def(38), NCαC def(21), H•••O str(11)
			189	NCαC def(28), CNCα def(23)
		216		CNCα def(34), CαCβ tor(18), CαCN def(16)
			230	CαCβ tor(62), CNCα def(16)
		247		CαCβ tor(76), CNCα def(14)
	256		256	CαCβ tor(32), CNCα def(34), H•••O str(10)
			279	C=O ipb(22), CNCα def(15), NCαC def(12), CαCN def(14), Cβ bend 1(10)
		276		C=O ipb(25), CNCα def(19), NCαC def(13), CαCN def(13)
			305	CαCN def(29), CCαN def(18), C=O ipb(13)
313		301		CαCN def(28), CCαN def(19), C=O ipb(13)
			335	Cβ bend 2(42)
333		331		Cβ bend 2(48), NH opb(10)
	370			α-helical structure
432	441	423	423	Cβ bend 1(25), NCαC def(22), Cβ bend 2(11), NH opb(11)
554	564		571	C=O opb(30), CαCN def(25), C=O ipb(12)
		573		CαCN def(28), C=O opb(28), C=O ipb(11)
600				
	618		619	C=O ipb(47), NCαC def(11)
630		622		C=O ipb(43), NCαC def(12)
		681		C=O opb(64)
			680	C=O opb(63)
		657		C=O opb(22), CN tor(13), NH opb(12)
			658	C=O opb(20), CN tor(16), NH opb(10)

Table 22. The observed and calculated frequencies for alanine **[Ban1983]**. The spectral resolution for the IR measurements was 1 cm^{-1}. Silicon was used as substrate.

IR Observed bands	Computed frequencies				Potential energy distribution
	a	b_1	b_2	b_3	
	55 49				σ_2 def (29), $CC^{\alpha}N$ def (17), CO_2 tor (10), NH_3 tor (10) $CC^{\alpha}N$ def (21), CO_2 tor (17), σ_1 str (10)
		59			$CC^{\alpha}N$ def (21), σ_1 def (20), σ_3 def (18), CO_2 tor (11)
73 m (74.5 m)			77		σ_3 def (27), $CC^{\alpha}N$ def (23), CO_2 tor (17)
				78	$CC^{\alpha}N$ def (21), σ_1 def (20), CO_2 tor (12)
85 m (87 m)		79			σ_1 def (22), σ_2 def (21), CO_2 tor (17)
			89		CH_3 tor (27), σ_2 def (18), σ_3 str (11)
94 w		96			CH_3 tor (21), σ_2 def (17), σ_3 str (9)
			98		σ_1 def (41), CO_2 tor (32), CH_3 tor (12), σ_2 def (9)
105 m (110 s)				101	CO_2 tor (22), σ_1 def (12)
112.5 m (125.8 s)				117	σ_3 str (32), σ_1 def (17), NH_3 tor (13)
	119				σ_1 def (31), σ_1 str (27), σ_1 str (17)
		125			CO_2 tor (37), $CC^{\alpha}N$ def (29), σ_1 str (11)
				127	σ_3 str (48), σ_1 def (22)
	133				σ_2 str (43), σ_1 def (31), σ_2 str (13)
145 sh (158 s) 139.5 sh (144 s) 150		140	153	151	σ_1 str (7), σ_2 str (43) σ_2 str (49), σ_1 str (41) σ_3 str (57), σ_1 str (33) σ_1 str (42), σ_3 def (21), CO_2 tor (11)
		201			CO_2 tor (81), $CC^{\alpha}N$ def (17)
200-220 br	203				CO_2 tor (66), $CC^{\alpha}N$ def (13)
				205	CO_2 tor (77), $CC^{\alpha}N$ def (13)
(258 m)			207		CO_2 tor (91)
258 m			277		$CC^{\alpha}N$ def (41), CH_3 tor (40)
282 s (280s 287s)		283			CH_3 tor (47), $CC^{\alpha}N$ def (33), NC^{α} str (10)
	293			291	$CC^{\alpha}N$ def (49), $C^{\alpha}C$ str (16) $CC^{\alpha}N$ def (49), CO_2 rock (12), $C^{\alpha}C$ str (9)
326 s (326 s)			316	317	CH_3 tor (47), $CC^{\alpha}N$ def (41), $C^{\alpha}C$ str (10) CH_3 tor (51), $CC^{\alpha}N$ def (21), NC^{α} str (10)
326 s (326 s)			325	326	$CC^{\alpha}N$ def (59), NH_3 tor (21) $CC^{\alpha}N$ def (56), CO_2 rock (13), $C^{\alpha}C$ str (9)
		327			$CC^{\alpha}N$ def (57), CO_2 rock (12)
	329				$CC^{\alpha}N$ def (63), $C^{\alpha}C$ str (16)
		407			CH_3 tor (69), NH_3 tor (19), NCα str (9)
408 vs 410 (vs)	409				CH_3 tor (89)
	411				$CC^{\alpha}N$ def (66), NH_3 tor (17)
408 vs (410 vs)		415	414	414	$CC^{\alpha}N$ def (81), NC^{α} str (10) $CC^{\alpha}N$ def (67), $C^{\alpha}C$ str (11), CO_2 rock (9) $CC^{\alpha}N$ def (79), NH_3 tor (9)
487 m (499 m)		489			NH_3 tor (76), $CC^{\alpha}N$ rock (12)
497 sh (505 sh)	495		498	496	NH_3 tor (83), CO_2 rock (10) NH_3 tor (77), CO_2 rock (18) NH_3 tor (79), CO_2 wag (10)
			533		CO_2 rock (61), NH_3 tor (13), CO_2 wag (10)
				533	CO_2 rock (66), NH_3 tor (17)
537 /539	542	540			CO_2 rock (71), CO_2 bend (21)/CO_2 rock (63), CO_2 wag 13

Table 23. Observed bands in the IR and Raman spectra of tyrosine, with their assignments: all IR and Raman values are in cm^{-1} **[Gra2002]**. The numbers indicated at the assignments represent the Wilson notation **[Wil1934]**.

IR, Nujol	Raman (rel.int.)	Assignment
	87 (19)	chain torsion
	108 (42)	$HOOCHNH_2$ torsion
	122 (75)	COOH torsion
	140 (7)	NH_2 torsion
	163 (54)	11
	255 (7)	15
	333 (7)	10b
	384 (7)	9b
	calc. 416	16a
434 (w)	427 (11)	6a
498 (m)		chain bend
535 (m-s)		16b
558 (vw)		chain bend
576 (m-s)		chain bend
639 (vw, sh)	641 (26)	6b
645 (m)		

Table 24. Observed and calculated frequencies (cm^{-1}) of PG I **[Fan1973]**.

Observed[a]		Calculated[b]	Assignments[c]
296 K	120 K		
		69	$\tau_{C'C}(30)$, $\tau_{CN}(29)$, $\omega_{N\text{-}H\cdots O}(18)$, $\tau_{C'N}(11)$, $\omega_{NH}(13)$
82(R)	87(R)	75	$\omega_{N\text{-}H\cdots O}(36)$, $\omega_{C\text{-}O\cdots H}(18)$, $\alpha_{N\text{-}H\cdots O}(17)$
111(R)	114(R)	106	$\omega_{NH}(22)$, $\tau_{C'N}(21)$, $\tau_{CC'}(20)$
		131	$\alpha_{NCC'}(33)$, $\tau_{CC'}(11)$, $r_{O\cdots H}(11)$
		137	$\alpha_{NCC'}(27)$, $\tau_{CC'}(10)$, $\tau_{C'N}(13)$
133(IR)		149	$r_{O\cdots H}(92)$
170(R)	175(R)		
211(R)	214(R)	201	$\alpha_{C'NC}(21)$, $\alpha_{CC'N}(11)$, $\omega_{NH}(30)$
215(R)		207	$\alpha_{C'NC}(43)$
260(R)	260(R)	257	$\alpha_{C'NC}(54)$, $r_{O\cdots H}(21)$
285(IR)		264, 267	$\alpha_{C'NC}(41)$, $\alpha_{C'O}(31)$
320()IR		329	$\alpha_{CC'N}(48)$, $\alpha_{NCC'}(15)$, $r_{NC}2(12)$
327(R)	328(R)	319	$\alpha_{CC'N}(48)$, $\alpha_{NCC'}(15)$, $r_{NC}2(12)$
587(R)		572	$r_{CC'}(12)$, $\alpha_{C'O}(26)$, $\omega_{C'O}(49)$
599(R)	599(R)	623	$\omega_{C'O}(49)$, $\alpha_{CC'N}(25)$

[a] Letters in paranthesis denote whether band is observed in the infrared (IR) or Raman (R).

[b] **[Abe1972]**

[c] r, bond stretch; ω, out-of-plane deformation; α, angle deformation, τ, torsion.

B. Normal modes calculation

In the next, it will be given the mathematical treatment of the vibration and rotation of a molecule. First, one needs to deduce the classical expressions for the kinetic and potential energies of the molecule in terms of the coordinates of the atoms, and to obtain with the help of these expressions, the wave equation for vibration, rotation, and translation.

It takes *3N* coordinates (*3N* degrees of freedom) to completely describe the space arrangement of a molecule with *N* nuclei, which corresponds to three Cartesian coordinates for each nucleus. Three of these specify the center of mass of the molecule (translational degrees of freedom), three coordinates describe the orientation of a nonlinear molecule about its center of mass (rotational degrees of freedom), and the rest of *3N-6* coordinates correspond to vibrational motion (vibrational degrees of freedom). In case of linear molecules it takes only two coordinates to specify the orientation about the center of mass. Accordingly, a linear molecule has only *3N-5* vibrational degrees of freedom.

If x_k, y_k, z_k are the coordinates of the k-th atom and a_k, b_k, c_k the values of the coordinates of the equilibrium position of the k-th atom, then the displacements from equilibrium are:

$$\Delta x_k = x_k - a_k, \qquad \Delta y_k = y_k - b_k, \qquad \Delta z_k = z_k - c_k \tag{B.1}$$

The kinetic energy is written as:

$$2T = \sum_{k=1}^{N} m_k \left[\left(\frac{d\Delta x_k}{dt} \right)^2 + \left(\frac{d\Delta y_k}{dt} \right)^2 + \left(\frac{d\Delta z_k}{dt} \right)^2 \right] \tag{B.2}$$

For convenience, the coordinates $\Delta x_k, \Delta y_k, \Delta z_k$ by another set of coordinates $q_1, \ldots, q_{3N}$ defined as:

$$q_1 = \sqrt{m_1}\Delta x_1,\ q_2 = \sqrt{m_1}\Delta y_1,\ q_3 = \sqrt{m_1}\Delta z_1,\ q_4 = \sqrt{m_2}\Delta x_2, \text{ etc.} \qquad \text{(B.3)}$$

These are the mass-weighted Cartesian coordinates. The kinetic energy becomes:

$$2T = \sum_{i=1}^{3N} \dot{q}_i^2 \qquad \text{(B.4)}$$

For small displacements, the potential energy in the new coordinates is written as a power series:

$$2V = 2V_0 + 2\sum_{i=1}^{3N}\left(\frac{\partial V}{\partial q_i}\right)_0 q_i + \sum_{i,j=1}^{3N}\left(\frac{\partial^2 V}{\partial q_i \partial q_j}\right)_0 q_i q_j + \text{higher terms} =$$

$$= 2V_0 + 2\sum_{i=1}^{3N} f_i q_i + \sum_{i,j=1}^{3N} f_{ij} q_i q_j + \text{higher terms} \qquad \text{(B.5)}$$

V_0 can be eliminated from equation for the cases where the energy of the equilibrium configuration is zero. When all q_i´s are zero, the atoms are in their equilibrium positions, which means that the energy should me a minimum for $q_i=0$. This is written as:

$$\left(\frac{\partial V}{\partial q_i}\right)_0 = f_i = 0 \qquad i = 1, 2, \ldots 3N \qquad \text{(B.6)}$$

The higher terms in equation (B.5) are neglected for small amplitudes:

$$2V = \sum_{1,j=1}^{3N} f_{ij} q_i q_j \quad (f_{ij}=f_{ji}) \qquad \text{(B.7)}$$

The equations of motion have the form:

$$\frac{d}{dt}\frac{\partial T}{\partial \dot{q}_j}+\frac{\partial V}{\partial q_j}=0 \qquad j=1, 2, \ldots 3N \qquad \text{(B.8)}$$

After substitution of (B.4) and (B.7) in (B.8), the equations of motion become:

$$\ddot{q}_j+\sum_{i=1}^{3N} f_{ij}q_i=0 \qquad j=1, 2, \ldots 3N \qquad \text{(B.9)}$$

(B.9) represents a set of 3N second-order linear differential equations. A solution for them is:

$$q_i=A_i\cos\left(\lambda^{1/2}t+\varepsilon\right) \qquad \text{(B.10)}$$

with A_i, λ, and ε constants. Substitution of the solution (B.10) in (B.9) gives the following set of algebraic equations in $3N$ unknown amplitudes A_i.

$$\sum_{i=1}^{3N}\left(f_{ij}-\delta_{ij}\lambda\right)A_i=0 \qquad j=1, 2, \ldots, 3N \qquad \text{(B.11)}$$

where δ_{ij} is the Kronecker symbol. The solutions are different from the trivial $A_i=0$, when λ satisfies the secular equation:

$$\begin{vmatrix} f_{11}-\lambda & f_{12} & \ldots & f_{1,3N} \\ f_{21} & f_{22}-\lambda & \ldots & f_{2,3N} \\ \ldots & \ldots & \ldots & \ldots \\ f_{3N,1} & f_{3N,2} & \ldots & f_{3N,3N}-\lambda \end{vmatrix}=0 \qquad \text{(B.12)}$$

For a fixed value of λ, say λ_k, which makes the determinant 0, the coefficients $(f_{ij} - \delta_{ij}\lambda)$ become fixed and is possible to obtain a solution A_{ik}. This is not uniquely determined. A unique mathematical solution can be determined by the quantities l_{ik}, defined as:

$$l_{ik} = \frac{A'_{ik}}{\left[\sum_i (A'_{ik})^2\right]^{1/2}} \tag{B.13}$$

where A'_{ik} is an arbitrary set obtained by putting $A_{1k} = 1$.
The solution for the physical problem is obtained as:

$$A_{ik} = K_k l_{ik} \tag{B.14}$$

where K_k are constants determined by the initial values of the coordinates q_i and velocities $\dot{q}_i$.

For a given λ_k, each atom has the same frequency and phase, even when the amplitudes of the oscillation are different. This means that all the atoms are reaching the position of maximum displacement at the same time, and they pass through the equilibrium position all together at the same time. The modes of vibration that have this characteristic are the *normal modes*, and the frequency is called *normal*, or *fundamental frequency* of the molecule. In a spectrum, the fundamental frequencies are, usually, the most intense. Other transitions, as overtones and combinations might appear, and might be comparatively intense.

C. Transition selection rules

The spectroscopic selection rules determine which transitions are allowed between two states. As a transition implies a time-dependent phenomenon, the spectroscopic selection rules are deduced from the time-dependent perturbation theory.

The time-dependent Schrödinger equation is written as:

$$\hat{H}\psi = i\hbar \frac{\partial \psi}{\partial t} \tag{C.1}$$

The solution of the equation is:

$$\psi_n(\vec{r},t) = \psi_n(\vec{r}) e^{-iE_1 t/\hbar} \tag{C.2}$$

where $\psi_n(\vec{r})$ is solution for the time-independent Schrödinger equation:

$$\hat{H}\psi_n(\vec{r}) = E_n \psi_n(\vec{r}) \tag{C.3}$$

A molecule may undergo a state transition upon interaction with electromagnetic radiation.

The presence of electromagnetic radiation can be considered a perturbation, and the new Hamiltonian is:

$$\hat{H} = \hat{H}^{(0)} + \hat{H}^{(1)} = \hat{H}^{(0)} - \mu\vec{E}_0 \cos 2\pi\nu t \tag{C.4}$$

The time-dependent term $\hat{H}^{(1)}$ is the reason for transitions between stationary states:

$$\hat{H}^{(1)} = -\mu\vec{E} \tag{C.5}$$

where μ is the dipole moment of the molecule, and $\vec{E}$ is the electromagnetic field which has the expression:

$$\vec{E} = \vec{E}_0 \cos 2\pi\nu t \tag{C.6}$$

where ν is the frequency of the radiation and $\vec{E}_0$ - the electric field vector. Considering an isolated molecule that has only two stationary states (in reality the number is infinite), the Hamiltonian in the absence of any perturbation is:

$$\hat{H}^{(0)}\psi = i\,\hbar\,\frac{\partial\psi}{\partial t} \tag{C.7}$$

and the stationary states are ψ_1, ψ_2 with:

$$\boldsymbol{\psi}_1(t) = \psi_1 e^{-iE_1 t/\hbar} \text{ and } \boldsymbol{\psi}_2(t) = \psi_2 e^{-iE_2 t/\hbar} \tag{C.8}$$

When the system evolutes from state 1 to state 2, the wave function $\boldsymbol{\psi}(t)$ is a linear combination of $\boldsymbol{\psi}_1(t)$ and $\boldsymbol{\psi}_2(t)$ with time-dependent coefficients:

$$\boldsymbol{\psi}(t) = a_1(t)\boldsymbol{\psi}_1(t) + a_2(t)\boldsymbol{\psi}_2(t) \tag{C.9}$$

Replacing this solution in the Schrödinger equation (x.1), one obtains:

$$\begin{aligned} &a_1(t)\hat{H}^{(0)}\boldsymbol{\psi}_1 + a_2(t)\hat{H}^{(0)}\boldsymbol{\psi}_2 + a_1(t)\hat{H}^{(1)}\boldsymbol{\psi}_1 + a_2(t)\hat{H}^{(2)}\boldsymbol{\psi}_2 \\ &= a_1(t)i\hbar\frac{\partial\boldsymbol{\psi}_1}{\partial t} + a_2(t)i\hbar\frac{\partial\boldsymbol{\psi}_2}{\partial t} + i\hbar\boldsymbol{\psi}_1\frac{da_1}{dt} + i\hbar\boldsymbol{\psi}_2\frac{da_2}{dt} \end{aligned} \tag{C.10}$$

The first two terms on both sides of the equation are equal, and this leads to:

$$a_1(t)\hat{H}^{(1)}\boldsymbol{\psi}_1 + a_2(t)\hat{H}^{(1)}\boldsymbol{\psi}_2 = i\hbar\boldsymbol{\psi}_1\frac{da_1}{dt} + i\hbar\boldsymbol{\psi}_2\frac{da_2}{dt} \qquad \text{(C.11)}$$

Multiplying the equation (C.11) with $\boldsymbol{\psi}_2^*$ and integrate over the spatial coordinates one obtains:

$$\begin{aligned} &a_1(t)\int\psi_2^*\hat{H}^{(1)}\boldsymbol{\psi}_1 d\tau + a_2(t)\int\boldsymbol{\psi}^*{}_2\hat{H}^{(1)}\boldsymbol{\psi}_2 d\tau = \\ &i\hbar\frac{da_1}{dt}\int\boldsymbol{\psi}^*{}_2\boldsymbol{\psi}_1 d\tau + i\hbar\frac{da_2}{dt}\int\boldsymbol{\psi}^*{}_2\boldsymbol{\psi}_2 d\tau \end{aligned} \qquad \text{(C.12)}$$

Because $\boldsymbol{\psi}_1 = \psi_1 e^{-iE_1t/\hbar}$, and because ψ_1 and ψ_2 are orthogonal $\int\psi_2^*\hat{H}^{(1)}\boldsymbol{\psi}_1 d\tau = 0$. On the other hand $\boldsymbol{\psi}_2 = \psi_2 e^{-iE_2t/\hbar}$ and ψ_2 is normalized which means that

$$i\hbar\frac{da_2}{dt}\int\boldsymbol{\psi}^*{}_2\boldsymbol{\psi}_2 d\tau = i\hbar e^{-iE_2t/\hbar}\frac{da_2}{dt} \qquad \text{(C.13)}$$

Solving the equation (C.12) for $i\hbar\frac{da_2}{dt}$ becomes:

$$i\hbar\frac{da_2}{dt} = a_1(t)\,e^{iE_2t/\hbar}\int\psi_2^*\hat{H}^{(1)}\boldsymbol{\psi}_1 d\tau + a_2(t)e^{-iE_2t/\hbar}\int\psi_2^*\hat{H}^{(1)}\boldsymbol{\psi}_2 d\tau \qquad \text{(C.14)}$$

After substitution of $\boldsymbol{\psi}_1(t) = \psi_1 e^{-iE_1t/\hbar}$ and $\boldsymbol{\psi}_2(t) = \psi_2 e^{-iE_2t/\hbar}$, (C.14) gives:

$$i\hbar\frac{da_2}{dt} = a_1(t)\exp\left[\frac{-i(E_1-E_2)t}{\hbar}\right]\int\psi_2^*\hat{H}^{(1)}\boldsymbol{\psi}_1 d\tau + a_2(t)\int\psi_2^*\hat{H}^{(1)}\boldsymbol{\psi}_2 d\tau$$

(C.15)

The initial values for the time dependent coefficient are $a_1(0) = 1$ and $a_2(0) = 0$, because the system is initially in state 1. As the perturbation is very small, the coefficients can be approximated with their initial values and get:

$$i\hbar \frac{da_2}{dt} = \exp\left[\frac{-i(E_1 - E_2)t}{\hbar}\right] \int \psi_2^* \hat{H}^{(1)} \psi_1 d\tau \qquad \text{(C.16)}$$

Next step is the replacement of $\hat{H}^{(1)}$ with the term that measures the electromagnetic field -molecule interaction:

$$\hat{H} = -\mu_z E_{0z} \cos 2\pi\nu t = -\frac{\mu_z E_{0z}}{2}(e^{i2\pi\nu t} + e^{-i2\pi\nu t}) \qquad \text{(C.17)}$$

where μ_z is the z component of the molecular dipole moment and E_{0z} is the electric field component along the z-axis. Defining $(\mu_z)_{12} = \int \psi_2^* \mu_z \psi_1 d\tau$ as the z component of the transition dipole moment between states 1 and 2 and introducing equation (C.17) in (C.16) gives:

$$\frac{da_2}{dt} \propto (\mu_z)_{12} E_{0z} \left\{ \exp\left[\frac{i(E_2 - E_1 + h\nu)t}{\hbar}\right] + \exp\left[\frac{i(E_2 - E_1 - h\nu)t}{\hbar}\right] \right\} \qquad \text{(C.18)}$$

If $(\mu_z)_{12}$ is 0, then $\frac{da_2}{dt}$ is also 0, and there is no transition from state 1 to state 2. The result is that transitions occur only between vibrational states for which the transition dipole moment is nonzero. The quantity $(\mu_z)_{12} = \int \psi_2^* \mu_z \psi_1 d\tau$ gives the intensity of the vibrational (infrared) transition.

D. Producing a spectrum with Michelson interferometer

Figure D.1 illustrates a Michelson interferometer. The source is emitting polychromatic radiation thatt is directed to the beamsplitter.

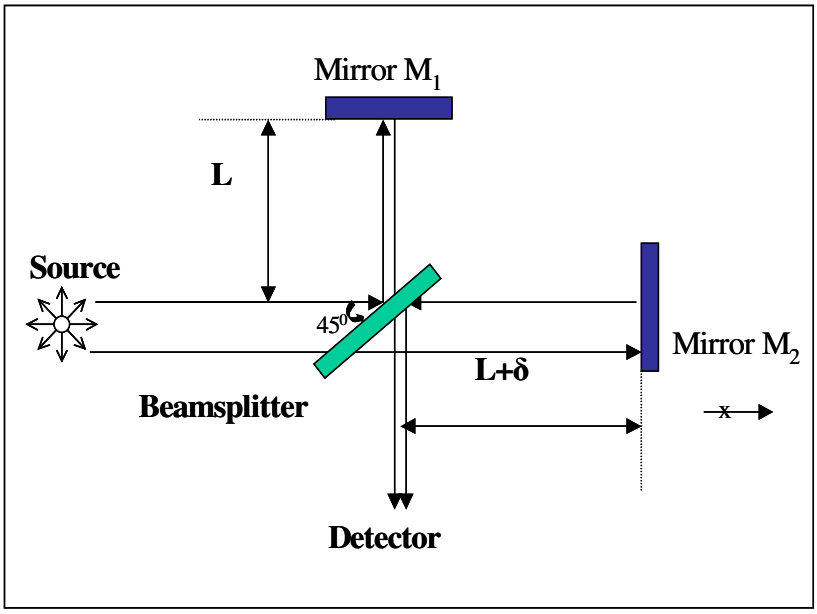

Fig. D.1 Michelson interferometer

Half of the incoming light passes through the beamsplitter, is reflected by the moving mirror

M_2 and is once more reflected on the beamsplitter before reaching the detector - after a total path length of $2(L+\delta)$. The other half of the incoming light is reflected perpendicularly by the beamsplitter , is reflected by the fixed mirror M_1, passes through the beamsplitter again and goes to the detector – after a total path length of $2L$. The difference between the two beams is 2δ. If the path difference is an integral number of wavelengths

$$2\delta = m\lambda, \quad m = 0,\pm1,\pm2,... \tag{D.1}$$

where λ is the wavelength, then the interference of the two beams is constructive. The quantity measured by the detector is thus the intensity $I(\delta)$ of the combined beams as a function of the displacement δ of the moving mirror. When 2δ is an odd multiple of $\lambda/2$, destructive interference occurs and the signal at the detector is minimum.

The amplitudes of the beams reaching the detector are equal, each of them undergoes one reflection and one transmission at the beamsplitter.

The electric field at the beamsplitter is:

$$\vec{E}(\delta,\nu) = \vec{E}_0(\nu)\exp\{i(2\pi\nu\delta - \omega t)\} \tag{D.2}$$

The electric field at the detector will be the sum of the electric field of the two beams:

$$\vec{E}(\delta,\nu) = |\hat{r}||\hat{t}|\vec{E}_0(\nu)\{\exp[i(4\pi\nu L - \omega t)] + \exp[i(4\pi\nu(L+\delta) - \omega t)]\} \tag{D.3}$$

Here, $\hat{r}$ and $\hat{t}$ are the complex reflection and transmission coefficients of the beamsplitter. The term $\vec{E}_0(\nu)\exp[i(4\pi\nu L - \omega t)]$ is due to the light beam that travels the distance of L, while the term $\vec{E}_0(\nu)\exp[i(4\pi\nu(L+\delta) - \omega t)]$ is due to the light beam that traveled the distance $2(L+\delta)$.

The intensity I detected is the time average of $\vec{E}\times\vec{H}$ (the Poynting vector), but because $|\vec{E}| \propto |\vec{H}|$ it can be considered that the intensity is proportional with the time average of E^2.

This means that:

$$I(\delta,\nu) \propto E_0^2(\nu)[1+\cos(2\pi\nu\delta)] \tag{D.4}$$

The intensity written as a function of path difference only is:

$$I(\delta) \propto \int_0^\infty E_0^2(\nu)[1+\cos(2\pi\nu\delta)]d\nu \tag{D.5}$$

After rearranging the terms, (3.1.5) becomes:

$$I(\delta) - E_0^2(\nu) \propto \int_0^\infty E_0^2(\nu)\cos(2\pi\nu\delta)d\nu \tag{D.6}$$

Which can be written as:

$$[I(\delta) - I(0)/2] \propto \int_0^\infty E_0^2(\nu)\cos(2\pi\nu\delta)d\nu \qquad \text{(D.7)}$$

The quantity of interest in the measurement is the power spectrum $B(\omega)$ which is the Fourier transform of $I(\delta)$. $B(\omega)$ is related to $I(\delta)$ by:

$$B(\nu) \propto \int_0^\infty [I(\delta) - I(0)/2]\cos(2\pi\nu\delta)d\delta \qquad \text{(D.8)}$$

The last relation means that an interferogram is produced as a function of path difference and the spectrum is reconstructed digitally.

E. Raman measurements

In **[Smi1969]**[32] Raman spectra for glycine molecule in different chain length were recorded in the region 150 to 1700 cm^{-1}, and assignments were made for the vibrational frequencies. It is worth to mention that the Amide V band, which corresponds to an N-H out-of-plane bending, can not be observed in the samples prepared as solution. It is observed both in Raman and infrared in the case of tetra- and pentaglycine, and in infrared in the case of polyglycine I and II. For polyglycine II the band is displaced to 740 cm^{-1}, while for the other molecules is situated at lower values, between 585 and 595 cm^{-1}. The vibrations under 400 cm^{-1} are assigned to skeletal deformations. However, the comments of the article are oriented toward the frequency range >800 cm^{-1}, leaving place for interpretations for the lower frequencies.

In **[Sma1970]** is reported a low-lying band observed in Raman spectra of polyglycines, which was not found in infrared absorption: 167 cm^{-1} for PGI which corresponds to a skeletal bending of the N-M-C and C-N-M angles, and 116 cm^{-1} for N-deuterated PGII which represents torsion about the M-C and N-M bonds. The latter band was calculated for N-deuterated PGII at 124 cm^{-1}, and for PGII at 126 cm^{-1}.

In **[Fan1973]**, new low-lying frequency were calculated for PGI (149, 137, 131, 106, 75, 69 cm^{-1}) and PGII (112, 93 and 83 cm^{-1}). The assignments are the following: the mode at 106 cm^{-1} for PGI is composed of torsions about the C´N and CC´ bonds and NH out-of-plane deformation; the mode at 149 cm^{-1} (calculated at 133 cm^{-1}) is due to the stretching of the NH•••O hydrogen bond; the mode at 75 cm^{-1} is a rotational mode that involves deformation of the out-of-plane NH•••O angle. For the other modes there were no definite assignments. In PGII, the mode at 83 cm^{-1} involves skeletal torsions, out-of-plane N-H deformation and NH•••O angle deformation. PGII has fewer bands under 200 cm^{-1} than PGI.

Raman studies of α-poly-L-alanine **[Koe1969]**[33] were made in parallel with those of infrared absorption **[Gup1968]**. In this reference all the bands under 474 cm^{-1} were assumed to be skeletal deformations. Although all of the optical modes of the α-helix are expected to be active in both Raman and infrared, it happens that some bands don't appear in both measurements, mainly because they are too weak to be detected. Amide V band is observed around 770 cm^{-1} where is mixed with a skeletal mode, more displaced than in other studies **[Gup1968]** and 650 cm^{-1}. Raman spectra indicate that dipeptides, the higher oligomers and the polymer of alanine exist in nonplanar β and α-helical conformations, respectively **[Sut1970]**[34]. From the comparison of the spectra of tri-L-alanine in the solid state and in aqueous solution, one can see the conformational change from the β structure to random coil. The spectrum of solid di-L-alanine has also the random like structure; this can be observed from comparison with the spectrum of tri-L-alanine in solution.

[32] **[Smi1969]** in Annex A is given the infrared and Raman spectra for polyglycine II, tetraglycine, pentaglycine, polyglycine I (only infrared), diglycine and triglycine (only Raman), table 11, page 151

[33] **[Koe1969]** in Annex A, table 10, page 150

[34] **[Sut1970]** in Annex A, table 13, page 152

F. Polyalanine

The polymer can assume both α and β conformations. Vibrational frequencies of α-poly-L-alanine are presented in Table F1. In the domain 60 - 200 cm^{-1}, the α-helix has 4 characteristic bands: ~100, 120, ~167, and ~190 cm^{-1} (Table F2).

Table F1. Observed and calculated frequencies (in cm^{-1}) of α-poly-L-alanine **[Dwi1984]**.

Observed	Calculated	Potential Energy Distribution
	38	$C^{\alpha}C$ t(53), H•••O s(18)
	40	NH ob(58), C^{β} b1(20), H•••O s(11)
	49	NH ob(38), NC^{α} t(24), H•••O s(23), CN t(15), C^{β} b1(13)
	87	NH ob(33), NH•••O ib(20), C^{β} b1(12), $NC^{\alpha}C$ d(10), CNC^{α} d(10)
84 W	94	CN t(27), NC^{α} t(23), $C^{\alpha}C$ t(22), H•••O s(15), NH ob(10)
113 M, sh	96	NH ob(24), $C^{\alpha}C$ t(20), NC^{α} t(18), CN t(18), H•••O s(10)
120 S	136	CNC^{α} d(34), $C^{\alpha}CN$ d(21), $NC^{\alpha}C$ d(16), C^{β} b1(12)
	151	NH ob(43), CNC^{α} d(20), $NC^{\alpha}C$ d(11)
163 M	155	CNC^{α} d(33), $C^{\alpha}CN$ d(19), C^{β} b1(14), NH ob(14), $NC^{\alpha}C$ d(12)
188 M	197	$C^{\alpha}CN$ d(15), C^{β} b2(12), CO ob(12)
	205	$C^{\alpha}CN$ d(27), C^{β} b2(25), C^{β} b1(12), CO ob(10)
233 VW	230	C^{α} C^{β} t(63)
	244	C^{α} C^{β} t(95)
240 W	245	C^{α} C^{β} t(91)
259 W, sh	264	C^{α} C^{β} t(35), C^{β} b2(14)
290 M	307	C^{β} b2(34), CO ib(29), CNC^{α} d(15)
	310	CNC^{α} d(30), CO ib(20), C^{β} b1(20), CO ob(17)
324 S	326	C^{β} b2(42), C^{β} b1(19), CO ib(16)
	366	C^{β} b2(49), $C^{\alpha}CN$ d(22), C^{β} b1(16)
366 M, sh	367	CO ob(21), C^{β} b1(17), $NC^{\alpha}C$ d(14), NH ob(13), C^{β} b2(11)
375 S	374	CO ob(16), NH ob(16), C^{β} b2(15), $C^{\alpha}CN$ d(15), CO ib(15), CNC^{α} d(10)
	492	$NC^{\alpha}C$ d(37), CO ib(17), $C^{\alpha}C$ s(16)
526 S	522	$NC^{\alpha}C$ d(31), $C^{\alpha}C$ s(14), $C^{\alpha}CN$ d(11), CO ib(11)
	537	CO ib(29), $C^{\alpha}CN$ d(21), $C^{\alpha}C$ s(17), C^{β} b2(17), NH ob(11)
	589	CN t(68), NH ob(36), CO ob(26), NH•••O ib(11)
618 S	608	CN t(47), NH ob(23), CO ob(15), CO ib(12)
	637	CN t(59), NH ob(43), NH•••O ib(13)
658 S	660	CN t(37), NH ob(21), $NC^{\alpha}C$ d(12)

S=strong, M=medium, W=weak, V=very, sh=shoulder
s=stretch, as=asymmetric stretch, ss=symmetric stretch, b=angle bend, ib=in-plane angle bend, ob=out-of-plane bend, ab=asymmetric angle bend, r=rock, d=deformation, t=torsion. Only contributions 10% or greater are included.

They were identified on the assumption that hydrogen bond stretching and bending vibrations, and the torsional vibrations about the axes C_α-C and C_α-N appear in this region.

Table F2. Infrared absorption frequencies in the region 60-700 cm^{-1} **[Ito1968]**& **[Ito1969]**. The samples were prepared as thin films cast from dichloroacetic acid and trifluoroacetic acid solutions.

α – helical			β – form	
Poly-L-Ala	^{15}N poly-L-Ala	Poly-L-Leu	Poly-L-Val	^{15}N poly-L-Val
90	Not measured	104	-	-
120		144	120	-
167		213	210	-
190		262	261	-
287		283	-	-
325		323	324	-
371		396	419	410
-	455	472	473	-
526	523	539	524	531
610	600	582	543	-
-	618	615	-	-
653	648	658	638	638
686	680	697	702	702

Above 200 cm^{-1} α-helix shows characteristic bands at around 380, 610, 650, and 690 cm^{-1} **[Ito1969]**. The bands at ~100, ~167, 380, and 690 cm^{-1} represent helix deformations. The other two, at 610 and 650 cm^{-1} are due to C=O out-of-plane bending[35] coupled with N-H out-of-plane bending.

From calculations, the α-helix characteristics should be situated at 93, 141, 162, and 203 cm^{-1} (**[Ito1970]**, Table F3). Beside these, there were two more bands calculated, but not observed: at 44 and 80 cm^{-1}.

For β form, only two bands are assigned as characteristic, at 120, 247, 440, and 700 cm^{-1}. The band at 700 cm^{-1} is assigned as amide V.

[35] This is one of the vibrations that is always present in single molecule-amino acid.

Table F3. Observed (dichroic measurements), calculated frequencies, and assignment of poly-L-alanine with right-handed α-helical conformation **[Ito1970]**. The measurements were made with oriented films. The calculations were carried out according to GF matrix method for infinite chain polymer.

Frequency, cm^{-1}		Assignment
Calculated	Observed	
44		Helix deformation
80		
93	113	
141	120	
162	163	Helix deformation+ $C_\alpha C_\beta$ bending
203	185	
259		Helix deformation
295	284	$C_\alpha C_\beta$ bending
333	324	
353		
368	371	Helix deformation
520	528	C=O in plane bending
531		
594	616	C=O out-of-plane bending N-H out-of-plane bending
621		
647	658	
654		
699	691	Helix deformation

The normal mode calculations have brought new information about the bands characteristic for a secondary structure. **[Miy1967]** and **[Fan1971]** (Table F4 & F5) filled the gap of knowledge with calculus of frequencies for all the infrared and Raman active modes by using a seven-atom model (the methyl group is considered to be only one atom) which includes hydrogen bonding between chains.

Table F4. Observed and calculated frequencies of α-poly-L-alanine **[Fan1971]**. The calculation model included the hydrogen bonding.

Frequencies, cm^{-1}			
Raman[a]	Infrared[b]	Calculated	Assignments[c]
		26 (E_1)	τCC´(33), τCN(18), τC´N(14)
		40 (E2)	rN•••O(34), τCN(21), τCC´
		53 (E2)	τCC´(47), rN•••O(10)
		79 (E2)	τCC´(19), ϕCC´N(12)
		80 (A)	τCC´(31), τC´N(23), ϕCC´N(14)
		90 (E1)	τCC´(26), τC´N(23), ϕCC´N(14)
	120	137 (A)	ϕNCC´(20), ϕC´NC(19), ϕNC´M(15)
159		125 (E2)	τC´N(34), τCN(16), πNH(13)
165	167	147 (E1)	ϕC´NC(19), τCC´(15), ϕNCC´(12)
194	190	173 (E1)	ϕMC´C(20), ϕNCC´(13)
		200 (A)	ϕCC´N(28), τCN(10), τCC´(10)
214			
		201 (E2)	ϕMC´(41), ϕNCC´(13)
294	287	304 (A)	ϕNC´M(35), ϕMC´M(22), ϕCC´N(11)
		313 (E2)	ϕC´CN(20), ϕCO(21), ϕC´NC(17)
314 d			
	325	324 (E1)	ϕNC´M(45), ϕMC´C(16)
		334 (A)	ϕMC´M(35), ϕC´NC(12), πCO(12)
378	371		
		339 (E1)	ϕCO(36), ϕMC´M(16), ϕC´NC(12)
		363 (E2)	ϕNC´M(62)
		472 (E2)	πCO(25), πNH(20)
469			
		493 (E1)	ϕCO(21), ϕNC´M(15), τCN(10)
531	526	530 (A)	ϕCO(36), rC´M(15), ϕNC´M(10)
		583 (E2)	πCO(26), πNH(24), τCN(11)
	595	599 (A)	πNH (31), πCO(15), τCN(13)
610 d	610	611 (E1)	πNH(30), πCO(29)
662 d	653	652 (E1)	ϕCO(28), πNH(12)
		673 (E2)	ϕCO(38), πNH(11)
695	686	691 (A)	πCO(29), ϕCC´N(17), ϕNCC´(13)

[a] from **[Sma1970]**
[b] from **[Ito1968], [Miy1967],** and **[Bam1956]**
[c] Potential energy distribution among diagonal elements of the force matrix: r, bond stretch; ϕ, angle bend; π, out-of-peptide-plane bend; τ, torsion
[d] from **[Koe1969]**

Table F5. Observed and calculated frequencies of N-deuterated α-poly-L-alanine **[Fan1971]**.

Frequencies, cm^{-1}			
Raman	Infrared[a]	Calculated	Assignments[b]
		26 (E_1)	$\tau_{CC'}(32)$, $\tau_{CN}(18)$, $\tau_{C'N}(12)$, $\pi_{ND}(11)$
		80 (A)	$\tau_{CC'}(31)$, $\tau_{C'N}(24)$
		90 (E1)	$\tau_{CC'}(31)$, $\tau_{C'N}(24)$, $\tau_{CN}(10)$, $\phi_{CC'N}(14)$
		142 (E_1)	$\phi_{C'NC}(19)$, $\phi_{NCC'}(10)$, $\tau_{CN}(11)$, $\tau_{CC'}(15)$
		169 (E_1)	$\phi_{MC'C}(21)$, $\phi_{CC'N}(17)$, $\phi_{NCC'}(14)$
		185 (A)	$\phi_{CC'N}(28)$, $\tau_{CN}(14)$, $\tau_{CC'}(13)$, $\tau_{C'N}(11)$
301		300 (A)	$\phi_{MC'C}(28)$, $\phi_{NC'M}(35)$
363		319 (E_1)	$\phi_{NC'M}(38)$, $\phi_{MC'C}(27)$
		331 (E_1)	$\phi_{CO}(21)$, $\phi_{NC'M}(12)$, $\phi_{C'NC}(14)$
374			
		330 (A)	$\phi_{MC'C}(27)$, $\pi_{CO}(12)$, $\phi_{C'NC}(14)$
433		460 (E_1)	$\pi_{ND}(18)$, $\phi_{CO}(14)$
	455	490 (A)	$\pi_{ND}(56)$, $\tau_{CN}(10)$, $\phi_{MC'C}(16)$
		522 (A)	$\phi_{CO}(35)$, $r_{C'M}(14)$, $\phi_{NC'M}(11)$
522	523		
		525 (E_1)	$\pi_{ND}(29)$
	600		
	618		
	648	641 (E_1)	$\phi_{CO}(27)$, $\pi_{CO}(20)$, $r_{C'M}(11)$
682	680	683 (A)	$\pi_{CO}(24)$, $\phi_{CC'N}(18)$, $\phi_{NCC'}(13)$

[a] from **[Ito1968]**

[b]Potential energy distribution among diagonal elements of the force matrix: r, bond stretch;

ϕ, angle bend; π, out-of-peptide-plane bend; τ, torsion

G. Other poly-amino acids in FIR

What was considered as characteristic frequency for each of the secondary structures of poly-L-alanine, can be found also in other homopolymers.

The broad band that is found in poly-L-valine at 700 cm^{-1} **[Ito1969]** is assigned as amide V[36].

Using FIR absorption it was possible to determine the secondary structure of poly-L-leucine. According to **[Blo1960]** poly-L-leucine exists as an α-helix in the solid state, as it has three infrared bands at 694, 657, and 614 cm^{-1}.

The FIR and Raman spectra of poly-L-leucine, poly-L-valine, and poly-L-serine are presented in **[Koe1971]**[37]. The absorption spectra of poly-L-proline, poly-L-leucine, and poly-DL-leucine were analysed in search for longitudinal acoustic modes predicted to appear at low frequencies[38], either at 80 and 44 cm^{-1} or at 75 and 43 cm^{-1}. However, there was just a single low lying mode observed, at 65 cm^{-1} that cannot be clearly assigned.

In **[Xie1999]** the authors attempted to provide "more precise data on the low-frequency modes of amino acid homopolymers than has been previously available", including, poly-L-valine poly-L-phenylalanine, poly-L-tryptophan, poly-L-leucine and poly-L-alanine. For the latter two, the spectra in the region 60-220 cm^{-1} appeared quite similar, except that the bands for poly-L-leucine are shifted to a higher frequency. It is not surprising that the absorption of the chains is alike, as the resemblance of single molecules is also not too much different.

---

[36] amide V is N-H in plane bending

[37] **[Koe1971]** in Annex A, table 17, page 154

[38] see **[Fan1971]** and **[Ito1969]**

LIST OF ABBREVIATIONS

Ala – alanine

Arg - arginine

Asn – asparagine

Asp – aspartic acid

Cys –cystine

DTGS – deuterated triglycine sulphate

EU – European Union

FIR – far infrared

Gln - glutamine

Glu – glutamic acid

Gly – glycine

His – histidine

Ile – isoleucine

IINS – inelastic incoherent neutron scattering

Leu – leucine

Lys – lysine

Met – methionine

MIR – mid infrared

PET – polyethylene

Phe - phenylalanine

Pro - proline

Ser - serine

Thr - threonine

THz – terahertz

Trp – tryptophan

Tyr – tyrosine

Val – valine

BIBLIOGRAPHY

[Abe1972] Y. Abe, *Biopolym.* **11**, 1817-1839 (1972)

[Ada1972] R. Adamowicz, E. Fishman, *Spectrochim. Acta* **28A**, 889-895 (1972)

[Alb1939] G. Albrecht, R. B. Corey, *J. Am. Chem. Soc.* **61**, 1087-1103 (1939)

[Ang1995] C. A. Angell, *Science* **267**, 1924-1935 (1995)

[Ast1949] W. T. Astbury, *Nature* **163**, 722 (1949)

[Bah1997] G. P. Bahuguna, P. Tandon, V. D. Gupta, S. Rastogi, C. Mehrotra, J. *Macromol. Sci.-Phys.* **B36(4)**, 535-552 (1997)

[Bam1955] C. H. Bamford, L. Brown, E. M. Cant, A. Elliot, W. E. Hanby, B. R. Malcolm, *Nature* **176**, 396-397 (1955)

[Bam1956] C. H. Bamford, A. Elliott, W. E. Hanby, in *Synthetic Polypetides*, Academic Press, New York, Chap. 5 (1956)

[Ban1983] J. Bandekar, L. Genzel, F. Kremer, L. Santo, *Spectrochim. Acta* **39A**, 357-366 (1983)

[Bar2000] A. Barth, *Prog. Biophys. Mol. Biol.* **74**, 141-173 (2000)

[Bar2002] M. Barthes, A. F. Vik, A. Spire, H. N. Bordallo, J. Eckert, *J. Phys. Chem. A* **106**, 5230-5241 (2002)

[Bel1975] L. J. Bellamy, The Infrared Spectra of Complex Molecules, Chapman and Hall, London, 1975, 3rd ed.

[Ber2002] P. F. Bernath, *Phys. Chem. Chem. Phys.* **4(9)**, 1501-1509 (2002)

[Biz2000] A. R. Bizzarri, A. Paciaroni, S. Cannistraro, *Phys. Rev. E* **62**, 3991-3999 (2000)

[Blo1960] E. R. Blout, C. Loze, S. M. Bloom, G. D. Fasman, *J. Amer. Chem. Soc.,* 3787-3789 (1960)

[Bog1971] R. Boggs, J. Donohue, *Acta Cryst.* **B27** 247 (1971)

[Bol1932] G. Bolla, *Nuovo Cimento* **9**, 290 (1932)

[Bow1989] D. I. Bower, W. F. Maddams, *The Vibrational spectroscopy of Polymers*, Cambridge University Press, 1989

[Bra1820] H. Braconnot, *Ann. chim. Phys.* **13**, 113 (1820)

[Bra1950] L. Bragg, J. C. Kendrew, M. F. Perutz, *Proc. R. Soc. London Ser. A* **203**, 321-357 (1950)

[Bro1972] K. G. Brown. S. C. Erfurth, E. W. Small, W. L. Peticolas, *Proc. Natl. Acad. Sci. U. S. A.* **69**, 1467-1469 (1972)

[Bro1988] C. L. Brooks, M. Karplus, B. M. Pettitt, *Proteins: A Theoretical Perspective of Dynamics, Structure, and Thermodynamics*, John Wiley& Sons, New York (1988)

[Bro1983] B. Brooks, M. Karplus, *Proc. Natl. Acad. Sci. U. S. A.*, **80**, 6571-6575 (1983)

[Bry1987] J. Bryngelson, P. Wolynes, *Proc. Natl. Acad. Sci. U. S. A.* **84**, 7524-7528 (1987)

[Bun1947] C. W. Bunn, E. V. Garner, *Proc. Roy. Soc., Ser. A* **189**, 39-68 (1947)

[Buo1971] U. Buontempo, G. Careri, P. Fasella, A. Ferarro, *Biopolym* .**10**, 2377-2386 (1971)

[Cal1981] S. Califano, V. Schettino, N. Neto, *Lattice Dynamics of Molecular Crystals*, Springer Verlag, 1981

[Car1999] G. Careri, G. Consolini, F. Bruni, *Solid State Ionics* **125**, 257- (1999)

[Cas1976] E. Castelucci, N. Neto, S. Sbrana, in Proceedings of the 5th International conference on Raman Spectroscopy, eds. E.D. Schmid, J., Brandmueller and W. Kiefer (Schulz Verlag, Freiburg, 1976) p.550

[Cas1995] J. Casado, J. T. Lopez Navarrete, F. J. Ramirez, *J. Raman Spectrosc.* **26**, 1003-1008 (1995)

[Cha1976] H. R. Chandrasekar, L. Genzel, J. Kuhl, *Optics Comm.* **17**, 106-110 (1976)

[Cha] M. Chapman *http://www.lsbu.ac.uk/water/index.html*

[Chi1973] Y. N. Chirgadze, A. M. Ovsepyan, *Biopolym.* **12**, 637-645 (1973)

[Cho1985] K. C. Chou, *Biophys. J.* **48**, 289-297 (1985)

[Coc1952] W. Cochran, B. R. Penfold, *Acta Cryst.* **5**, 644-653 (1952)

[Cri1955] F. H. C. Crick, A. Rich, *Nature* **176**, 780-781 (1955)

[Cus1989] S. Cusack, *Chem. Scr.* **29A**, 103–107 (1989)

[Cus1990] S. Cusack, W. Doster, *Biophys. J.* **58**, 243–251 (1990)

[Der1968] J. L. Derissen, H. J. Endeman, A. F. Peerdeman, *Acty Cryst.* **B24**, 1349-1354 (1968)

[Des1971] C. Destrade, C. Garrigou-Lagrange, M.-T. Forel, *J. Mol. Struct,* **10**, 203-219 (1971)

[Des1988] R. Destro, R. E. Marsh, *J. Phys. Chem.* **92**, 966-973 (1988)

[Dha1991] P.Dhamelincourt, F. J. Ramirez, *J. Raman. Spectrosc.* **22**, 577 (1991)

[Dha1993] P. Dhamelincourt, F. J. Ramirez, *Appl. Spectrosc.* **47**, 446-451 (1993)

[Die1982] [M. Diem, P. L. Polavarapu, Obodi, L. A. Nafie, *J. Am. Chem. Soc.* **104**, 3392 (1982)

[Dos1989] W. Doster, S. Cusack, W. Petry, *Nature (London)* **337**, 754– 756 (1989)

[Dov1998] G. Dovbeshko, L. Berezhinsky, *J. Mol. Struct.* **450**, 121-128 (1998)

[Dov2000] M. T. Dove, M. J. Harris, A. C. Hannon, J. M. Parker, I. P. Swanson, M. Gambhir, *Phys. Rev. Lett.* **78**, 1070-1073 (1997)

[Dow1975] H. D. Downing, D. Williams, *J. Geophys.Res.* **80**, 1656-1661 (1975)

[Dwi1972] A. M. Dwivedi, A.M., Gupta, V. D., *Biopolym.* **11**, 2091-2098 (1972)

[Dwi1973] A. M. Dwivedi, R. B. Srivastava, V. D. Gupta, *Indian Journal of Pure and Applied Physics* **11**, 764-768 (1973)

[Dwi1982] A. M. Dwivedi, S. Krimm, *Biopolym.* **21**, 2377-2397 (1982)

[Dwi1982I] A. M. Dwivedi, S. Krimm, *Macromol.* **15**, 177-185 (1982)

[Dwi1984] A. M. Dwivedi, S. Krimm, *Biopolym.* **23**, 923-943 (1984)

[Ell1996] S. R. Elliott, *Phys. Rev. Lett.* **77**, 4105 (1996)

[Fan1971] B. Fanconi, E. W. Small, W. L. Peticolas, *Biopolym.* **10**, 1277-1298 (1971)

[Fan1972] B. Fanconi, *J. Chem. Phys.*, **57**, 2109-2116 (1972)

[Fan1973] B. Fanconi, *Biopolym.* **12**, 2759-2776 (1973)

[Fill1976] F. Fillaux, C. de Loze, *J. Chim. Phys. Physicochim Biol.* **73**, 1010-1017 (1976)

[Fox2001] M. Fox, *Optical Properties of Solids*, Oxford University Press (2001)

[Fri1992] M. J. Frisch, G. W. Trucks, M. Head-Gordon, P. M. W. Gill, M. W. Wong, "Gaussian 92", Revision C, Gaussian Inc., Pittsburg, PA (1992)

[Fuk1963] K. Fukushima, Y. Ideguchi, T. Shimanouchi, T. Miyazawa, *Bull. Chem. Soc. Japan* **36**, 1301-1307 (1963)

[Gai2001] V. I. Gaiduk, *Phys. Chem. Chem. Phys.* **3 (23)**, 5173-5181 (2001)

[Gen1976] L. Genzel *et al., Biopolymers* **15**, 219-225 (1976)

[Gen1983] L. Genzel, F. Kremer, A. Poglitsch, G. Bechtold, *Coherent Excitations in Biological Systems*, Ed. by H. Fröhlich and F. Kremer, Springer-Verlag Berlin Heidelberg, 58 (1983)

[Gen1983I] L. Genzel, F. Kremer, A. Poglitsch, G. Bechtold, *Biopolym.* **22**, 1715-1729 (1983)

[Gen1983II] L. Genzel, L. Santo, S. C. Shen, In „Spectroscopy of Biological Molecules", C. Sandori, T. Theophanides eds., D. Reidel, 609-619 (1983)

[Gio2004] N. Giovambattista, C. A. Angell, F. Sciortino, H. E. Stanley, *Phys. Rev. Lett.* **93**, 047801-047804 (2004)

[Gra2002] L. I. Grace, R. Cohen, T. M. Dunn, D. M. Lubman, M. S. de Vries, *J. Molec. Spectrosc.* **215**, 204-219 (2002)

[Gre1972] Y. Grenie, C. Garrigou-Lagrange, *J. Molec. Spectrosc.* **41**, 240-248 (1972)

[Gru1987] A. Grunenberg, D. Bougeard, *J. Macromolec. Struct.* **160**, 27-36 (1987)

[Gub2002] A. V. Gubskaya, P. G. Kusalik, *J. Chem. Phys.* **117,** 5290-5302 (2002)

[Gup1968] V. D. Gupta, S. Trevino, H. Boutin, *J. Chem. Phys.* **48**, 3008-3015 (1968)

[Gup1972] V. D. Gupta, R. D. Singh, *Biopolym.* **11**, 2099-2108 (1972)

[Gup1975] V. D. Gupta, M. K. Gupta, K. Nath, *Biopolym.* **14**, 1987-1990 (1975)

[Gup1977] M. K. Gupta, V. D. Gupta, *Indian J. Phys.* **51B**, 462-472 (1972)

[Gup1997] A. Gupta, P. Tandon, V. D. Gupta, S. Rastogi, *Polymer* **38**, 2389-2397 (1997)

[Hal1989] A. Hallbruker, E. Mayer, G. P. Johari, *J. Phys. Chem.* **92**, 7751-7752 (1989)

[Har1968] M. J. Harding, H. A. Long, *Acta Cryst.* **B24**, 1096-1102 (1968)

[Har2000] M. J. Harris, M. T. Dove, M. J. Parker, *Mineralogical Magazine* **64 (3)**, 435-440 (2000)

[Has1983] J. B. Hasted, S. K. Husain, A. Y. Ko, D. Rosen, Elisabeth Nicol, in "Coherent Excitations in Biological Systems", Ed. By H. Fröhlich and F. Kremer, by Springer-Verlag Berlin Heidelberg p. 71-83 (1983)

[Has1985] J. B. Hasted, S. K. Husain, F. A. M. Frescura, J. R. Birch, *Chem. Phys. Lett.* **118,** 622-625 (1985)

[Hei1935] E. Heintz, *Comptes rendus hebdomadaires des séances de l'Académie des Sciences* / Académie des Sciences <Paris> **201**, 1478-1480 (1935)

[Hir1955] S. Hirokawa, *Acta Cryst.* **8**, 637-641 (1955)

[Hig1953] P. W. Higgs, *Proc. Roy. Soc.* (London) **A220,** 472 (1953)

[Hug1950] E. W. Hughes, W. J. Moore, *Acta Cryst.* 3, 313 (1950)

[Hu1995] B. B. Hu, M. C. Nuss, *Opt. Lett.* **20(16)**, 1716-1718 (1995)

[Hus1984] S. K. Husain, J.B. Hasted, D. Rosen, E. Nicol, J.R. Birch, *Infrared Phys.* **24**, 201-208 (1984)

[Ito1968] K. Itoh, T. Nakahara, T. Shimanouchi, M. Oya, K. Uno, I. Iwakura, *Biopolym.* **6**, 1759-1766 (1968)

[Ito1969] K. Itoh, T. Shimanouchi, M. Oya, *Biopolym.* **7**, 649-658 (1969)

[Ito1970] K. Itoh, T. Shimanouchi, *Biopolym.* 9, 383-399 (1970)

[Ito1972] K. Itoh, H. Katabuchi, *Biopolym.* **11**, 2593-2605 (1972)

[Ito1999] K. Ito, C. T. Moynihan, C. A. Angell, *Nature* **398**, 492-495 (1999)

[Ket1989] S.E. Kettle, E. Lugwisha, J. Eckert, N.K. McGuire, *Spectrochim. Acta* **45A**, 533-539 (1989)

[Kha1969] B. Khawas, G. S. R. Krishna Murti, *Acta Cryst.* **B25**, 1006-1009 (1969)

[Kha1970] B. Khawas, *Acta Cryst.* **B26**, 1919-1922 (1970)

[Kha1985] B. Khawas, *Indian. J. Phys. A* **59**, 219-226 (1985)

[Kis1974] T. J. Kistenmacher, G. A. Rand, R. E. Marsh, *Acta Cryst.* **B30**, 2573-2578 (1974)

[Koe1969] J. L. Koenig, P. L. Sutton, *Biopolym.* **8**, 167-171 (1969)

[Koe1971] J. L. Koenig, P.L. Sutton, *Biopolym.* **10**, 89-106 (1971)

[Lag1983] P. Lagant, P., Vergoten, G., Loucheux-Lefebvre, M.H., Fleury, G., *Biopolymers*, **22**, 1267-1283 (1983)

[Lea1969] A. J. Leadbetter, *J. Chem. Phys.* **51**, 779 (1969)

[Leh1972] M. S. Lehman, T. F. Koetzle, W. C. Hamilton, *J. Am. Chem. Soc.* **94**, 2657-2660 (1972)

[Len1932] F. V. Lenel, *Z. Krystallogr.* **81**, 224 (1932)

[Lev1999] A. Levstik, C. Filipic, Z., Kutnjak, G. Careri, G. Consolini, F. Bruni, *Phys. Rev. E* **60**, 7604-7607 (1999)

[Mac1977] K. Machida, A. Kagayama, Y. Saito, Y. Kuroda, T. Uno, *Spectrochim. Acta*, **33A**, 569-574 (1977)

[Mac1978] K. Machida, A. Kagayama, Y. Saito, T. Uno, *Spectrochim. Acta* **34 A**, 909-914 (1978)

[Mac1979] K. Machida, M. Izumi, A. Kagayama, *Spectrochim. Acta* **35A**, 1333-1339 (1979)

[Mad1972] J. J. Madde, E. L. McGandy, N.C. Seeman, M. M. Harding, A. Hoy, *Acta Cryst.* **B28**, 2382-2389 (1972)

[Mat2003] A. Matei, M. Dressel, *J. Biol. Phys.* **29**, 101-108 (2003)

[McQ1997] Donald A. McQuarrie, John D. Simon, John Choi, *Physical Chemistry: A Molecular Approach,* p. 496, 1997

[Mel1999] S. Melchionna, A. Desideri, *Phys. Rev. E* **60(4)**, 4664-4669 (1999)

[Mir2002] I. Mirebeau, *Nature* **420**, 35-38 (2002)

[Mis1998] O. Mishima, H. E. Stanley, *Nature* **396**, 329-335 (1998)

[Miy1967] T. Miyazawa, K. Fukushima, S. Sugano, *Conformation of Biopolymers*, Ed., Ramachandran, G.N., Academic Press, New York, **vol. 2**, p. 557 (1967)

[Miy2003] F. M. Miyamaru, M. Yamaguchi, M. Tani, K. Hangyo, K. Yamamoto, K. Tominaga Conference on Lasers and Electro-Optics (CLEO 2003) June (2003), Baltimore, USA

[Moe1992] K. D. Moeller *et al.*, *Biophys. J.* **61**, 276-280 (1992)

[Moo1976I] W. H. Moore, S. Krimm, *Biopolym.* **15**, 2439-2464 (1976)

[Moo1976II] W. H. Moore, S. Krimm, *Biopolym.* **15**, 2465-2483 (1976)

[Nav1994] J. T. L. Navarrete, V. Hernandez, F. J. Ramirez, *J. Raman Spectr.* **25**, 861-867 (1994)

[Ohs1995] K. Ohshima, H. Okabayashi, T. Yoshida, *Vibr. Spectrosc.* **8**, 401-410 (1995)

[Pac1998] A. Paciaroni, A. R. Bizzarri, S. Cannistraro, *Phys. Rev. E* **57**, 6277-6280 (1998)

[Pac1999] A. Paciaroni, A. R. Bizzarri, S. Cannistraro, *Phys. Rev. E* **60**, R2476-2479 (1999)

[Pad1965] F. J. Padden, H. D. Keith, *J. Appl. Phys.* **36**, 2987-2995 (1965)

[Pad2003] A. Padró, J. Marti, *J. Chem. Phys.* **118**, 452-453 (2003)

[Pai1982] P. Painter, L. Mosher, C. Rhoads, *Biopolym.* **21**, 1469–1472 (1982)

[Pal1991] E. D. Palik, *Handbook of Optical Constants of Solids*, Academic Press (1997)

[Pau1951] L. Pauling, R. B. Corey, H. R. Branson . *Natl. Acad. Sci U. S. A.,* **37(4)**, 205-211 (1951)

[Paw1995] A. Pawlukojc *et al.*, *Spectrochim. Acta A* **51**, 303-307 (1995)

[Paw1996] A. Pawlukojc, J. Leciejewicz, I. Natkaniec, *Spectrochim. Acta A* **52**, 29-32 (1996)

[Paw1997] A. Pawlukojc, K. Bajdor, J. C. Dobrowolski, *Spectrochim. Acta A* **53**, 927-931 (1997)

[Paw2001] A. Pawlukojc, J. Leciejewicz, J. Tomkinson, S. F. Parker, *Spectrochim. Acta A* **57**, 2513-2523 (2001)

[Paw2002] A. Pawlukojc, J. Leciejewicz, J. Tomkinson, S. F. Parker, *Spectrochim. Acta A* **58**, 2897-2904 (2002)

[Pey2001] M. Peyrard, *Phys. Rev. E* **64,** 0111091-0111095 (2001)

[Piz2001] E. Pizzitutti, F. Bruni, *Phys. Rev. E* **64**, 0529051-0529054 (2001)

[Pow1979] B. M. Powell, P. Martel, *Chem. Phys. Lett.* **67**, 165-167 (1979)

[Qia1991] W. Qian, J. Bandekar, S. Krimm, *Biopolym.* **5(31)** 193-210 (1991)

[Ram1967] G. N. Ramachandran, V. Sasisekharan, *Proc. Conf. Conformation of Biopolymers*, Madras 1967, Academic Press (1967)

[Ram1995] F. J. Ramirez, J. T. Lopez Navarrete, *Spectrochim. Acta* **2**, 293-302 (1995)

[Rev1994] I. D. Reva, S. G. Stepanian, A. M. Plokhotnichenko, E. D. Radchenko, G. G. Sheina, Yu. P. Blagoi, *J. Molec. Struct.* **318**, 1-13 (1994)

[Ric1981] J. S. Richardson, *Adv. Prot. Chem.* **34,** 167-339 (1981)

[Sch1989] D. Schrader, "Raman, Infrared Atlas of Organic Compunds", Verlag Chemie, Weinheim (1989)

[Seg1931] E. Segre, *Rend. Licei* **13**, 929 (1931)

[Set1996] M. Setteles, W. Doster, *Faraday Discuss.* **103**, 269-279 (1996)

[Sho1974] W. J. Shotts, A. J. Sievers, *Biopolym.* **13**, 2593-2614 (1974)

[Sil1998] B. L. Silva, P. T. C. Freire, I. G. Melo, M. A. Araujo Silva, J. Mendes, A. J. Filho, D. Moreno, *Braz. J. Phys.* **28**, 19-24 (1998)

[Sim1966] H. J. Simpson, R. E. Marsh, *Acta Cryst.* **20**, 550-555 (1996)

[Sin1971] R. D. Singh, V. D. Gupta, *Spectrochim. Acta* **27**, 385-393 (1971)

[Sma1970] E. W. Small, B. Fanconi, W. L. Peticolas, *J. Chem. Phys.* **52**, 4369-4379 (1970)

[Smi1969] M. Smith, A. G. Walton, J. L. Koenig, *Biopolym.* **8**, 29-43 (1969)

[Ste1998] S. G. Stepanian, I. D. Reva, E. D. Radchenko, M. T. S. Rosado, M. L. T. S. Duarte, R. Fausto, L. Adamowicz, *J. Phys. Chem. A* **102**, 1041-1054 (1998)

[Sun1989] T. Sundius, J. Bandekar, S. Krimm, *J. Molec. Struct.* **214**, 119-142 (1989)

[Sus1983] H. Susi, D. M. Byler, W. V. Gerasimowicz, *J. Molec. Struct.* **102**, 63-79 (1983)

[Sut1970] P. Sutton, J. L. Koenig, *Biopolym.* **9**, 615-634 (1970)

[Suw1972] M. Suwalski, W. Traub, *Biopolym.* **11**, 623-629 (1972)

[Suz1959] S. Suzuki, T. Ohshima, N. Tamiya, K. Fukushima, T. Shimanouchi, S. I. Mizushima, *Spectrochim. Acta* **11**, 969-976 (1959)

[Suz1963] S. Suzuki, T. Shimanouchi, M. Tsuboi, *Spectrochim. Acta* **19**, 1195-1208 (1963)

[Suz1966] S. Suzuki, Y. Iwashita, T. Shimanouchi, *Biopolym.* **4**, 337-350 (1966)

[Tar1997I] S. N. Taraskin, S. R. Elliot, *Europhys. Lett.* **39**, 37-42 (1997)

[Tar1997II] S. N. Taraskin, S. R. Elliot, *Phys. Rev. B* **56**, 8605-8622 (1997)

[Tor1971] K. Torii, Y. Iitaka, *Acta Cryst.* **B27**, 2237-2246 (1971)

[Tor1971II] K. Torii, Y. Iitaka, *Acta Cryst.* **B26**, 1317-1326 (1970)

[Tsu1958] M. Tsuboi, T. Onishi, I. Nakagawa, T. Shimanouchi, S. Mizushima, *Spectrochim. Acta* **12**, 253-261 (1958)

[Vel2001] V. Velikov, S. Borick, C. A. Angell, *Science* **294**, 2335-2338 (2001)

[Ver1972] J. J. Verbist, M. S. Lehmann, T. F. Koetzle, W. C. Hamilton, *Acta Crystallogr. Cryst. Chem.* **28**, 3006-3013 (1972)

[Vij1992] A. Vijay, D.N. Sathyanarayana, *J. Phys. Chem.* **96**, 10735-10739 (1992)

[Wan1971] C.H. Wang, R. D. Storms, *J. Chem. Phys.* **55**, 3291-3299 (1971)

[Wan2004] K. Wang, D. M. Mittelman, *Nature* **432**, 376-379 (2004)

[Whi1940] S. E. Whitcomb, H. H. Nielsen, L. H. Thoma, *J. Chem. Phys.* **8**, 143 (1940)

[Whi2003] S. E. Whitmire, D. Dolpert, A. G. Markelz, J. R. Hillebrecht, J. Galan, R. R. Birge, *Biophys. J.* **85**, 1269-1277 (2003)

[Wil1934] E. B. Wilson, *Phys. Rev.* **45**, 706-711 (1934)

[Wil1939] E. B. Wilson, *J. Chem. Phys.* **7**, 1047 (1939)

[Woo2003] R. M Woodward, V. P. Wallace, D. D. Arnone, E. H. Linfield, M. Pepper, *J. Biol. Phys.* **29**, 257-261 (2003)

[Wri1939] N. Wright, *J. Biol. Chem.* **120**, 641 (1937); **127**, 137-141 (1939)

[Wri1949] B. A. Wright, P. A. Cole, *Acta Cryst.* **2**, 129-130 (1949)

[Xie1999] A. Xie, Q. He, L. Miller, B. Sclavi, M. R. Chance, *Biopolym.* **49**, 591-603 (1999)

[Yak1952] H. L. Yakel Jr., E. W. Hughes, *Acta Cryst.* **5**, 847-848 (1952)

[Yak2002] V. A. Yashin, A. A. Yakovenko, A. E. Kovalev, E. E. Fesenko, *Biophys.* **47**, 965-969 (2002)

[Yam2002] K. Yamamoto, K. Tominaga, H. Sasakawa, A. Tamura, H. Murakami, H. Ohtake, N. Sarukura, *Bull. Chem. Soc. Jpn.* **75**, 1083-1092 (2002)

[Zbi1969] R. Zbindin, *Infrared Spectroscopy of High Polymers*, Academica Press, New York and London, p. 96 (1969)

[Zel1995] H. R. Zelsmann, *J. Mol. Struct.* **350**, 95-114 (1995)

[Zon2003] C. Zandonella, *Nature* **424**, 721-722 (2003)

Curriculum Vitae

December 13th, 1975	Born in Bucharest, Romania
1990 - 1994	High School, Bucharest, Romania
1994 - 1998	BSc, Faculty of Physics University of Bucharest, Romania
1998 - 2000	MSc, Faculty of Physics, Biophysics Department, University of Bucharest University of Bucharest, Romania
2001 - 2005	PhD student, 1. Physikalisches Institut, Universität Stuttgart, Germany Title: Optical Investigations of Biological Samples in Far Infrared